1

Conjugated Polymer Donors for Organic Solar Cells

Xiaopeng Xu[1], Xiyue Yuan[2], Qunping Fan[3], Chunhui Duan[2], Maojie Zhang[3], and Qiang Peng[1]

[1] *Sichuan University, School of Chemical Engineering, State Key Laboratory of Polymer Materials Engineering, No. 24 South Section 1, Yihuan Road, Chengdu 610065, P.R. China*
[2] *South China University of Technology, Institute of Polymer Optoelectronic Materials and Devices, State Key Laboratory of Luminescent Materials and Devices, 381 Wushan Road, Tianhe District, Guangzhou 510640, P.R. China*
[3] *Soochow University, Laboratory of Advanced Optoelectronic Materials, College of Chemistry, Chemical Engineering and Materials Science, 199 Ren'ai Road, Suzhou 215123, P.R. China*

1.1 Introduction

Organic solar cells (OSCs) are the devices that can directly convert solar energy into electricity with the advantages of low cost, light weight, and the potential for roll-to-roll fabrication on flexible substrates, which make them promising candidates for inexpensive renewable power sources [1–3]. At present, the highest power conversion efficiency (PCE) of OSCs in laboratory has exceeded 18% [4]. Important progresses have been also made in scalability and device stability, which demonstrated the great application prospect of this technology [5, 6]. These progresses were greatly benefitted from the design and synthesis of donor polymers with wide spectral absorption coverage to the solar spectrum and matched energy levels. Based on the optical bandgaps (E_g^{opt}s), donor polymers employed in OSCs can be divided into three major types: low bandgap (LBG) polymers ($E_g < 1.6$ eV), medium bandgap (MBG) polymers (1.6 eV $< E_g <$ 1.8 eV), and wide bandgap (WBG) polymers ($E_g > 1.8$ eV) (Figure 1.1a) [7]. In the early stage of OSCs field, fullerene derivatives were the dominant acceptors, which are poor light absorbers. As a result, the donor polymers are responsible for light harvesting in the resulting OSCs. Correspondingly, the LBG polymers played a more important role than the MBG and WBG polymers at that stage [8]. Nevertheless, LBG polymers with reduced E_g^{opt} generally had a high-lying highest occupied molecular orbital (HOMO) energy level, which resulted in a limited open-circuit voltage (V_{oc}) in the corresponding OSCs [9]. MBG polymers could have more potential to deepen the HOMO level without significantly increasing the bandgap, which afforded higher V_{oc} without

Xiaopeng Xu, Xiyue Yuan, and Qunping Fan have contributed equally to this work.

Organic Solar Cells: Materials Design, Technology and Commercialization, First Edition. Edited by Liming Ding.

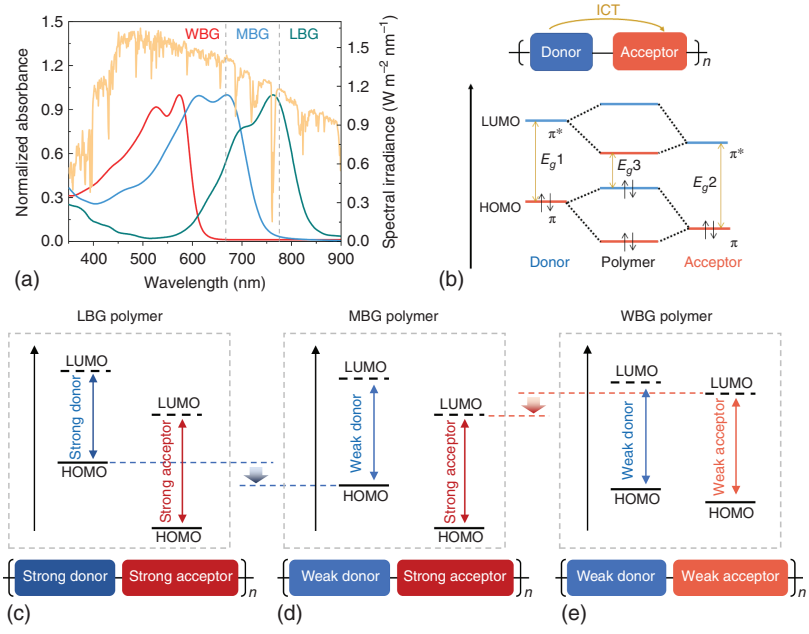

Figure 1.1 (a) UV–vis–near-infrared (NIR) absorption of different bandgap polymers. (b) Principle of bandgap lowering by donor–acceptor interaction. (c) LBG polymers constructed by using "strong donor-strong acceptor" configuration. (d) MBG polymers constructed by using "weak donor-strong acceptor" configuration. (e) WBG polymers constructed by using "weak donor-weak acceptor" configuration. Source: Xiaopeng Xu.

sacrificing short-current density (J_{sc}) in the resulted OSCs [9, 10]. Although the J_{sc}s of OSCs based on WBG polymers were limited by their narrow absorptions, they were also key components to complement the absorption spectra with LBG counterparts and achieve high V_{oc} in the multi-junction, ternary blend, or the currently prevailing non-fullerene OSCs [8–11].

Constructing donor–acceptor (D–A)-type copolymers has been demonstrated to be the most successful strategy to develop high-performance donor polymers (Figure 1.1b). With rational choice of electron-donating and electron-withdrawing units, the absorption ranges and frontier energy levels can be readily tuned. The "push-pull" effect between D and A units has distinct effect on the bandgaps of the resulted polymers: (i) the combination of "strong donor" and "strong acceptor" could be a feasible way to achieve a LBG polymer (Figure 1.1c); (ii) the pair of "weak donor" and "strong acceptor" could be employed to construct a MBG polymer (Figure 1.1d); and (iii) the utilization of "weak donor" and "weak acceptor" could be effective to build a WBG polymer (Figure 1.1e). Compared to the LBG polymer, the weak electron-donating ability of donor motif delivers a low-lying HOMO energy level of the MBG and WBG polymers, which is beneficial to realize high V_{oc} in the resulting polymer solar cells (PSCs) [10, 11]. Compared to the WBG polymer, the strong electron-withdrawing ability of acceptor block lowers the lowest unoccupied molecular orbital (LUMO) energy level of the MBG polymer, which enables a

reduced bandgap *via* intramolecular charge transfer (ICT) [12]. In the following part, we will introduce the design strategies of LBG, MBG, and WBG polymers and analyze their photovoltaic properties.

1.2 LBG Polymers

LBG-conjugated polymers are usually obtained *via* the design strategies as follows [13, 14]. First, stabilization of the quinoidal resonance structure in conjugated polymers. Generally, two kinds of resonance structures, i.e. aromatic and quinoidal form coexist in conjugated polymers. As compared to the aromatic form, the quinoidal form has a smaller bandgap but is energetically less stable due to the destruction of the original aromaticity. Second, copolymerization of D unit and A unit alternatively to afford the so-called D–A copolymers [15]. Reduced optical gaps (E_g3 in Figure 1.1b) in an alternating copolymer can be achieved due to the molecular orbital hybrid of the electron-rich (D) and electron-deficient (A) moiety. Besides, the HOMO level of the polymers is mainly influenced by the donor units, while the LUMO level is determined by the acceptor units. Donor units employed in high-performance LBG polymers are mostly thiophene ring-containing building blocks with strong electron-donating capability. Compared to donor units, acceptor units play a more important role in constructing LBG polymers because the absorption spectra, energy levels, and aggregation properties can be more easily tuned by selecting appropriate acceptor units [16]. The common acceptor units with stronger electron-accepting ability include 2,1,3-benzothiadiazole (BT), isoindigo (IID), and diketopyrrolopyrrole (DPP). In this section, we will introduce the design strategies of LBG polymers at first. After that, several representative types of LBG polymers and their photovoltaic properties will be analyzed.

1.2.1 LBG Polymers Based on Benzothiadiazole (BT)

2,1,3-Benzothiadiazole (BT) is a widely used acceptor unit for constructing LBG polymers in a D–A-type framework (Figure 1.2). One of the representative LBG polymers is P1 [17, 18], a copolymer-based on cyclopentadithiophene (CPDT) and BT with an E_g of 1.47 eV. By replacing the carbon atom with silicon atom on CPDT, the polymer P2 [19, 20] with a higher crystallinity and improved charge transport properties was generated, which afforded a certified PCE of 5.2% when blended with a fullerene derivative in OSCs. When introducing P2 as the third component into the PTB7:PC_{71}BM blend host, a higher fill factor (FF) of 77% was obtained due to the reduction of recombination losses. Correspondingly, a PCE improvement from 7.52% to 8.60% was achieved [21]. Replacing S with O in heteroaromatic rings tends to offer a more positive oxidation potential, which is beneficial for obtaining a higher V_{oc} in OSCs [18]. This was reflected by P3, which exhibited much deeper-lying HOMO level and higher V_{oc} than P1 in OSCs. However, this polymer could not generate photocurrent, which was possibly caused by the reduced driving force for exciton dissociation.

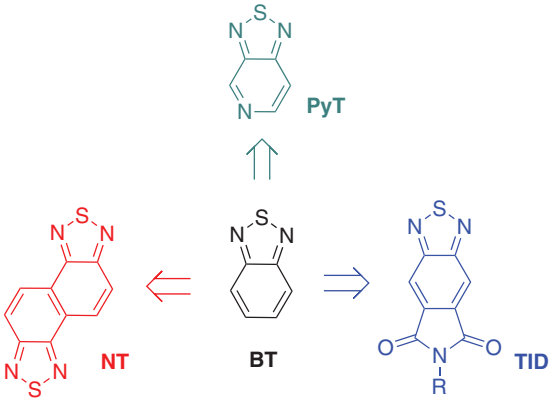

Figure 1.2 The chemical structures of BT and its derived building blocks. Source: Xiyue Yuan.

Fluorination is effective to improve the photovoltaic properties of conjugated polymers *via* tuning the frontier orbital energy levels and improving molecular ordering. However, fluorination can also bring negative effects on resulting polymers, such as poor solubility and excessive aggregation in organic solvents. Hence, the degree of fluorination shall be optimized to achieve a high-efficiency OSCs. Neher and coworkers [22] showed that the polymer with mono-fluorination on BT (P4) exhibited better photovoltaic performance than the polymers with non- and di-fluorination on BT (P1, P5) due to the stronger tendency to take face-on orientation when blended with $PC_{71}BM$. Similar fluorination effects were also observed by Jo et al. on the polymers P6–P8 [23]. Yang et al. [24] inserted a strong electron-donating oxygen atom into the CPDT unit to form the dithienopyran (DTP) unit for lowering E_g. The resulting polymer P9 exhibited a narrow E_g of 1.38 eV, and a deep HOMO level of −5.26 eV. Single-junction OSCs based on P9:$PC_{71}BM$ blend showed over 60% external quantum efficiency (EQEs) and effective optical response up to 900 nm. Moreover, a certified PCE of 10.6% in tandem OSCs based on this polymer was achieved. Guo and coworkers [25] reported a BT-based polymer P10 with an E_g of 1.46 eV by using a head-to-head substituted bithiophenes as the donor units, which afforded a promising PCE of 9.8% in fullerene-based OSCs. Replacing the phenyl ring on BT unit with pyridine ring leads to a new building block, thiadiazolo[3,4-*c*]pyridine (PyT), which possesses higher electron affinity and affords narrower bandgap in conjugated polymers. You and coworkers [26] reported a LBG polymer P11 based on PyT, which exhibited an E_g of 1.51 eV and a PCE of 6.3% in OSCs. When utilizing 4,4-bis(2-ethylhexyl)-4*H*-germolo[3,2-*b*:4,5-*b*′]dithiophene (DTG) as the electron-rich unit, the polymer P12 based on PyT exhibited a very low E_g of 1.32 eV and a decent PCE of 6.6% in inverted OSCs [27]. The chemical structures of P1–P12 are showed in Figure 1.3, and the corresponding photovoltaic parameters of OSCs are summarized in Table 1.1.

Fusing two BT units leads to the formation of naphtho[1,2-*c*:5,6-*c*′]bis[1,2,5]thiadiazole (NT), which possesses a larger planar structure and higher electron affinity than BT unit (Figure 1.4). The pioneering work based on NT was done by Cao and coworkers along with the creation of P13, which exhibited an E_g of

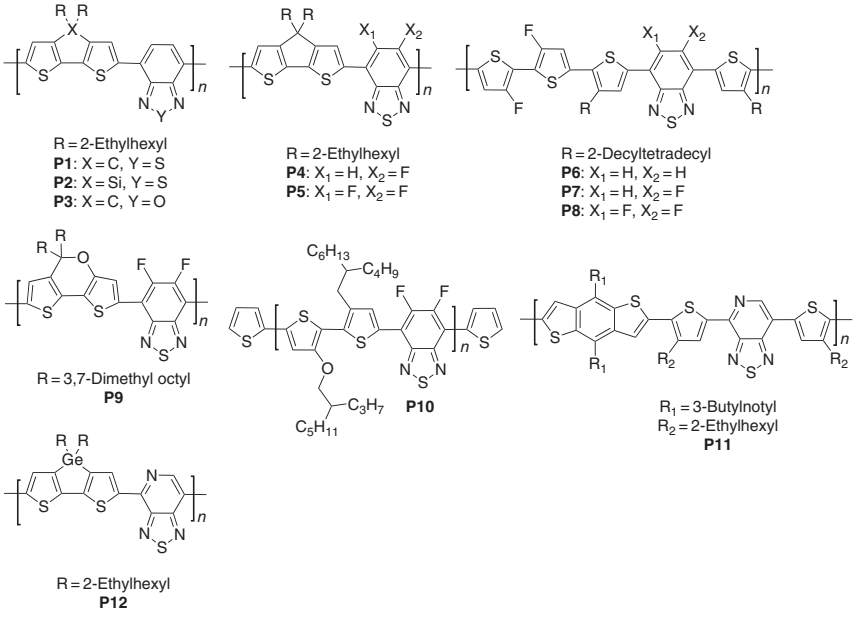

Figure 1.3 Chemical structures of the BT-derived conjugated polymers P1–P12. Source: Xiyue Yuan.

Table 1.1 Optoelectronic properties and device performances of P1–P12.

Polymer	E_g^{opt} (eV)	HOMO/ LUMO (eV)	Acceptor	V_{oc} (V)	J_{sc} (mA cm^{-2})	FF	PCE (%)	References
P1	1.47	−5.30/−3.55	$PC_{61}BM$	0.65	11.0	0.47	3.2	[17]
P2	1.45	−5.05/−3.27	$PC_{61}BM$	0.58	14.9	0.61	5.2	[20]
P3[a)]	1.47	−5.39/−3.71	$PC_{61}BM$	0.78	5.2	0.60	2.5	[18]
P4	1.45	−5.35/−3.90	$PC_{71}BM$	0.74	14.1	0.58	5.9	[22]
P5	1.51	−5.34/−3.52	$PC_{71}BM$	0.85	12.6	0.52	5.6	[24]
P6	1.57	−5.33/−3.76	$PC_{71}BM$	0.80	14.1	0.63	7.1	[23]
P7	1.57	−5.37/−3.80	$PC_{71}BM$	0.82	15.7	0.71	9.1	[23]
P8	1.59	−5.46/−3.87	$PC_{71}BM$	0.82	13.3	0.59	6.4	[23]
P9	1.38	−5.26/−3.61	$PC_{71}BM$	0.68	17.8	0.65	7.9	[24]
P10	1.46	−5.20/−3.74	$PC_{71}BM$	0.66	20.7	0.71	9.8	[25]
P11	1.51	−5.47/−3.64	$PC_{61}BM$	0.85	12.8	0.58	6.3	[26]
P12	1.32	−4.90/−3.60	$PC_{71}BM$	0.59	19.6	0.57	6.6	[27]

a) For P3, energy levels are determined from cyclic voltammetry ($E^{(Fc/Fc^+)} = -5.20$ eV).
Source: Based on Hendriks et al. [28].

Table 1.2 Optoelectronic properties and device performances of P13–P20.

Polymer	E_g^{opt} (eV)	HOMO/ LUMO (eV)	Acceptor	V_{oc} (V)	J_{sc} (mA cm^{-2})	FF (%)	PCE (%)	References
P13	1.58	−5.19/−3.26	$PC_{71}BM$	0.80	11.7	0.61	6.0	[29]
P14	1.54	−5.16/−3.77	$PC_{71}BM$	0.71	19.4	0.73	10.1	[30]
P15	1.52	−5.48/−3.65	$PC_{71}BM$	0.96	14.5	0.64	8.9	[34]
P16	1.56	−5.14/−3.46	$PC_{61}BM$	0.71	19.4	0.73	10.1	[33]
P17	1.60	−5.38/−3.53	$PC_{71}BM$	0.82	19.3	0.67	10.5	[33]
P18	1.42	−5.36/−3.48	$PC_{71}BM$	0.77	20.2	0.72	11.3	[32]
P19	1.52	−5.42/−3.48	$PC_{71}BM$	0.84	16.5	0.72	10.0	[32]
P20	1.40	−5.29/−3.40	$PC_{71}BM$	0.72	19.1	0.73	10.3	[31]

1.58 eV and a PCE of 6.0% when blended with $PC_{71}BM$ [29]. After that, more narrow bandgap polymers based on NT were developed for application in OSCs. For example, the polymer P14 bearing quaterthiophene donor units and NT acceptor units exhibited a high PCE of 10.1% in OSCs with an inverted structure at the active layer thickness of 290 nm due to the high crystallinity and hole mobility of the polymer [30]. More remarkably, high-performance thick-film OSCs were achieved by more NT-based polymers (P16–P20), which suggested the prospect of NT-based polymers in large-scale manufacturing of OSCs [31–33]. To reduce the energy loss (E_{loss}) of NT polymer-based OSCs, Takimiya and coworkers created a new building block naphtho[1,2-*c*:5,6-*c*′]bis[1,2,5]oxadiazole (NOz) by replacing the sulfur atom on NT unit with oxygen atom. The resulting polymer P15 exhibited similar E_g as P14 but significantly enhanced V_{oc} and greatly reduced E_{loss} in OSCs when blended with the same electron acceptor (≈0.85 versus ≈0.55 eV) [34]. The chemical structures of P13–P20 are showed in Figure 1.4, and the corresponding photovoltaic parameters of OSCs are summarized in Table 1.2.

[1,2,5]Thiadiazolo[3,4-*f*]isoindole-5,7-dione (TID) is another strong acceptor unit derived from BT (Figure 1.5). McCulloch and coworkers [35] reported a LBG polymer P21 based on this acceptor unit, which exhibited ideal frontier orbital energy levels for OSCs. This polymer can be solution-processed in a blend with $PC_{71}BM$ from a single solvent to reproducibly afford OSCs with the best PCE reaching 8.3%. Wang et al. [36] reported P22 with a low E_g of 1.49 eV, which was copolymerized from TID and the electron-rich unit indacenodithieno[3,2-*b*]thiophene (IDTT). The OSCs based on P22:$PC_{71}BM$ attained a good PCE of 6.7% with a high V_{oc} of 1.0 V, leading to the E_{loss} as low as 0.49 eV. In addition to TID, Facchetti and coworkers [37] reported a new electron-accepting building block benzo[1,2-*d*:4,5-*d*′]bis([1,2,3]thiadiazole) (iso-BBT). The resulting polymer P23 exhibited an E_g of 1.40 eV and afforded a PCE of 10.3% when blended with $PC_{61}BM$. Li and coworkers [38] introduced quinoidal structure design concept into the BT-derived unit and obtained the polymer P24 with an E_g of 1.45 eV. When employed in fullerene-based OSCs, P24 showed a PCE of

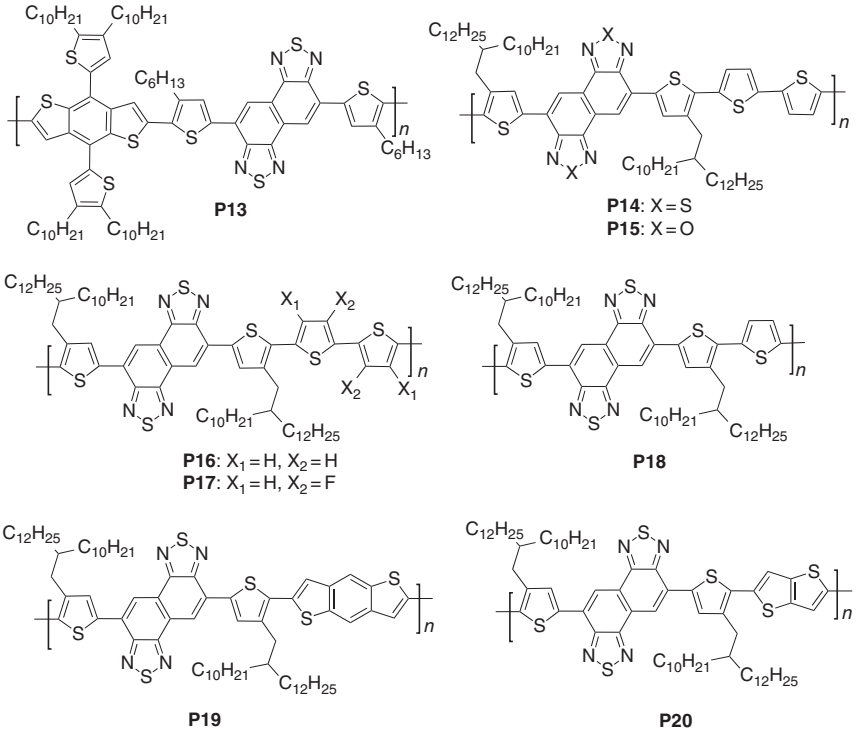

Figure 1.4 Chemical structures of the NT-derived conjugated polymers P13–P20. Source: Xiyue Yuan.

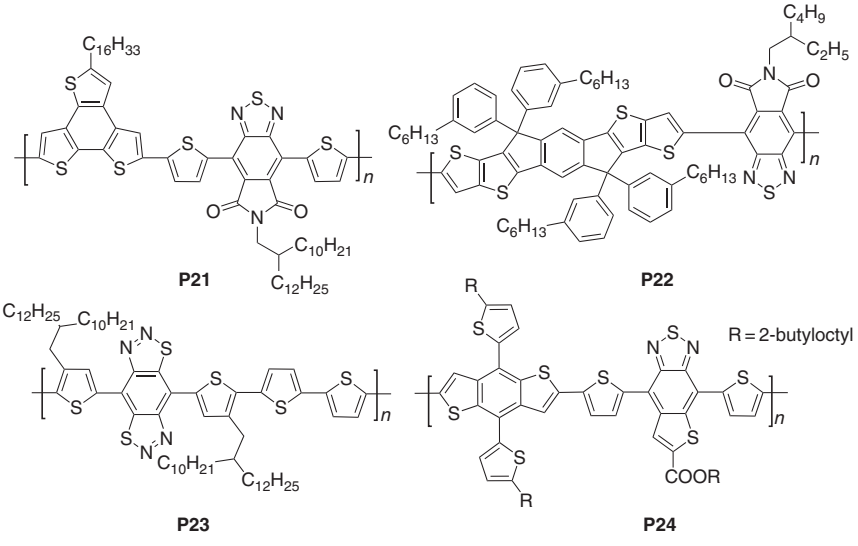

Figure 1.5 Chemical structures of the BT-derived conjugated polymers P21–P24. Source: Xiyue Yuan.

Table 1.3 Optoelectronic properties and device performances of P21–P24.

Polymer	E_g^{opt} (eV)	HOMO/ LUMO (eV)	Acceptor	V_{oc} (V)	J_{sc} (mA cm^{-2})	FF	PCE (%)	References
P21[a)]	1.50	−5.20/−3.70	$PC_{71}BM$	0.80	16.5	0.63	8.3	[35]
P22	1.49	−5.89/−3.84	$PC_{71}BM$	1.00	12.6	0.53	6.7	[36]
P23	1.40	−5.43/−4.03	$PC_{61}BM$	0.81	20.8	0.61	10.3	[37]
P24	1.45	−5.35/−3.39	$PC_{71}BM$	0.75	13.2	0.63	6.1	[38]

a) For P21, E_{LUMO} is determined by E_{HOMO} and E_g^{opt}.

6.1%. The chemical structures of P21–P24 are showed in Figure 1.5, and the corresponding photovoltaic parameters of OSCs are summarized in Table 1.3.

1.2.2 LBG Polymers Based on Isoindigo (IID)

Isoindigo (Figure 1.6a) is an isomer of the natural dye indigo, which was first known as a therapeutic agent for leukemia [39, 40]. In 2010, Reynolds and coworkers [41] introduced isoindigo-based materials into OSCs firstly. Although the highest PCE was only 1.76% achieved in that study, the unique electronic

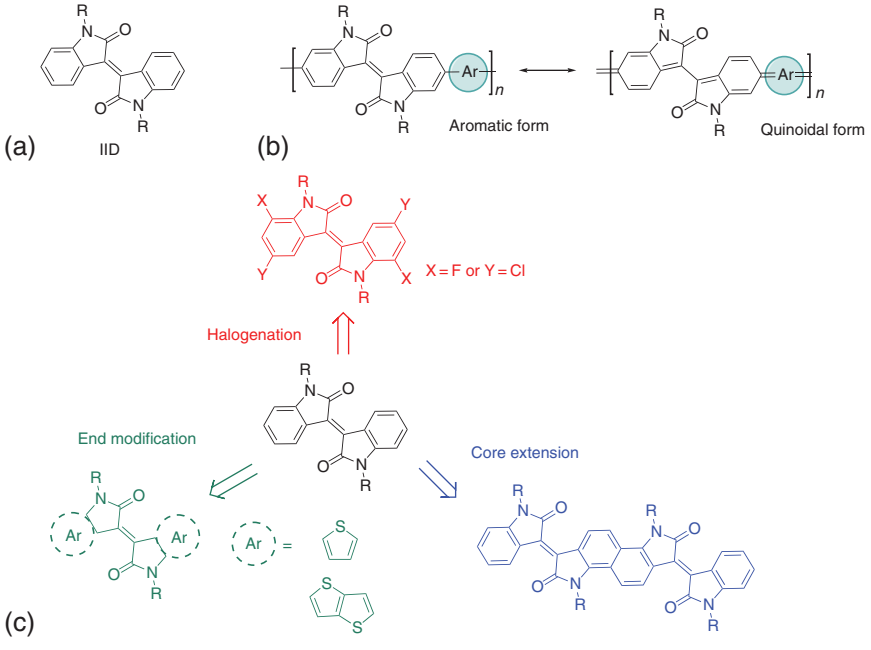

Figure 1.6 (a) The chemical structure of isoindigo. (b) The aromatic (left) and quinoidal form (right) of isoindigo-based polymers. (c) Structural modification based on isoindigo. Source: Xiyue Yuan.

Table 1.4 Optoelectronic properties and device performances of P25–P31.

Polymer	E_g^{opt} (eV)	HOMO/ LUMO (eV)	Acceptor	V_{oc} (V)	J_{sc} (mA cm^{-2})	FF	PCE (%)	References
P25	1.60	––	$PC_{61}BM$	0.91	9.1	0.54	4.5	[46]
P26	1.55	−5.43/−3.88	$PC_{71}BM$	0.84	3.9	0.53	1.7	[43]
P27	1.50	−5.69/−3.97	IT-M	0.72	14.6	0.66	6.9	[47]
P28	1.49	−5.34/−3.79	$PC_{71}BM$	0.77	9.3	0.65	4.7	[48]
P29	1.52	−5.43/−3.81	$PC_{71}BM$	0.72	7.6	0.60	3.2	[48]
P30	1.54	−5.20/−3.66	$PC_{71}BM$	0.71	7.9	0.34	1.9	[43]
P31	1.56	−5.71/−3.96	$PC_{61}BM$	0.94	8.6	0.50	4.0	[49]

properties and excellent light absorption capabilities made isoindigo an ideal building block for D–A conjugated polymers. The solubility of unsubstituted isoindigo is very poor in common organic solvents, but it can be improved by introducing various alkyl chains onto the amide nitrogen atoms. Due to its two lactam rings, isoindigo has strong electron-withdrawing properties [42]. Besides, the optoelectronic properties of isoindigo-based conjugated polymers can be tuned by structural modification including heteroatom substitution, end modification, and core extension (Figure 1.6c). Subsequently, conjugated polymers based on isoindigo and its derivatives were widely used in OSCs [43–45]. The comprehensive study on the energy levels of isoindigo-based polymers showed that LUMO levels were located on the isoindigo unit and the change of donor units could effectively manipulate the HOMO levels of isoindigo-based D–A polymers, leading to different V_{oc} values in OSCs (Figure 1.7, Table 1.4) [43, 46–52]. Meanwhile, the absorption spectra and the optical bandgaps of the resulting conjugated polymers could be readily tuned [43, 46–48].

Heteroatomic substitution (Figure 1.8) is another important method to tune the optoelectronic properties of isoindigo-based polymers, including light absorption, energy level, and solubility, etc. For example, the introduction of fluorine and chlorine atoms is effective to reduce the HOMO levels and improve charge mobility of the polymers [53]. Pei and coworkers [54] synthesized a set of fluorinated and chlorinated isoindigo-based polymers P32, P33 for using as the donor materials in OSCs. When blended with $PC_{71}BM$, the chlorinated polymer P33 performed much better than the fluorinated polymer P32 in J_{sc}. This was because that the smaller radius of F atoms endows the polymer P32 with better planarity and crystallinity, while the increased polymer crystallinity reduced the mixing between the polymer and $PC_{71}BM$. Yan and coworkers [55] studied the influence of fluorine substitution on aggregation characteristics and optical properties of the polymers in solution. The polymer P34 with fluorination on the donor unit exhibited the strongest extent of temperature-dependent aggregation, which led to a higher hole mobility for the polymer as compared to the fluorine-free polymer. Geng and coworkers [56] reported LBG polymers (P37–P39) based on dithienocarbazole and isoindigo. The HOMO

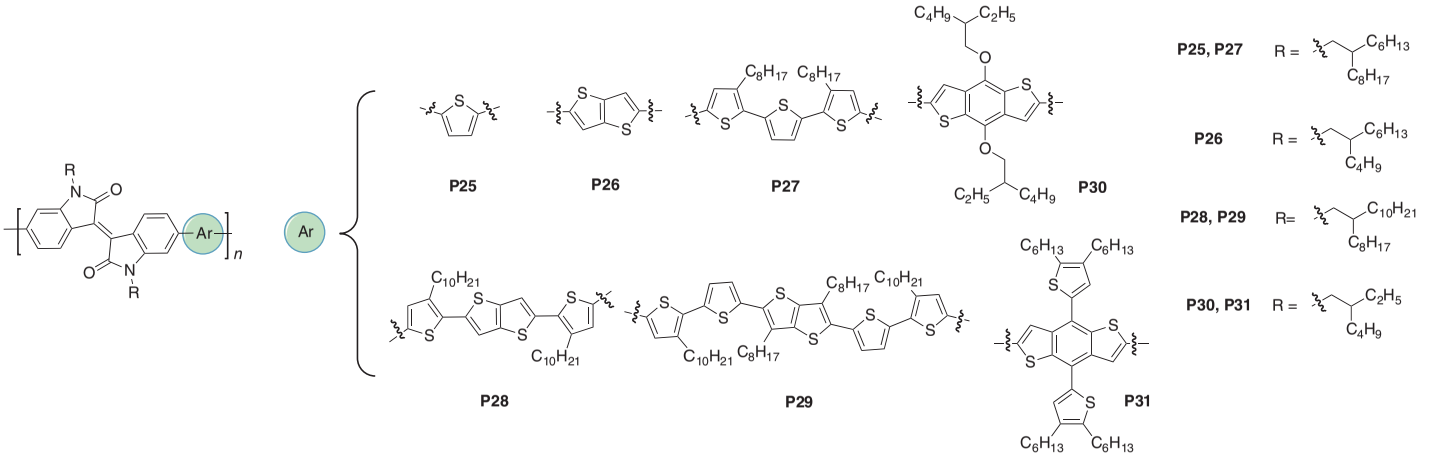

Figure 1.7 Chemical structures of the isoindigo-based conjugated polymers P25–P31. Source: Xiyue Yuan.

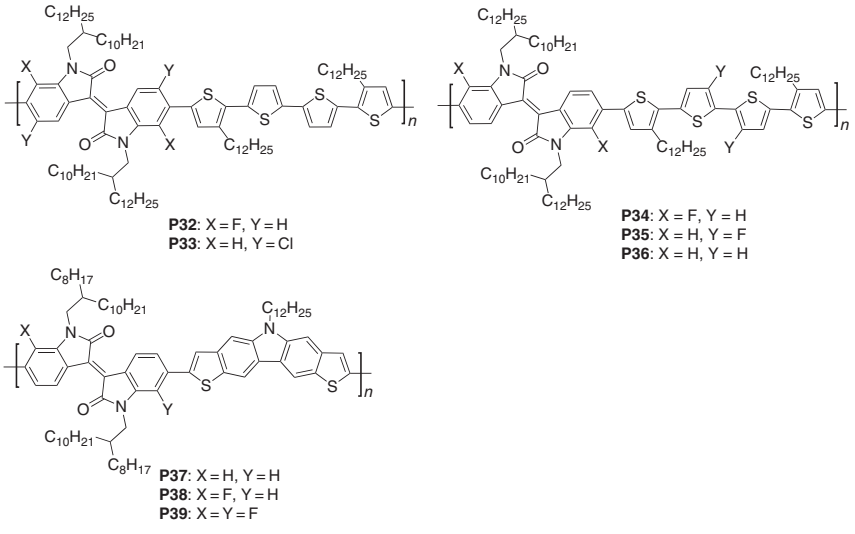

Figure 1.8 Chemical structures of the isoindigo-based conjugated polymers P32–P39. Source: Xiyue Yuan.

Table 1.5 Optoelectronic properties and device performances of P32–P39.

Polymer	E_g^{opt} (eV)	HOMO/ LUMO (eV)	Acceptor	V_{oc} (V)	J_{sc} (mA cm^{-2})	FF	PCE (%)	References
P32	1.45	−5.51/−3.92	$PC_{71}BM$	0.63	4.3	0.44	1.2	[54]
P33	1.50	−5.53/−3.85	$PC_{71}BM$	0.75	10.0	0.61	4.6	[54]
P34	1.51	−5.18/−3.67	$PC_{71}BM$	0.73	10.3	0.47	3.5	[55]
P35	1.52	−5.30/−3.78	$PC_{71}BM$	0.83	13.3	0.61	6.7	[55]
P36	1.51	−5.28/−3.77	$PC_{71}BM$	0.73	11.4	0.55	4.6	[55]
P37	1.61	−5.22/−3.54	$PC_{71}BM$	0.79	14.6	0.62	7.2	[56]
P38	1.59	−5.30/−3.67	$PC_{71}BM$	0.81	12.6	0.69	7.1	[56]
P39	1.59	−5.36/−3.74	$PC_{71}BM$	0.86	12.3	0.68	7.2	[56]

energy levels of the polymers were pushed down with the increase of F-substitution degree in isoindigo unit, which were helpful to obtain high V_{oc} in the resulting OSCs. However, the champion OSCs were achieved by the non-fluorinated polymer P37, which afforded the best PCE of 7.2% in conventional devices and 8.2% in inverted devices. The reason for the poorer device performance of fluorinated polymers was the poor phase separation. The chemical structures of P32–P39 are showed in Figure 1.8, and the corresponding photovoltaic parameters of OSCs are summarized in Table 1.5.

The other two types of isoindigo-based conjugated polymers involve skeleton changes of isoindigo (Figure 1.9): (i) changing the isoindigo terminal groups from

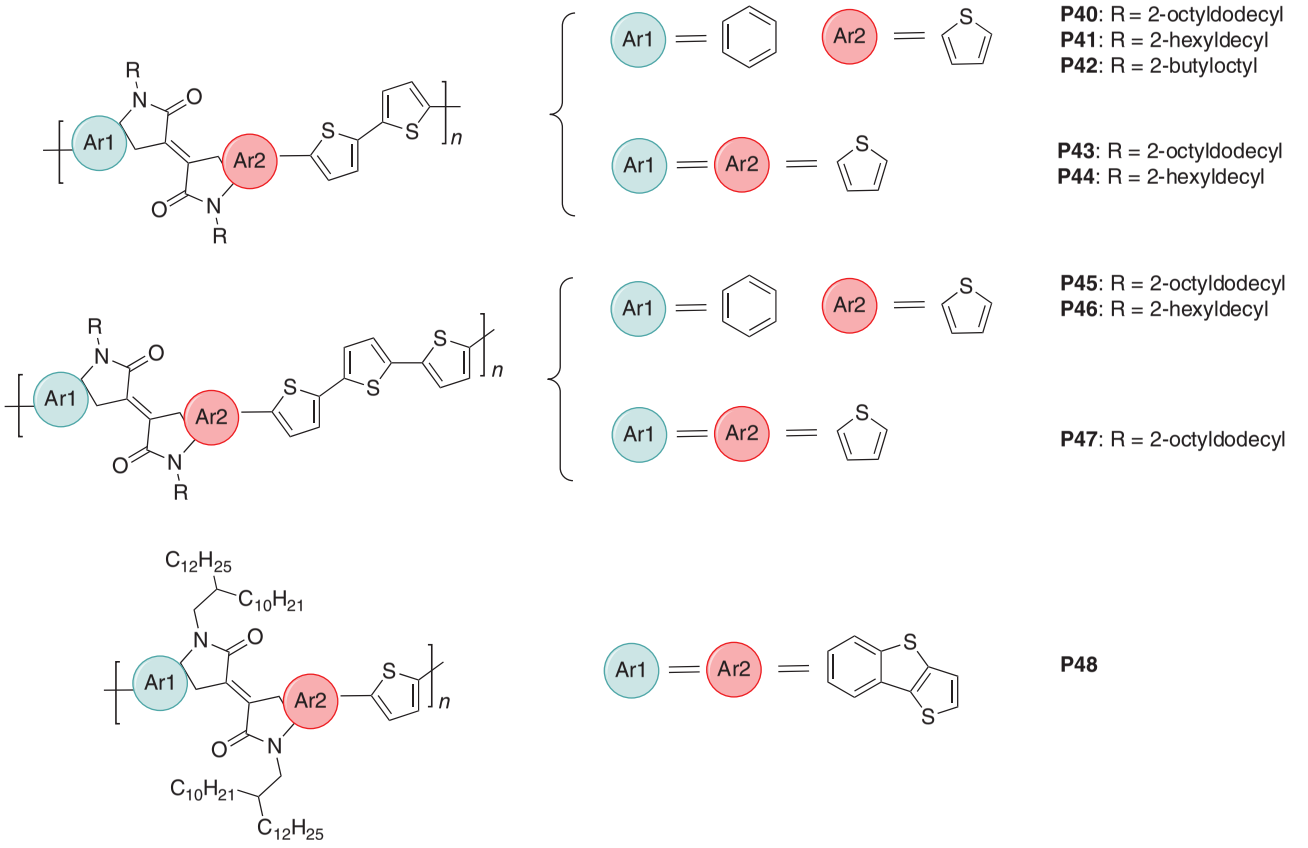

Figure 1.9 Chemical structures of the isoindigo-derived conjugated polymers P40–P48. Source: Xiyue Yuan.

phenyl rings to heterocyclic rings or fusing additional heteroaromatic rings onto the terminal phenyl rings; (ii) inserting additional conjugated units into the exocyclic double bond between the lactam rings in isoindigo core. Fréchet and coworkers [57] reported isoindigo-derived polymers with increased coplanarity by replacing isoindigo terminal phenyl rings with thiophene rings. Upon thin-film analysis by atomic force microscopy (AFM) and grazing incidence X-ray diffraction (GIXD), the thiophene-terminated isoindigo polymers favor a face-on orientation in thin films, while the phenyl-terminated isoindigo polymers favor an edge-on orientation. As a result, P45, the polymer with modest planarity, showed the highest PCE in OSCs due to the face-on-dominated orientation. McCulloch and coworkers [58] reported an eight-ring fused isoindigo-based acceptor unit thieno[3,2-*b*][1]benzothiophene isoindigo (TBTI) by fusing isoindigo core with thieno[3,2-*b*]thiophene and obtained a polymer P48 (Figure 1.9), which had a low E_g of 1.60 eV. Benefitted from its high hole mobility (0.31 $cm^2\ V^{-1}\ s^{-1}$) and suitable LUMO level (−3.50 eV), P48 afforded a high PCE of 9.1% in fullerene-based OSCs. The chemical structures of P40–P48 are showed in Figure 1.9, and the corresponding photovoltaic parameters of OSCs are summarized in Table 1.6.

Kelly and coworkers [59] used diisoindigo and ring-fused bisisoindigo dimer to study the effect of acceptor unit number and size on the optoelectronic properties of donor–acceptor–acceptor (D–A–A)-type polymers (Figure 1.10). It was found that the diisoindigo-containing polymers had lower LUMO levels as well as lower hole mobilities and higher electron mobilities than their isoindigo analogs. The polymers P51 and P52 containing bisisoindigo had the lowest LUMO levels and much smaller E_g than the isoindigo- and diisoindigo-containing polymers, consistent with their increased conjugation length. When incorporated into OSCs, the isoindigo-based polymers performed better than the diisoindigo analogs, and the bisisoindigo-based polymers performed poorer than the other polymers. The lower LUMO level of the diisoindigo- and bisisoindigo-based polymers reduced the energetic driving force for exciton dissociation at the polymer:$PC_{71}BM$ interface, leading to low J_{sc} and PCE

Table 1.6 Optoelectronic properties and device performances of P40–P48.

Polymer	E_g^{opt} (eV)	HOMO/ LUMO (eV)	Acceptor	V_{oc} (V)	J_{sc} (mA cm^{-2})	FF	PCE (%)	References
P40	1.37	−5.54/−3.84	$PC_{71}BM$	0.54	10.4	0.57	3.2	[57]
P41	1.39	−5.43/−3.87	$PC_{71}BM$	0.52	13.6	0.57	4.0	[57]
P42	1.37	−5.33/−3.86	$PC_{71}BM$	0.45	7.6	0.41	1.4	[57]
P43	1.12	−5.22/−3.78	$PC_{71}BM$	0.19	4.0	0.53	0.4	[57]
P44	1.09	−5.04/−3.82	$PC_{71}BM$	−−	−−	−−	−−	[57]
P45	1.39	−5.30/−3.72	$PC_{71}BM$	0.49	14.7	0.66	4.7	[57]
P46	1.39	−5.21/−3.72	$PC_{71}BM$	0.42	10.8	0.51	2.3	[57]
P47	1.23	−5.06/−3.77	$PC_{71}BM$	0.18	5.4	0.45	0.4	[57]
P48	1.60	−5.10/−3.50	$PC_{71}BM$	0.72	17.7	0.71	9.1	[58]

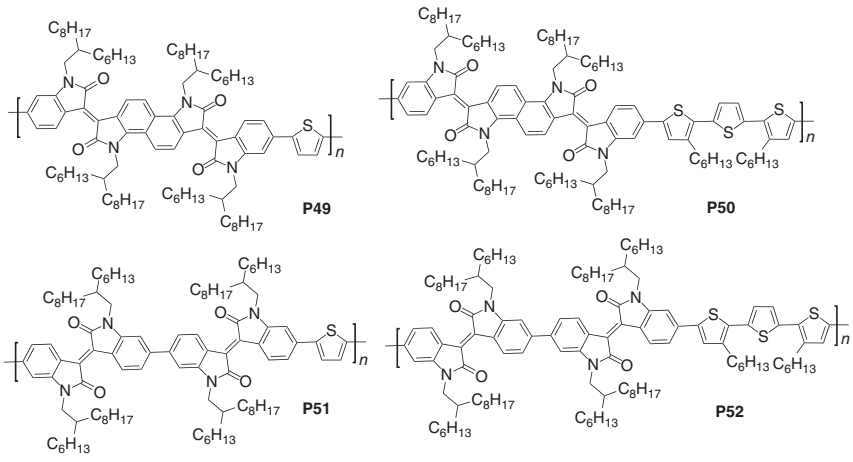

Figure 1.10 Chemical structures of the isoindigo-derived polymers P49–P52. Source: Xiyue Yuan.

Table 1.7 Optoelectronic properties and device performances of P49–P52.

Polymer	E_g^{opt} (eV)	HOMO/ LUMO (eV)	Acceptor	V_{oc} (V)	J_{sc} (mA cm^{-2})	FF	PCE (%)	References
P49	1.30	−5.83/−3.97	$PC_{71}BM$	0.80	0.8	0.54	0.3	[59]
P50	1.60	−5.90/−3.91	$PC_{71}BM$	0.86	4.2	0.50	1.8	[59]
P51	1.31	−5.67/−3.97	$PC_{71}BM$	0.66	2.4	0.58	0.9	[59]
P52	1.54	−5.68/−3.85	$PC_{71}BM$	0.77	5.9	0.61	2.8	[59]

values. The chemical structures of P49–P50 are showed in Figure 1.10, and the corresponding photovoltaic parameters of OSCs are summarized in Table 1.7.

1.2.3 LBG Polymers Based on Diketopyrrolopyrrole (DPP)

DPP (Figure 1.11) is a widely used electron-deficient building block for constructing LBG polymers with strong light absorption and high carrier mobility [60–64], which has two lactam rings with eight π-electrons. Generally, DPP polymers have E_gs lower than 1.50 eV with light absorption extended to 1000 nm. Figure 1.12 shows the chemical structures of a few DPP polymers (P53–P64) [28, 65–74], and the basic optoelectronic and photovoltaic properties of these polymers are summarized in Table 1.8. By changing electron-rich comonomers with different electron-donating ability, the E_g^{opt}s of the polymers can be finely tuned. Besides, the donor units have a profound influence on the morphology of donor:acceptor blends, thus affecting exciton dissociation and charge carrier transport [65]. In a set of DPP-based polymers with different donor units (P53–P55, P57, and P60), the polymers with poorer solubilities resulted in the formation of fibers with smaller widths (Figure 1.13), which

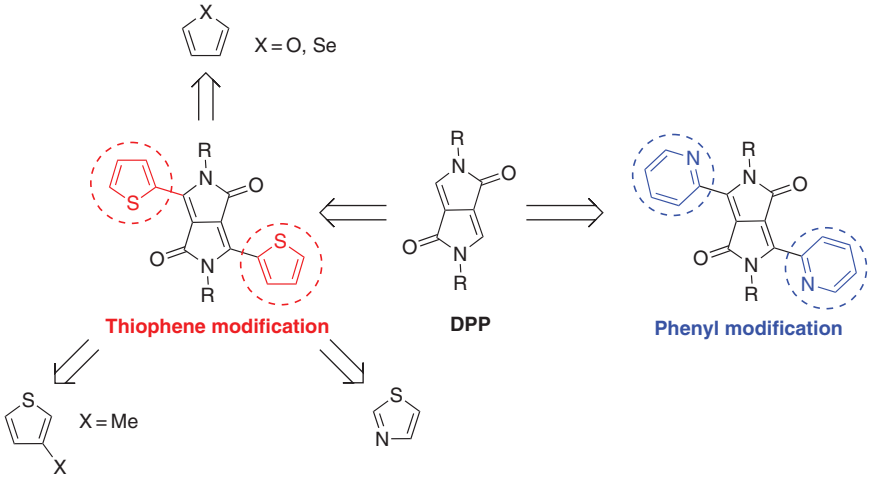

Figure 1.11 The chemical structure of DPP and its derived building blocks. Source: Xiyue Yuan.

thereby contributed to higher EQEs and PCEs in OSCs. The length of branched alkyl chains also had a critical influence on the device performance. For example, the PCE could be increased from 3.2% to 7.4% in blends of P65–P67 upon decreasing the length of the side chains [75]. This was caused by a progressive increase in the photocurrent due to the decreased phase separated domain size in the polymer:$PC_{71}BM$ blends (Figure 1.14).

Changing the flanking units is a general strategy to tune the properties of DPP polymers. A few representative DPP polymers with different flanking units are shown in Figure 1.15. Janssen and coworkers [65] reported a DPP polymer (P69) with two additional methyl substituents on the 3-position of the flanking thiophene rings to raise the LUMO energy level of the parent DPP polymer (P68) [18]. This small change led to improved EQEs (60% for P69 versus 50% for P68). To further improve the V_{oc} of DPP polymers, Janssen and coworkers [76] replaced the electron-rich thiophene (T) rings with electron-deficient thiazoles (Tz) and obtained the polymer P71. The polymer gave a very high V_{oc} of 0.96 V but a very low PCE of 1.1% when blended with $PC_{71}BM$. This was caused by the imbalanced electron–hole mobilities and reduced energetic driving force for exciton dissociation. Yang and coworkers [77] showed that the substitution of thiophene flanking units by furan and selenophene could lead to reduced E_g^{opt}s and enhanced hole mobilities (P72–P74). The polymer with the lowest E_g^{opt} (P74, E_g^{opt} = 1.38 eV) resulted in high-performance tandem and semi-transparent OSCs with PCEs of 9.5% and 4.5%, respectively. McCulloch and coworkers [78] reported a set of DPP-based polymers (P75–P77) with different chalcogenophene comonomers (thiophene, selenophene, and tellurophene) to study the effect of the heteroatom substitution on the optoelectronic and photovoltaic properties. Upon increasing the size of the chalcogen atom (S → Se → Te), the E_gs of the polymers were reduced due to the upshifting of the HOMO energy levels. When 2-pyridine was used as the flanking unit [79],

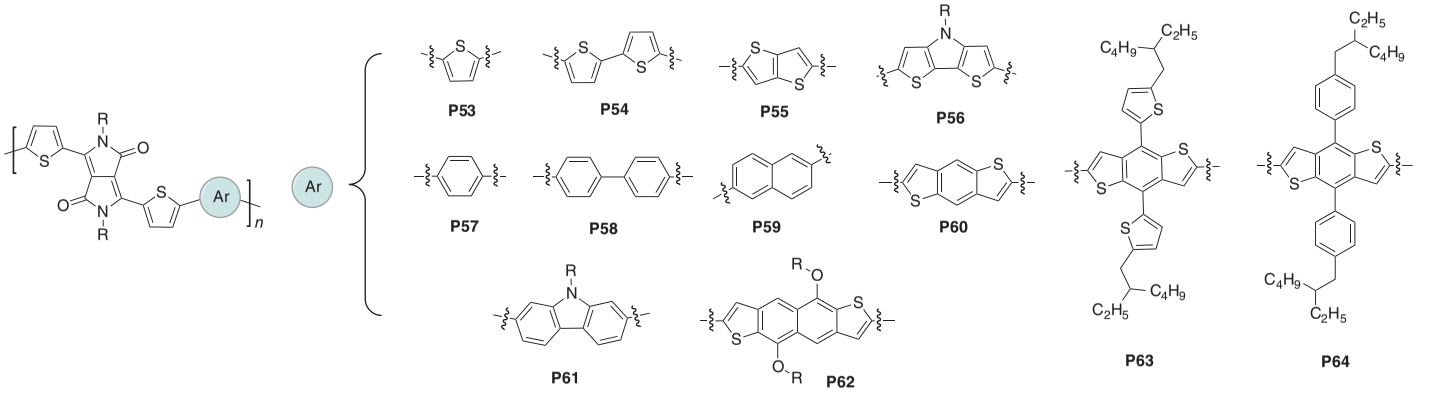

Figure 1.12 Chemical structures of the DPP polymers P53–P64. Source: Xiyue Yuan.

Table 1.8 Optoelectronic properties and device performances of P53–P67.

Polymer	E_g^{opt} (eV)	HOMO/ LUMO (eV)	Acceptor	V_{oc} (V)	J_{sc} (mA cm^{-2})	FF	PCE (%)	References
P53	1.33	−5.17/−3.61	$PC_{71}BM$	0.67	15.4	0.69	7.1	[28]
P54[a)]	1.43	−5.09/−3.64	$PC_{71}BM$	0.64	16.0	0.69	7.1	[65]
P55	1.35	−5.10/−3.68	$PC_{71}BM$	0.67	20.1	0.70	9.4	[66]
P56	1.23	−5.26/−3.68	$PC_{61}BM$	0.43	16.6	0.54	3.9	[67]
P57	1.53	−5.48/−3.66	$PC_{71}BM$	0.80	14.0	0.67	7.4	[28]
P58	1.63	−5.39/−3.59	$PC_{71}BM$	0.80	11.5	0.63	5.7	[68]
P59	1.55	−5.29/−3.79	$PC_{71}BM$	0.76	11.8	0.52	4.7	[69]
P60[a)]	1.51	−5.36/−3.81	$PC_{71}BM$	0.77	13.2	0.68	6.9	[65]
P61	1.57	−5.40/−3.90	$PC_{71}BM$	0.77	9.0	0.52	3.6	[71]
P62	1.36	−5.33/−3.74	$PC_{71}BM$	0.76	13.3	0.68	6.9	[72]
P63	1.44	−5.30/−3.63	$PC_{71}BM$	0.74	13.5	0.65	6.5	[73]
P64	1.46	−5.35/−3.56	$PC_{71}BM$	0.76	13.6	0.60	6.2	[74]
P65	1.52	−−/−−	$PC_{71}BM$	0.80	14.0	0.67	7.4	[75]
P66	1.52	−−/−−	$PC_{71}BM$	0.79	11.9	0.60	5.7	[75]
P67	1.52	−−/−−	$PC_{71}BM$	0.81	6.6	0.59	3.2	[75]

a) For P54 and P60, energy levels are determined from cyclic voltammetry $\left(E^{(Fc/Fc^+)} = -5.23\,eV\right)$.
Source: Based on Hendriks et al. [28].

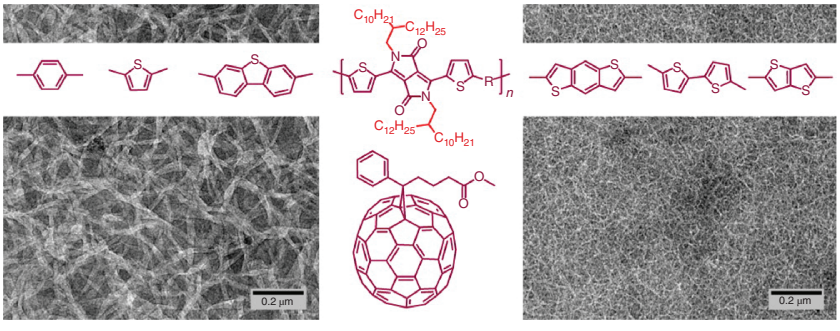

Figure 1.13 Bright field transmission electron microscopy (TEM) images ($1.2 \times 1.2\ \mu m^2$) of the polymer:$PC_{71}BM$ blend films based on several DPP polymers. Source: Li et al. [65] with permission of American Chemical Society.

good coplanarity in the resulting polymer (P78) could be guaranteed. The sp^2 hybridization nitrogen of pyridine also downshifted the HOMO energy level of the polymer and thereby led to high V_{oc} in resulting OSCs. The chemical structures of P68–P78 are showed in Figure 1.15, and the corresponding photovoltaic parameters of OSCs are summarized in Table 1.9.

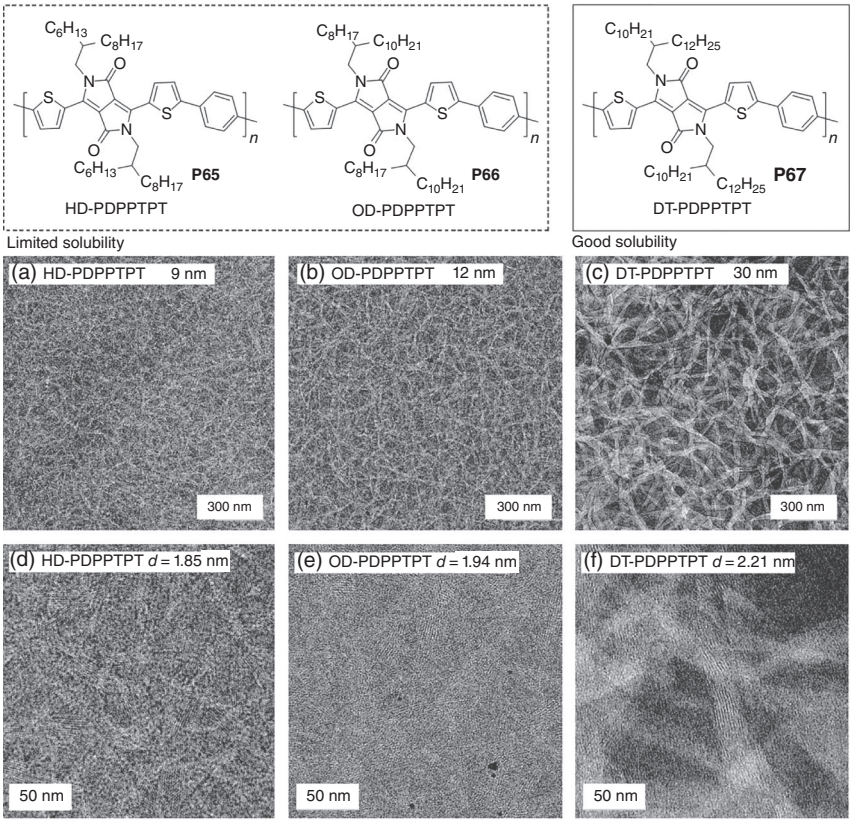

Figure 1.14 Bright field TEM images of the P65-P67:$PC_{71}BM$ blends for different length of the side chains. (a,b,c) Image size: $1.2 \times 1.2\ \mu m^2$. (d,e,f) Image size: $225 \times 225\ nm^2$. Source: Li et al. [65] with permission of John Wiley & Sons, Inc.

Besides, Janssen and coworkers reported a set of regular alternating D1-A-D2-A terpolymers and demonstrated its superior performance in fullerene-based OSCs compared to the parent D–A copolymers (Figure 1.16). Compared to the polymer with random alternation of D1 and D2 with A, the D1-A-D2-A regular polymer allows exact chemical composition [28, 82] and controlled local variations in HOMO/LUMO energy levels. Among these polymers, the polymer containing a terthiophene and a thiophene–phenylene–thiophene (TPT) donor segment (P79) showed optimal energy levels and optical bandgap as compared to the parent copolymers. As a result, this polymer afforded a high PCE of 8.0% when blended with $PC_{71}BM$. The chemical structures of P79–P81 are showed in Figure 1.16, and the corresponding photovoltaic parameters of OSCs are summarized in Table 1.10.

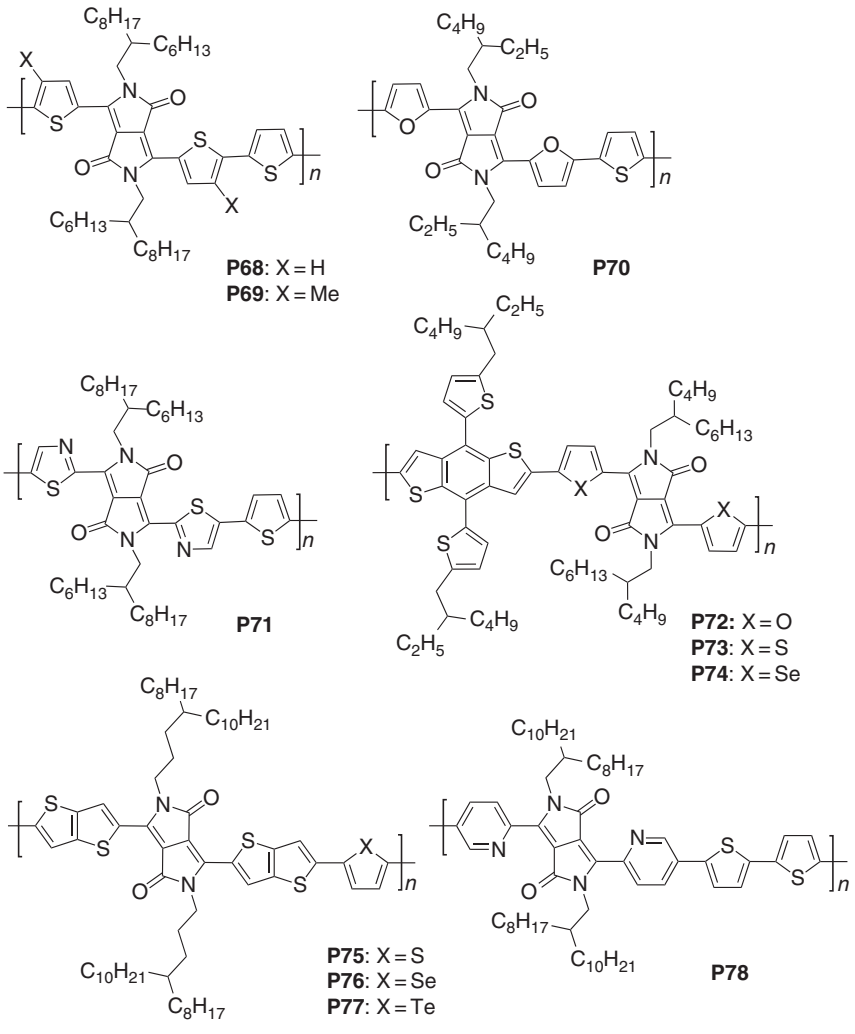

Figure 1.15 Chemical structures of the DPP polymers P68–P78. Source: Xiyue Yuan.

1.3 MBG Polymers

As discussed in the previous section, in the early stage of PSCs using fullerene derivatives as the electron acceptors, extensively researches on the development of conjugated donor polymers have been focused on design and synthesis of LBG polymers to extend the light absorption range over 800 nm and thereby improve the J_{sc} of resulted PSCs [10]. Nevertheless, LBG polymers with reduced E_g^{opt} generally had a

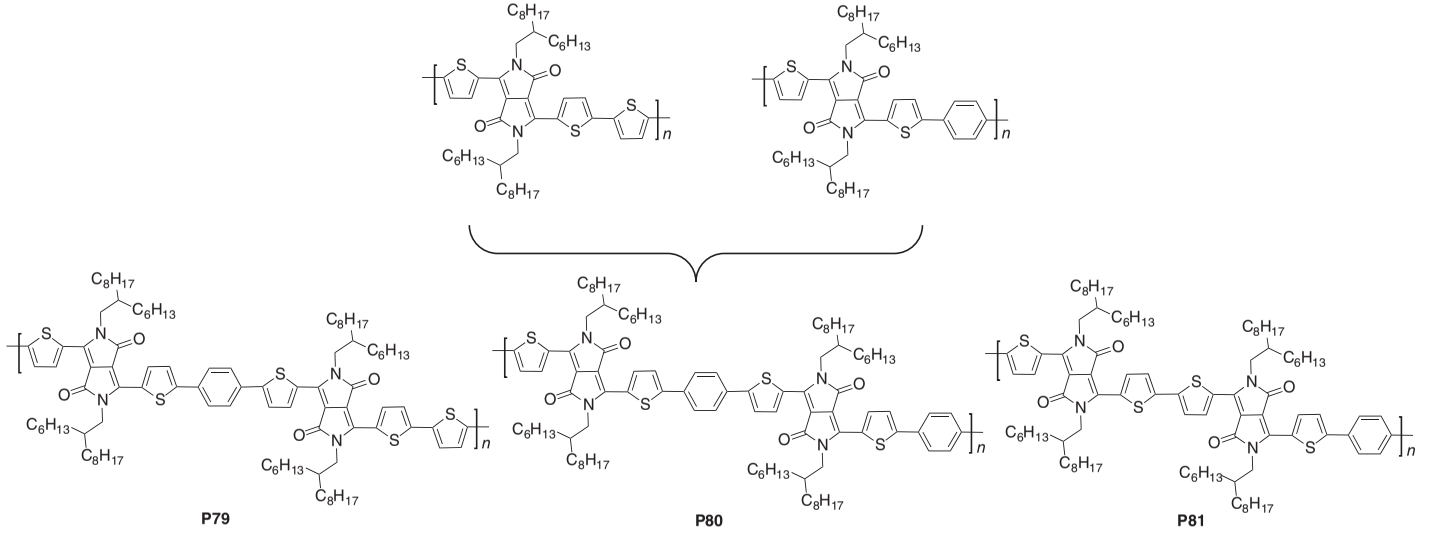

Figure 1.16 Chemical structures of the DPP polymers P79–P81. Source: Xiyue Yuan.

Table 1.9 Optoelectronic properties and device performances of P68–P78.

Polymer	E_g^{opt} (eV)	HOMO/LUMO (eV)	Acceptor	V_{oc} (V)	J_{sc} (mA cm^{-2})	FF	PCE (%)	References
P68	1.33	−5.17/−3.61	$PC_{71}BM$	0.67	15.4	0.69	7.1	[80]
P69[a)]	1.30	−5.43/−3.68	$PC_{71}BM$	0.60	17.8	0.66	7.0	[65]
P70	1.40	−5.20/−−	$PC_{71}BM$	0.65	14.8	0.64	6.5	[81]
P71[a)]	1.44	−5.97/−4.07	$PC_{71}BM$	0.96	2.0	0.58	1.1	[76]
P72	1.51	−5.26/−3.64	$PC_{71}BM$	0.77	10.9	0.56	4.7	[77]
P73	1.46	−5.30/−3.63	$PC_{71}BM$	0.73	13.7	0.65	6.5	[77]
P74	1.38	−5.25/−3.70	$PC_{71}BM$	0.69	16.8	0.62	7.2	[77]
P75	1.39	−5.08/−3.69	$PC_{71}BM$	0.57	13.5	0.66	8.8	[78]
P76	1.37	−5.07/−3.70	$PC_{71}BM$	0.56	21.5	0.63	7.6	[78]
P77	1.32	−5.05/−3.73	$PC_{71}BM$	0.52	21.7	0.63	7.1	[78]
P78	1.68	−5.77/−3.86	$PC_{71}BM$	0.92	8.0	0.66	4.9	[79]

a) For P69 and P71, energy levels determined from cyclic voltammetry $\left(E^{(Fc/Fc^+)} = -5.23\ eV\right)$.
Source: Based on Hendriks et al. [28].

Table 1.10 Optoelectronic properties and device performances of P79–P81.

Polymer	E_g^{opt} (eV)	HOMO/LUMO (eV)	Acceptor	V_{oc} (V)	J_{sc} (mA cm^{-2})	FF	PCE (%)	References
P79	1.47	−−/3.73	$PC_{71}BM$	0.75	15.9	0.67	8.0	[28]
P80	1.57	−5.79/−3.79	$PC_{71}BM$	0.80	13.8	0.67	7.5	[82]
P81	1.42	−5.69/−3.86	$PC_{71}BM$	0.74	6.4	0.67	3.2	[82]

high-lying HOMO energy level, which resulted in a limited V_{oc} and a large E_{loss} [9]. LBG polymers also intrinsically displayed narrow absorption range, which made them could hardly realize an ideal broad photon absorption to make full use of the solar spectrum [10]. In these regards, making a trade-off wisely between the J_{sc} and V_{oc} is quite essential to improve the performance of PSCs. Despite the limited light absorption (< 780 nm) of MBG polymers, the strategy of molecular design and morphology control could enable to improve exciton generation and charge transport for achieving high J_{sc}s that were comparable to LBG polymers. Importantly, MBG polymers could have more potential to deepen the HOMO level without increasing the bandgap, which afforded higher V_{oc} without sacrificing J_{sc} in the resulted PSCs [9, 10]. In addition, the MBG polymers have also played an important role to harvest high-energy photons in ternary and tandem devices. The pair of "weak donor" and "strong acceptor" is an effective way to construct an MBG polymer. Several typical strong acceptor blocks including BT, quinoxaline (Qx), thienopyrrolodione (TPD),

and functionalized thieno[3,4-*b*]thiophene (TT) derivatives have been widely used to build MBG polymers. In the following part, we will introduce the design strategies of MBG polymers based on the above acceptor blocks and analyze their photovoltaic properties.

1.3.1 MBG Polymers Based on Benzothiadiazole (BT)

As aforementioned, BT is a widely used "strong acceptor" unit not only in LBG polymers but also in MBG polymers. On the other hand, benzo[1,2-*b*:4,5-*b*′]dithiohpene (BDT) is an ideal "weak donor" block for building MBG polymers. Both BT and BDT have high chemical stability, rigid planar structure, and ease of preparation. BDT–BT-based polymers (Figure 1.17) have shown promising PCEs over 10%, implying the combination of BDT and BT is one of the ideal pairs for high-performance PSCs [83, 84]. What's more, the optical, electrical, and morphological properties of the resulted polymers can be feasibly modulated by introducing various side chains of BDT and functional groups on BDT as well as π-bridges between BDT and BT, which enable the optimization of the final photovoltaic performances (Figure 1.17) [85]. In 2008, Hou et al. reported P82 ($E_g^{opt} = 1.70$ eV) based on the BT acceptor block and alkoxy-substituted BDT donor block, which produced a poor PCE of 0.90% [86]. By replacing the one-dimensional (1D) alkoxy side chains with two-dimensional (2D) alkylthienyl groups on the BDT block, the resulting polymer P83 exhibited lowered HOMO level (−5.45 versus − 5.10 eV) and extended light absorption than P82, which improved the V_{oc} from 0.68 V of P82 to 0.92 V of P83 and PCE up to 9.4% [87]. Yang and coworkers introduced thiophene units as the bridges between BDT and BT, which extended the conjugation length and developed P84 [88]. Peng et al. introduced alkoxy and fluorine atom, respectively, onto the BT block and developed P85 and P86 [89]. The fluorination effectively lowered the HOMO level of P86 (−5.41 eV), improving the V_{oc} (0.86 V) and PCE (6.21%).

Note that quite a few researches focused on the side chain modification of BDT units, including unsubstituted (P87) [90], alkyl (P88–P90) [91], alkylthienyl (P83–P86, P91) [84, 87–89], fluorinated alkylthienyl (P92, P93), chlorinated alkylthienyl (P94), alkylthiothienyl (P92) side chains, etc. Peng and coworkers combined fluorination and sulfuration on the alkylthienyl side chains and developed P96, which improved the absorption and lowered the HOMO level compared to the fluorinated polymer of P92 and sulfurated polymer of P95 [84]. The resulted devices achieved a much higher PCE of 10.69% in fullerene PSCs and 11.66%

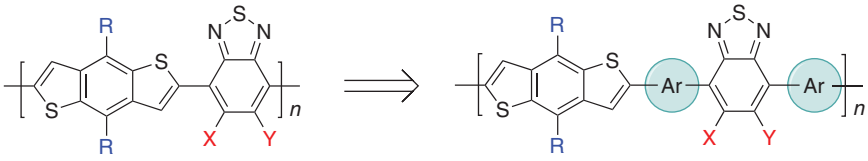

Figure 1.17 The chemical modification strategy of BDT-BT-based polymers. Source: Xiaopeng Xu.

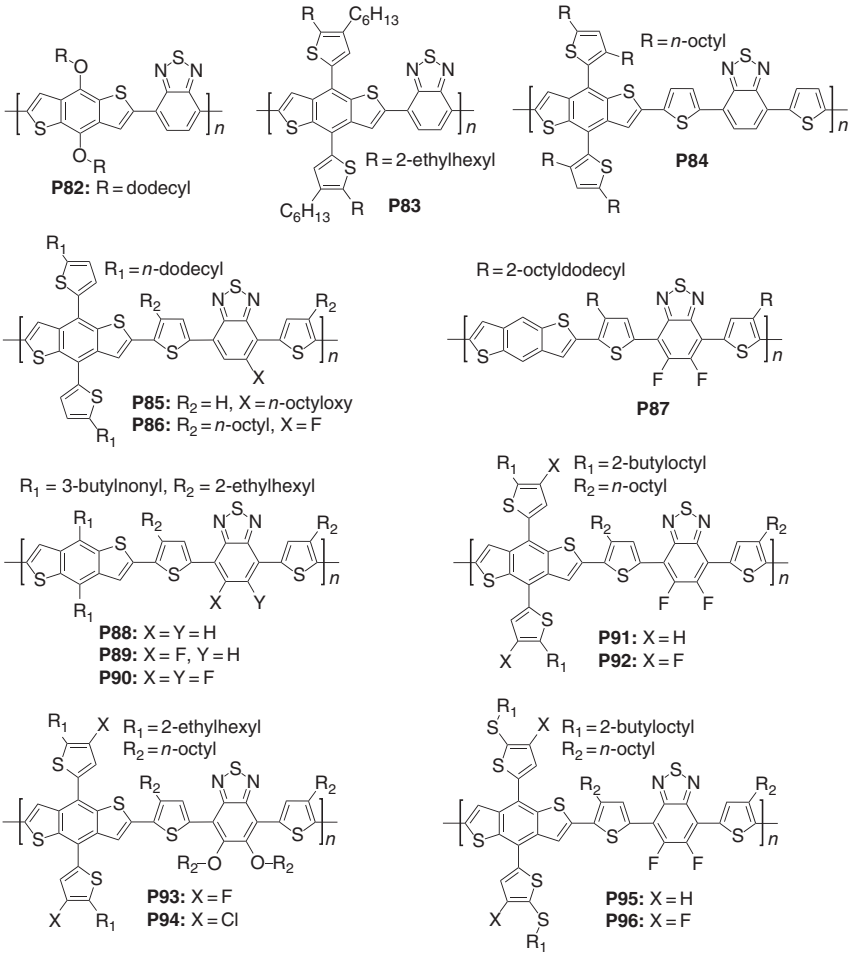

Figure 1.18 Chemical structures of the BT-derived copolymers P82–P96. Source: Xiaopeng Xu.

in non-fullerene PSCs. The chemical structures of P82–P96 are presented in Figure 1.18. The corresponding optoelectronic properties and device performances are listed in Table 1.11.

Compared to the thiophene unit, the benzene ring is featured with symmetry and lower electron-donating ability [93]. Using benzene ring as the side group, the overall properties of the resulted polymers would be modulated. Hou and coworkers [94] attached alkylphenyl groups onto BDT block and developed P97, which exhibited an E_g^{opt} of 1.70 eV and deep HOMO of −5.35 eV. The resulting devices produced a high V_{oc} of 0.88 V and a PCE of 8.07%. Sulfur and oxygen atoms could be inserted into the alkylphenyl group to modulate the energy levels and intermolecular interactions (P98–P101) [95, 96]. Furthermore, the alkoxyphenyl side chains could be further modified by introducing fluorine atom at the meta-position [96–98], ortho-position

Table 1.11 Optoelectronic properties and device performances of P82–P96.

Polymer	E_g^{opt} (eV)	HOMO/ LUMO (eV)	Acceptor	V_{oc} (V)	J_{sc} (mA cm^{-2})	FF	PCE (%)	References
P82	1.70	−5.10/−3.19	$PC_{61}BM$	0.68	2.97	0.44	0.90	[86]
P83	1.65	−5.45/−3.65	$PC_{71}BM$	0.92	15.4	0.66	9.4	[87]
P84	1.75	−5.31/−3.44	$PC_{71}BM$	0.92	10.70	0.575	5.66	[88]
P85	1.67	−5.32/−3.58	$PC_{71}BM$	0.82	12.53	0.549	5.64	[89]
P86	1.63	−5.41/−3.72	$PC_{71}BM$	0.86	12.05	0.599	6.21	[89]
P87	1.73	−5.40/−3.67	$PC_{71}BM$	0.85	14.56	0.751	9.29	[90]
P88	1.65	−5.42/−−	$PC_{61}BM$	0.78	11.7	0.476	4.33	[91]
P89	1.67	−5.48/−−	$PC_{61}BM$	0.85	11.4	0.506	5.28	[91]
P90	1.73	−5.53/−−	$PC_{61}BM$	0.90	12.2	0.621	7.16	[91]
P91	1.69	−5.14/−3.35	$PC_{71}BM$	0.79	15.41	0.682	8.31	[84]
P91	1.69	−5.14/−3.35	ITIC	0.82	13.73	0.638	7.15	[84]
P92	1.71	−5.34/−3.53	$PC_{71}BM$	0.86	16.47	0.687	9.74	[84]
P92	1.71	−5.34/−3.53	ITIC	0.90	15.38	0.663	9.17	[84]
P93	1.77	−5.39/−3.65	IT-4F	0.778	21.73	0.545	9.14	[92]
P94	1.78	−5.51/−3.60	IT-4F	0.782	21.03	0.70	11.60	[92]
P95	1.70	−5.20/−3.40	$PC_{71}BM$	0.84	16.28	0.683	9.33	[84]
P95	1.70	−5.20/−3.40	ITIC	0.89	14.63	0.659	8.58	[84]
P96	1.71	−5.41/−3.59	$PC_{71}BM$	0.92	16.60	0.70	10.69	[84]
P96	1.71	−5.41/−3.59	ITIC	1.03	17.09	0.663	11.66	[84]

[98] or more than one fluorine atom in each alkoxyphenyl side chain (P102–P104) [96]. Shin et al. [96, 98] found that introducing one fluorine at the ortho-position or two fluorine atoms onto each alkoxyphenyl side chain would enlarged the E_g^{opt} to more than 1.8 eV due to the large steric hindrance at ortho-position and high electron-withdrawing effect of fluorine atom. In contrast, introducing fluorine atom onto the ortho-position of alkoxyphenyl side chain did not induce any steric hindrance but lowered the HOMO level of the resulting polymers (P103, P104) [96, 98]. The π-conjugated side chains efficiently increased the electron density and interchain aggregation among conjugated polymers, thereby enhancing light absorption and charge transport properties of the related PSCs. Cho and coworkers [99] employed oligothienyl side chains to further extend the 2D conjugation lengths of conjugated copolymer systems and developed a series MBG polymers (P105–P107). With the thiophene numbers increasing, the E_g^{opt} was reduced, and the HOMO level was lowered. P106 with the optimum size of the chromophoric side chains exhibited an extended absorption spectrum and high carrier transport, leading to the highest PCE of 6.5%. Yang and coworkers [100] replaced the alkylthienyl side chains on BDT with the extended alkylbenzothienyl side chains and developed P108. Fusing benzene on the flanking thiophene ring of BDT side chains

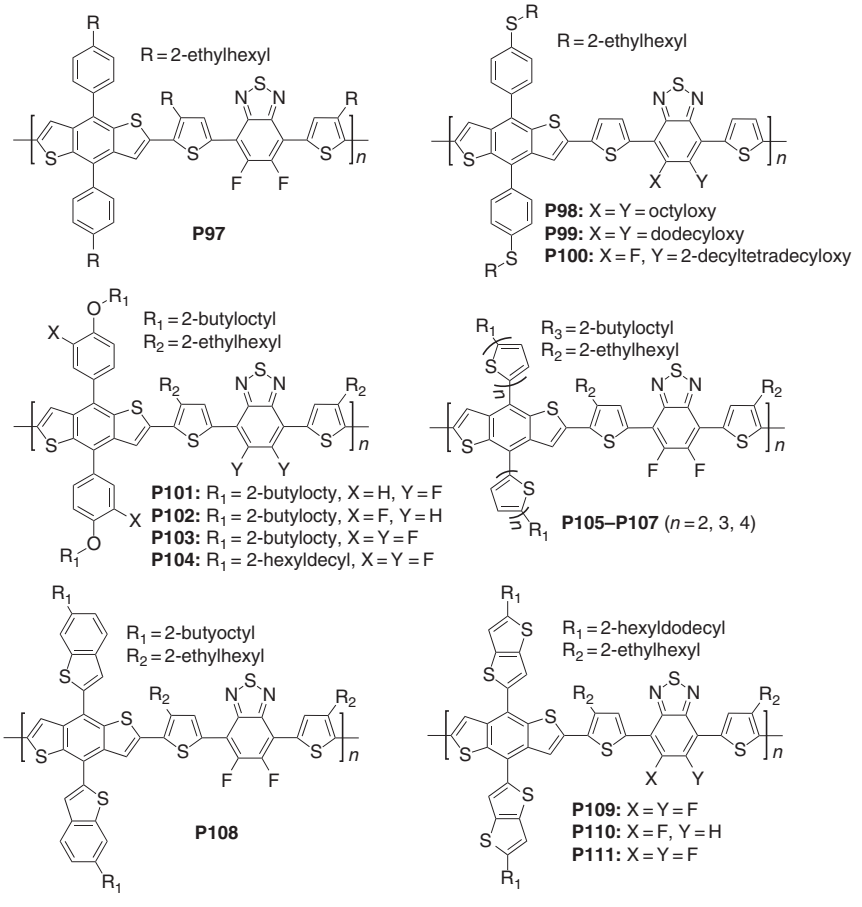

Figure 1.19 Chemical structures of the BT-derived copolymers P97–P111. Source: Xiaopeng Xu.

slightly red-shifted the absorption bands, obviously enhanced the intermolecular interactions, and pronouncedly downshifted the HOMO and LUMO energy levels of P110, which improved the PCE to 7.30%. Yang and coworkers [101] used alkyl-substituted thieno[3,2-*b*]thiophene as the extended side chains and developed P109–P111. Devices based on the three polymers maintained ~90% of the initial efficiency after annealing for 30 days at 100 °C, showing their long-term stability. The chemical structures of P97–P111 are presented in Figure 1.19. The corresponding optoelectronic properties and device performances are listed in Table 1.12.

Most of the BDT-based polymers are based on the symmetric 1D BDT and 2D BDT units. To combine the two kinds of BDTs, Yang and coworkers proposed a symmetry-breaking strategy to combine the advantages of both 1D and 2D symmetric BDT building blocks and constructed a series of high-performance donor polymers (P112–P119) [102, 103]. The asymmetric BDT blocks efficiently triggered a modulation of the preferential ordered microstructure, formed the

Table 1.12 Optoelectronic properties and device performances of P97–P111.

Polymer	E_g^{opt} (eV)	HOMO/ LUMO (eV)	Acceptor	V_{oc} (V)	J_{sc} (mA cm^{-2})	FF	PCE (%)	References
P97	1.70	−5.35/−3.34	$PC_{71}BM$	0.88	12.94	0.709	8.07	[94]
P98	1.79	−5.42/−3.63	$PC_{71}BM$	0.74	11.60	0.63	5.4	[95]
P99	1.78	−5.41/−3.63	$PC_{71}BM$	0.76	11.26	0.72	6.1	[95]
P100	1.76	−5.60/−3.84	$PC_{71}BM$	0.82	12.28	0.73	7.4	[95]
P101	1.70	−5.12/−3.42	$PC_{71}BM$	0.83	11.33	0.663	6.23	[93]
P102	1.73	−5.42/−3.69	$PC_{71}BM$	0.83	12.23	0.618	6.28	[96]
P102	1.73	−5.39/−3.66	$PC_{71}BM$	0.83	13.11	0.653	7.02	[97]
P103	1.77	−5.56/−3.79	$PC_{71}BM$	0.91	11.25	0.646	6.62	[98]
P104	1.76	−5.58/−3.77	$PC_{71}BM$	0.90	13.18	0.644	7.64	[96]
P105	1.73	−5.37/−3.61	$PC_{71}BM$	0.90	10.6	0.547	5.22	[99]
P106	1.70	−5.31/−3.62	$PC_{71}BM$	0.86	12.3	0.614	6.48	[99]
P107	1.68	−5.30/−3.63	$PC_{71}BM$	0.84	6.35	0.405	2.17	[99]
P108	1.76	−5.36/−3.60	$PC_{61}BM$	0.90	12.93	0.627	7.30	[100]
P109	1.71	−5.29/−−	$PC_{71}BM$	0.74	11.76	0.655	5.70	[101]
P110	1.69	−5.39/−−	$PC_{71}BM$	0.80	11.95	0.662	6.29	[101]
P111	1.75	−5.48/−−	$PC_{71}BM$	0.86	11.71	0.653	6.54	[101]

Table 1.13 Optoelectronic properties and device performances of P112–P119.

Polymer	E_g^{opt} (eV)	HOMO/ LUMO (eV)	Acceptor	V_{oc} (V)	J_{sc} (mA cm^{-2})	FF	PCE (%)	References
P112	1.73	−5.03/−3.30	$PC_{71}BM$	0.83	13.92	0.665	7.68	[102]
P113	1.72	−5.01/−3.29	$PC_{71}BM$	0.84	13.64	0.717	8.22	[102]
P114	1.76	−5.06/−3.29	$PC_{71}BM$	0.88	14.92	0.719	9.44	[102]
P115	1.75	−5.03/−3.28	$PC_{71}BM$	0.88	13.98	0.739	9.09	[102]
P116	1.76	−5.35/−3.59	$PC_{71}BM$	0.892	15.17	0.755	10.22	[103]
P117	1.75	−5.33/−3.58	$PC_{71}BM$	0.884	14.86	0.750	9.84	[103]
P118	1.75	−5.32/−3.57	$PC_{71}BM$	0.876	14.98	0.709	9.30	[103]
P119	1.74	−5.32/−3.58	$PC_{71}BM$	0.868	14.05	0.703	8.57	[103]

intense molecular stacking, and shortened the π–π stacking distance to enhance π–π overlap from the extended conjugated aryl units, which was beneficial for charge transport. Based on such strategy, a high PCE reaching 10.22% was realized when using $PC_{71}BM$ as the acceptor in PSCs. The chemical structures of P112–P119 are presented in Figure 1.20. The corresponding optoelectronic properties and device performances are listed in Table 1.13.

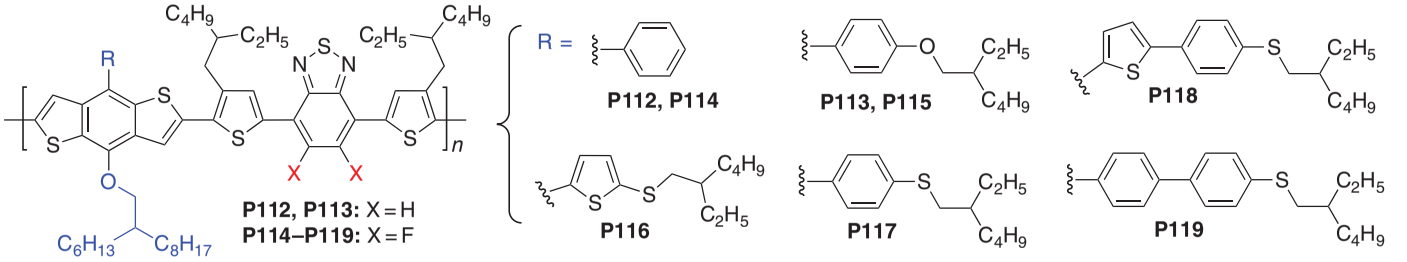

Figure 1.20 Chemical structures of the BT-derived copolymers P112–P119. Source: Xiaopeng Xu.

Modulation of the π-spacers between BDT and BT have also shown great potential in developing efficient MBG polymers. Introducing a bulky bridge between the BDT and BT blocks, such as a hexylthiophene-substituted thiophene bridge (P120), could introduce large steric hindrance into the polymer backbone, which had less effect on the E_g^{opt}, but effectively lowered the HOMO, thereby increasing the V_{oc} of the resulted PSCs [104]. Replacing thiophene with furan as the π-spacers between BDT and BT blocks could enlarge the E_g^{opt} and lower the HOMO of the resulting polymers (P121, P122) [105], while replacing thiophene with selenophene as the π-spacers could reduce the E_g^{opt} and increase the HOMO of the resulting polymers (P123, P124) [106]. Moreover, the BDT block could also be modulated by replacing the sulfur atoms with oxygen atoms. The thieno[2,3-*f*]benzofuran and benzo[1,2-*b*:4,5-*b*′]difuran-derived polymers exhibited reduced E_g^{opt}s and increased HOMOs (P125–P128). The chemical structures of P120–P128 are presented in Figure 1.21. The corresponding optoelectronic properties and device performances are listed in Table 1.14.

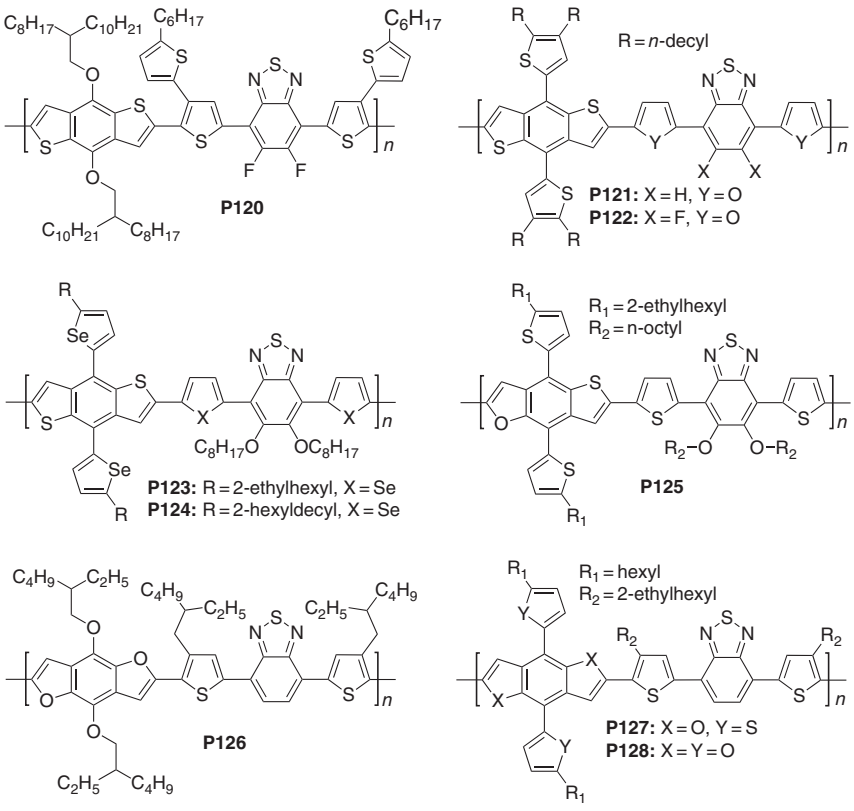

Figure 1.21 Chemical structures of the BT-derived copolymers P120–P128. Source: Xiaopeng Xu.

Table 1.14 Optoelectronic properties and device performances of P120–P128.

Polymer	E_g^{opt} (eV)	HOMO/ LUMO (eV)	Acceptor	V_{oc} (V)	J_{sc} (mA cm^{-2})	FF	PCE (%)	References
P120	1.70	−5.47/−3.74	$PC_{71}BM$	0.80	12.56	0.604	6.19	[104]
P121	1.76	−5.36/−3.59	$PC_{71}BM$	0.86	7.9	0.55	3.7	[105]
P122	1.78	−5.28/−3.60	$PC_{71}BM$	0.86	8.7	0.59	4.4	[105]
P123	1.69	−5.26/−3.57	$PC_{71}BM$	0.70	12.28	0.589	5.07	[106]
P124	1.63	−5.40/−3.77	$PC_{71}BM$	0.73	12.22	0.594	5.34	[106]
P125	1.63	−5.20/−3.57	$PC_{71}BM$	0.78	13.51	0.61	6.42	[107]
P126	1.60	−5.10/−3.24	$PC_{71}BM$	0.78	11.77	0.546	5.01	[108]
P127	1.68	−5.08/−3.39	$PC_{71}BM$	0.73	9.94	0.609	4.42	[109]
P128	1.61	−5.11/−3.60	$PC_{71}BM$	0.80	5.84	0.556	2.60	[109]

In addition, there also had many other BT-based polymers using various donor blocks. For example, Ashraf et al. employed indacenodithiophene (IDT) and it derivatives silaindacenodithiophene (SiIDT) and germaindacenodithiophene (GeIDT) as the donor blocks and developed P129–P131 [110, 111]. These polymers exhibited an MBG around 1.7 ∼ 1.8 eV, a low HOMO around −5.2 ∼ −5.3 eV. Jen and coworkers reported the IDTT-based ladder-type polymer of P132, which exhibited a medium E_g^{opt} of 1.78 eV and a high hole mobility of 2×10^{-2} cm^2 V^{-1} s^{-1} [112]. The resulting PSCs realized a high PCE of 7.03%. Yan and coworkers developed the terthiophene-based D–A polymer of P133 with an asymmetric arrangement of alkyl chains [113]. The asymmetric arrangement of alkyl chains enabled highly efficient thick-film PSCs with PCE up to 10.7% without the need of processing additives. Woo and coworkers introduced dialkoxylphenylene as the donor block and developed a series of semi-crystalline photovoltaic polymers (P134–P136) [114]. The noncovalent intramolecular interactions (N···S, N···H, O···S, O···H, F···S, F···H) served as conformational lock to enhance chain planarity, intermolecular ordering, and thermal stability without losing solution processability. The polymers formed well-distributed interpenetrating nano-fibrillar-networked morphologies with $PC_{71}BM$, showing well-balanced hole and electron mobilities. P136 exhibited a high PCE up to 9.39% in a 290-nm thick conventional single-cell device structure without any additional interfacial layer. Using P136 in the all-PSCs, a high PCE of 5.10% was realized [115]. Ding and coworkers introduced different lactam-containing tricyclic blocks and developed a series of BT-based polymers (P137–P139), which had medium E_g^{opt}s around 1.65 ∼ 1.72 eV [116, 117]. Among them, the P138 displayed less bimolecular recombination and balanced charge transport in the active layer, P138:$PC_{71}BM$ solar cells gave a PCE of 10.16% with an active layer thickness of 267 nm. He and coworkers developed P141, in which a chlorine atom was introduced at the 4-position in the middle thiophene unit [118].

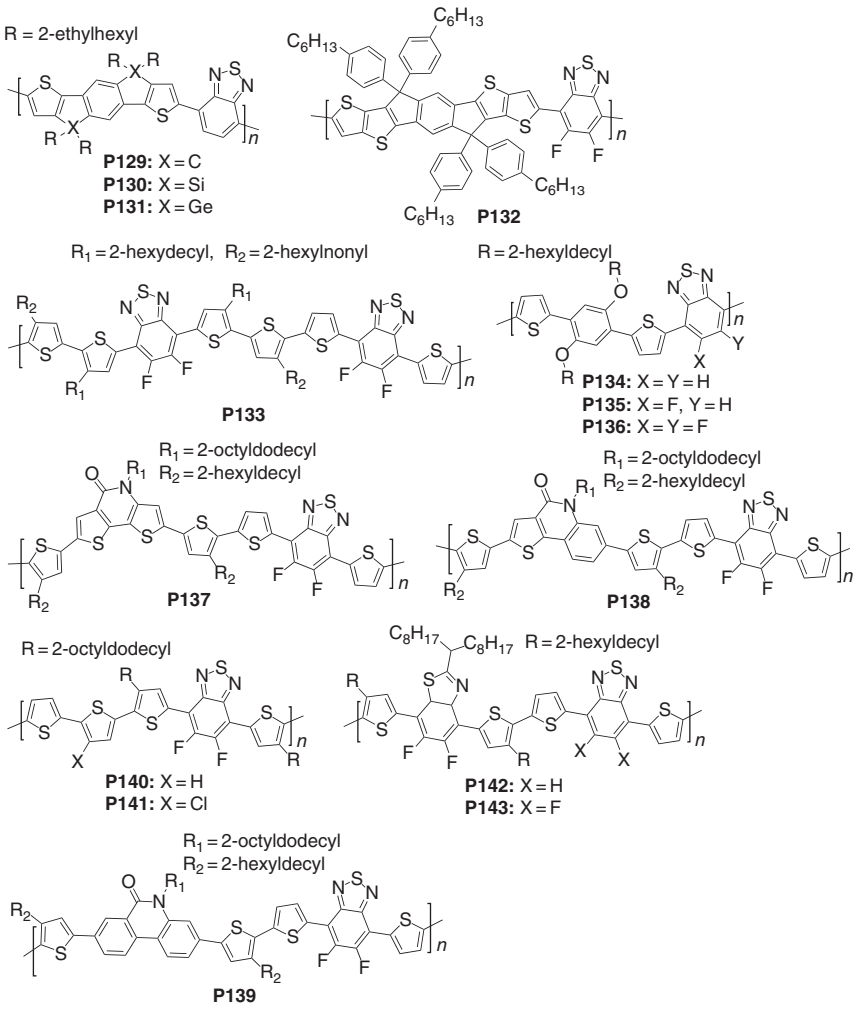

Figure 1.22 Chemical structures of the BT-derived copolymers P129–P143. Source: Xiaopeng Xu.

Compared to the non-chlorinated P140, the chlorination lowered the HOMO level of P60 (−5.33 versus −5.19 eV) and enhanced the intermolecular π–π interactions in the active layer film. The PSCs based on P141:$PC_{71}BM$ exhibited enhancements both in V_{oc} and FF, resulting in further improvement of PCE from 10.17% of P140:$PC_{71}BM$ to 11.18%. Feng et al. introduced the weak electron-withdrawing 5,6-difluorobenzo[*d*]thiazole (BTA-2f) and developed two new BT-based MBG polymers (P142, P143) [119]. P143 with difluorinated BT exhibited lowered HOMO level, enhanced ICT, and improved crystallinity. The PCE of resulting fullerene-free PSCs using Y6 as the acceptor was significantly improved from 2.61% (P142) to 16.08% (P143). The chemical structures of P129–P143 are presented in Figure 1.22. The corresponding optoelectronic properties and device performances are listed in Table 1.15.

Table 1.15 Optoelectronic properties and device performances of P129–P143.

Polymer	E_g^{opt} (eV)	HOMO/ LUMO (eV)	Acceptor	V_{oc} (V)	J_{sc} (mA cm^{-2})	FF	PCE (%)	References
P129	1.7	−5.3/−3.6	$PC_{71}BM$	0.80	14.48	0.56	6.5	[110]
P130	1.8	−5.3/−3.5	$PC_{71}BM$	0.91	12.18	0.52	5.8	[110]
P131	1.7	−5.2/−3.4	$PC_{71}BM$	0.85	13.95	0.55	6.5	[110]
P131	1.74	−−/−−	$PC_{71}BM$	0.86	10.1	0.58	5.02	[111]
P132	1.78	−5.30/−3.50	$PC_{71}BM$	0.95	12.21	0.61	7.03	[112]
P133	1.63	−5.31/−3.68	$PC_{71}BM$	0.82	18.7	0.683	10.5	[113]
P134	1.72	−5.29/−3.57	$PC_{71}BM$	0.81	10.4	0.61	5.08	[114]
P135	1.72	−5.35/−3.63	$PC_{71}BM$	0.81	10.2	0.62	5.11	[114]
P136	1.76	−5.45/−3.69	$PC_{71}BM$	0.86	11.4	0.74	7.26	[114]
P136	1.76	−5.45/−3.69	P(NDI2OD-T2)	0.85	11.9	0.51	5.03	[115]
P137	1.62	−5.26/−3.21	$PC_{71}BM$	0.82	15.35	0.696	8.75	[116]
P137	1.62	−5.26/−3.21	ITIC	0.90	14.18	0.593	7.58	[116]
P137	1.65	−5.44/−3.05	$PC_{71}BM$	0.84	14.64	0.703	8.61	[117]
P138	1.67	−5.41/−3.01	$PC_{71}BM$	0.82	17.27	0.721	10.16	[117]
P139	1.72	−5.48/−2.99	$PC_{71}BM$	0.89	13.60	0.699	8.47	[117]
P140	1.65	−5.19/−3.53	$PC_{71}BM$	0.75	19.23	0.705	10.17	[118]
P141	1.67	−5.33/−3.64	$PC_{71}BM$	0.80	18.71	0.746	11.18	[118]
P142	1.69	−5.45/−3.76	Y6	0.90	10.07	0.289	2.61	[119]
P143	1.73	−5.55/−3.82	Y6	0.81	27.25	0.727	16.08	[119]

1.3.2 MBG Polymers Based on Quinoxaline (Qx)

The quinoxaline (Qx) skeleton is a simple but effective system in organic photovoltaics and has been extensively studied as a strong electron deficient unit for building high-performance MBG copolymers [120, 121]. The Qx can be modified by introducing side chains on the 1,2- or 5,6-positions, introducing halogen atoms on the 5,6-positions and fusing aromatic rings to extend Qx core (Figure 1.23). BDT-Qx-based polymers are quite representative in this filed. The side chains on both BDT and Qx can be easily modified by introducing alkoxy, alkylthienyl, or alkoxyphenyl groups (P144–P151) [122–124]. In addition, the side chains of Qx block can be further modified by introducing fluorine atoms (P152–P154) [125–127]. For example, Zou and coworkers introduced the monofluorinated and difluorinated alkoxyphenyl groups, respectively, on the 1,2-positions of Qx as the side chains and developed P153 and P154 [126, 127]. P154 with difluorinated alkoxyphenyl groups exhibited blue-shifted absorption (E_g^{opt}, 1.76 versus 1.73 eV), lower HOMO level (−5.45 versus −5.36 eV) than those of P153 with monofluorinated alkoxyphenyl groups. Using ITIC as the acceptor in fullerene-free solar

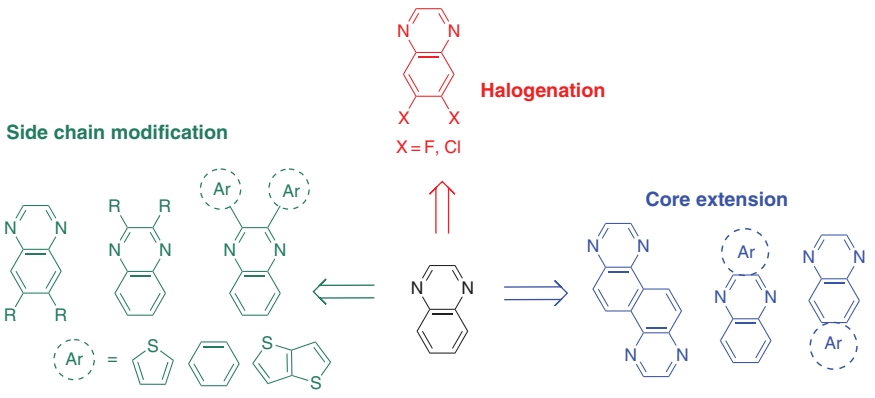

Figure 1.23 The chemical structure of quinoxaline and the structural modification based on quinoxaline. Source: Xiaopeng Xu.

Table 1.16 Optoelectronic properties and device performances of P144–P154.

Polymer	E_g^{opt} (eV)	HOMO/ LUMO (eV)	Acceptor	V_{oc} (V)	J_{sc} (mA cm^{-2})	FF	PCE (%)	References
P144	1.68	−4.79/−2.27	$PC_{71}BM$	0.78	13.2	0.708	7.29	[122]
P145	1.72	−4.83/−2.22	$PC_{71}BM$	0.88	11.4	0.759	7.61	[122]
P146	1.66	−4.76/−2.28	$PC_{71}BM$	0.72	13.4	0.708	6.82	[122]
P147	1.72	−4.77/−2.25	$PC_{71}BM$	0.85	11.3	0.757	7.25	[122]
P148	1.78	−5.25/−3.2	$PC_{71}BM$	0.82	12.34	0.601	6.08	[123]
P149	1.75	−5.29/−3.58	$PC_{71}BM$	0.85	12.13	0.635	6.54	[123]
P150	1.72	−5.20/−3.50	$PC_{71}BM$	0.86	12.77	0.699	7.68	[123]
P151	1.78	−5.51/−3.57	$PC_{71}BM$	0.94	11.28	0.647	6.9	[124]
P152	1.66	−5.52/−−	$PC_{71}BM$	0.87	11.4	0.73	7.2	[125]
P153	1.73	−5.36/−3.56	ITIC	0.87	16.33	0.596	8.47	[126]
P154	1.76	−5.45/−3.50	ITIC	0.90	14.89	0.66	9.07	[127]

cells, the higher V_{oc} and FF values contributed to the improved PCE from 8.47% to 9.07%. The chemical structures of P144–P154 are presented in Figure 1.24. The corresponding optoelectronic properties and device performances are listed in Table 1.16.

Introducing halogen atoms on the Qx skeleton shows more impact on the energy levels of Qx-based polymers. Wang and coworkers developed P155–P157 by introducing different numbers of fluorine atom on the Qx block [128]. The E_g^{opt} was gradually enlarged, while the HOMO level was stepwise downshifted from the non-fluorinated P155 to the monofluorinated P156 and difluorinated P157. With number of fluorine atom increasing, the molecular packing orientation changed from edge-on direction to face-on direction, facilitating the vertical charge transport

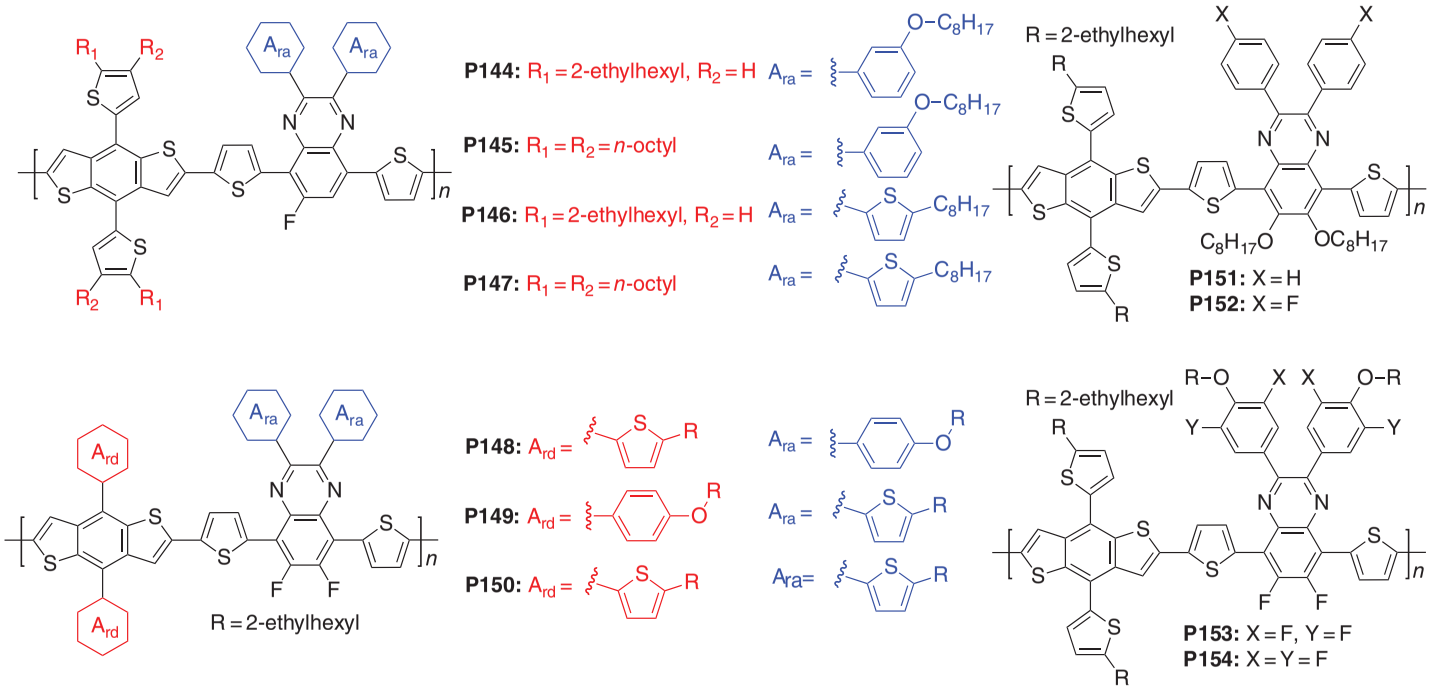

Figure 1.24 Chemical structures of the Qx-derived copolymers P144–P154. Source: Xiaopeng Xu.

and enhancement in hole mobilities. The significantly improved V_{oc} (from 0.60 to 0.77 V) and J_{sc} (from 9.10 to 12.62 mA cm^{-2}) boosted the PCE from 2.82% to 5.19%. Chang and coworkers introduced fluorine atoms on the side chains and/or the skeleton of Qx block and developed a series of Qx-based polymers (P158–P161) to elucidate the positional and populational effects of fluorine atoms on the properties of Qx-based polymers [129]. The gradual but noticeable improvements in the PCEs of these polymers in inverted-type PSCs were observed by increasing the number or changing the position of fluorine substituents on the Qx unit. Hou and coworkers reported P162–P164 by introducing fluorine atoms on the Qx block or on both the side chains of BDT block and the skeleton of Qx block [130]. The fluorination made the HOMO level offset and LUMO level offset between the P164 and ITIC acceptor to 0.24 and 0.04 eV, respectively. This energy level modulation effectively improved the V_{oc} from 0.69 to 0.95 V in the fullerene-free PSCs, without sacrificing the charge extraction. Moreover, the polymer with more fluorine tended to form stronger interchain π–π interaction when it was blended with ITIC, which was helpful for efficient charge transport. As a result, P164:ITIC devices yielded a high PCE of 11.34%. Zhang et al. replaced fluorine atom on P165 with chlorine atom and developed P166 [131]. The chlorination reduced the E_g^{opt} and lowered the HOMO level of P166. The simultaneously increased V_{oc}, J_{sc}, and FF resulted in the improved PCE from 6.12% to 8.16%. The chemical structures of P155–P166 are presented in Figure 1.25. The corresponding optoelectronic properties and device performances are listed in Table 1.17.

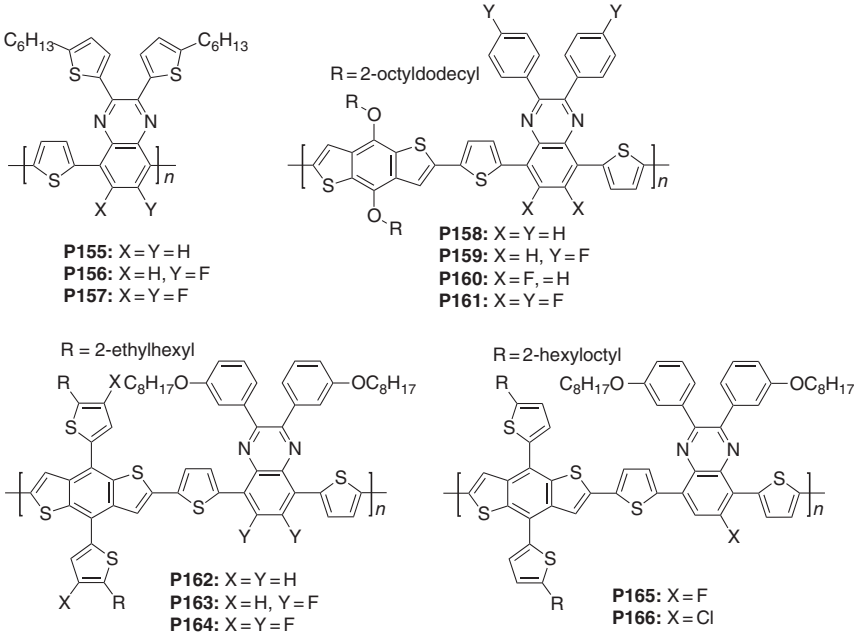

Figure 1.25 Chemical structures of the Qx-derived copolymers P155–P166. Source: Xiaopeng Xu.

Table 1.17 Optoelectronic properties and device performances of P155–P166.

Polymer	E_g^{opt} (eV)	HOMO/ LUMO (eV)	Acceptor	V_{oc} (V)	J_{sc} (mA cm^{-2})	FF	PCE (%)	References
P155	1.61	−5.10/−3.53	$PC_{71}BM$	0.60	9.10	0.518	2.82	[128]
P156	1.68	−5.18/−3.54	$PC_{71}BM$	0.68	11.05	0.549	4.14	[128]
P157	1.77	−5.33/−3.54	$PC_{71}BM$	0.77	12.62	0.531	5.19	[128]
P158	1.67	−5.29/−3.62	$PC_{71}BM$	0.61	8.08	0.637	3.14	[129]
P159	1.71	−5.35/−3.64	$PC_{71}BM$	0.78	8.76	0.661	4.52	[129]
P160	1.73	−5.36/−3.63	$PC_{71}BM$	0.82	9.62	0.705	5.56	[129]
P161	1.73	−5.47/−3.74	$PC_{71}BM$	0.91	10.15	0.715	6.60	[129]
P162	1.70	−5.18/−3.48	ITIC	0.69	16.16	0.599	6.68	[130]
P163	1.72	−5.34/−3.62	ITIC	0.83	17.16	0.645	8.90	[130]
P164	1.79	−5.49/−3.70	ITIC	0.95	17.87	0.668	11.34	[130]
P165	1.68	−5.31/−3.50	$PC_{71}BM$	0.93	12.40	0.53	6.12	[131]
P166	1.66	−5.33/−3.56	$PC_{71}BM$	0.95	14.08	0.61	8.16	[131]

The Qx block can also be further modified by fusing more aromatic rings to extend the π-conjugation. Bo and coworkers employed the fluorinated dibenzo[*a,c*]phenazine and acenaphtho[1,2-*b*]quinoxaline as the acceptor units, respectively, and developed P167 and P168 [132, 133]. These polymers exhibited MBGs and low HOMO levels. P167 exhibited a high hole mobility of 3.56×10^{-3} cm^2 V^{-1} s^{-1}. The resulting PSCs based on P167 realized a good PCE of 6.0%. Zhang et al. fused two pyrazine rings onto a benzene core and developed P169 [134]. P169 combined with $PC_{71}BM$ demonstrated decent J_{sc} and remarkable V_{oc}. Huang and coworkers fused two Qx blocks and developed quinoxalino[6,5-*f*]quinoxaline (NQx) with an angular shape [135]. By changing the alkoxy side chains on NQx block, a series of MBG polymers of P170–P172 were developed. With carefully device engineering, Peng and coworkers improved the PCE of P172 from 1.7% to 7.02% [136]. The chemical structures of P167–P172 are presented in Figure 1.26. The corresponding optoelectronic properties and device performances are listed in Table 1.18.

1.3.3 MBG Polymers Based on Thienopyrrolodione (TPD)

Thieno[3,4-*c*]pyrrole-4,6-dione (TPD) is a simple, compact, symmetric, and planar structure, which can be beneficial for electron delocalization when it is incorporated into various conjugated polymers [137]. TPD has strong electron-withdrawing ability and is able to form quinoidal resonance structure in the polymers. Using the N-bridged dithieno[3,2-*b*:2′,3′-*d*]pyrrole (DTP), which has strong electron-donating ability, as the donor block, the resulted polymers exhibited relatively LBGs (P173) [138, 139]. The bandgap of the resulting polymers can be enlarged and HOMO level can be downshifted by replacing the N-bridged

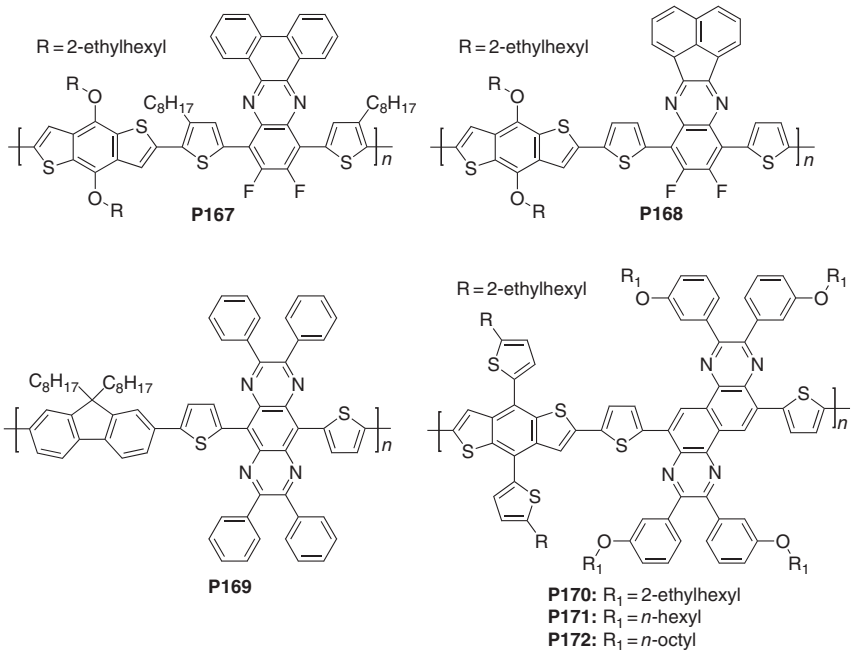

Figure 1.26 Chemical structures of the Qx-derived copolymers P167–P172. Source: Xiaopeng Xu.

Table 1.18 Optoelectronic properties and device performances of P167–P172.

Polymer	E_g^{opt} (eV)	HOMO/ LUMO (eV)	Acceptor	V_{oc} (V)	J_{sc} (mA cm^{-2})	FF	PCE (%)	References
P167	1.66	−5.30/−3.64	$PC_{71}BM$	0.74	12.50	0.65	6.0	[132]
P168	1.76	−5.54/−3.78	$PC_{71}BM$	0.77	10.75	0.57	4.72	[133]
P169	1.75	−5.70/−3.90	$PC_{71}BM$	0.83	4.9	0.41	1.70	[134]
P170	1.77	−5.16/−3.39	$PC_{71}BM$	0.88	9.1	0.48	3.8	[135]
P171	1.70	−5.16/−3.46	$PC_{71}BM$	0.79	8.0	0.42	2.7	[135]
P172	1.65	−5.16/−3.51	$PC_{71}BM$	0.80	4.9	0.43	1.7	[135]
P172	1.79	−5.36/−3.38	$PC_{71}BM$	0.82	14.24	0.601	7.02	[136]

DTP with C-bridged cyclopenta[2,1-*b*:3,4-*b*′]dithiophene (CPDT) and Si-bridged dithieno[3,2-*b*:2′,3′-*d*]silole (DTS) donor blocks (P174–P177) [139–143]. Compared to DTS, the dithieno[3,2-*b*:2′,3′-*d*]germole (DTG) with the larger Ge bridge could result in enhancement of ordering and electron delocalization [144]. The relative polymers exhibited lowered bandgaps and upshifted HOMO levels (P178) [144]. This variation trend could be further enhanced by introducing more germanium atoms, the diseleno[3,2-*b*:2′,3′-*d*]germole (DSG)-based P179 displayed a E_g^{opt}

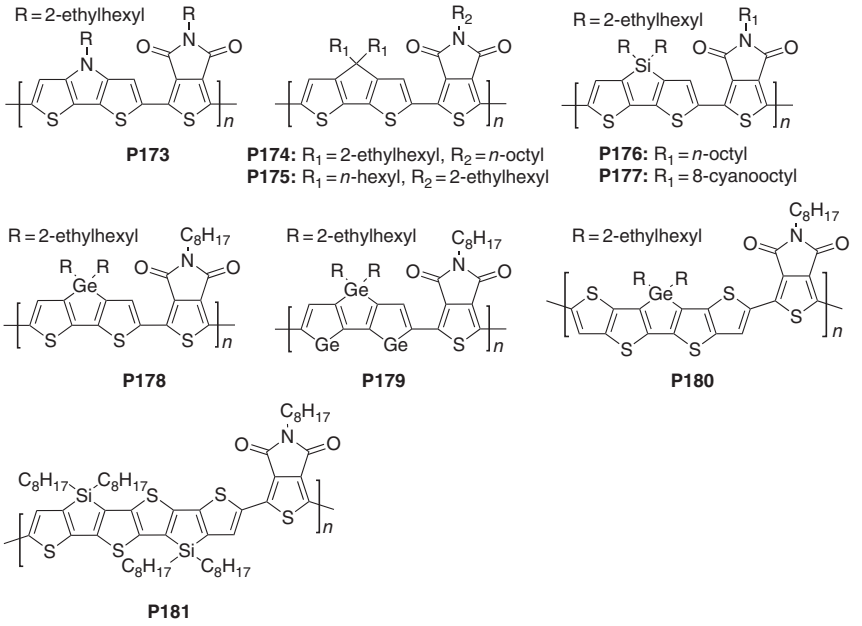

Figure 1.27 Chemical structures of the TPD-derived copolymers P173–P181. Source: Xiaopeng Xu.

of 1.60 eV and HOMO of −5.29 eV [145], which were smaller than the above DTS-based polymers. Extending the DTG by fusing two more thiophene afforded the dithienogermolodithiophene (DTTG). The resulted polymer P180 exhibited a medium E_g^{opt} of 1.75 eV and a deep HOMO level of −5.68 eV [146]. Fusing two DTS blocks produced the thieno[3,2-*b*]thienobis (silolothiophene) (Si4T) block, the resulted polymer P181 displayed slightly upshifted energy levels with minimal changed E_g^{opt} [147]. The chemical structures of P173–P181 are presented in Figure 1.27. The corresponding optoelectronic properties and device performances are listed in Table 1.19.

TPD-based polymers using thiophene derivatives as the donor block and spacers have been extensively studied. Their optoelectronic properties and energy levels can be finely tuned by introducing other heteroatoms (P182–P184) [148, 149], or fluorination on the thiophene blocks (P185) [150]. Moreover, Li and coworkers found that using bi-TPD block as the acceptor unit would be able to downshift the HOMO levels and redshift the absorptions (P186, P187) [151]. Along with suitable side chains introducing, the resulted polymer P187 based PSCs exhibited a high V_{oc} of 0.89 V and PCE of 9.08% [151]. They further lowered the energy levels of bi-TPD-based polymers by introducing the electron-deficient BT and fluorinated BT into the polymers, the resulted P188-based devices achieved a high V_{oc} of 1.02 V with a PCE of 6.46% [152]. While P189 with fluorinated BT could not match well with $PC_{71}BM$ to afford enough driving force for charge separation, resulting in poor device performance [152]. The chemical structures of P182–P189 are presented in Figure 1.28. The corresponding optoelectronic properties and device performances are listed in Table 1.20.

Table 1.19 Optoelectronic properties and device performances of P173–P181.

Polymer	E_g^{opt} (eV)	HOMO/ LUMO (eV)	Acceptor	V_{oc} (V)	J_{sc} (mA cm^{-2})	FF	PCE (%)	References
P173	1.62	−5.09/−3.42	$PC_{71}BM$	0.70	6.97	0.39	1.90	[138]
P174	1.67	−5.43/−3.25	$PC_{71}BM$	0.80	10.04	0.47	3.74	[139]
P175	1.61	−5.24/−3.55	$PC_{71}BM$	0.84	12.9	0.535	5.80	[140]
P176	1.70	−5.44/−3.17	$PC_{71}BM$	0.85	6.58	0.37	2.13	[139]
P176	1.73	−5.57/−3.88	$PC_{71}BM$	0.88	12.2	0.68	7.3	[141]
P176	1.73	−5.57/−3.88	$PC_{71}BM$	0.91	12.13	0.70	7.7	[142]
P177	1.73	−5.66/−3.68	$PC_{71}BM$	0.89	14.0	0.676	8.4	[143]
P178	1.69	−5.60/−3.50	$PC_{71}BM$	0.85	12.6	0.68	7.3	[144]
P179	1.60	−5.29/−3.40	$PC_{71}BM$	0.74	12.2	0.58	5.2	[145]
P180	1.75	−5.68/−3.88	$PC_{71}BM$	0.81	13.85	0.64	7.2	[146]
P181	1.70	−5.3/−3.6	$PC_{71}BM$	0.80	9.42	0.46	3.46	[147]

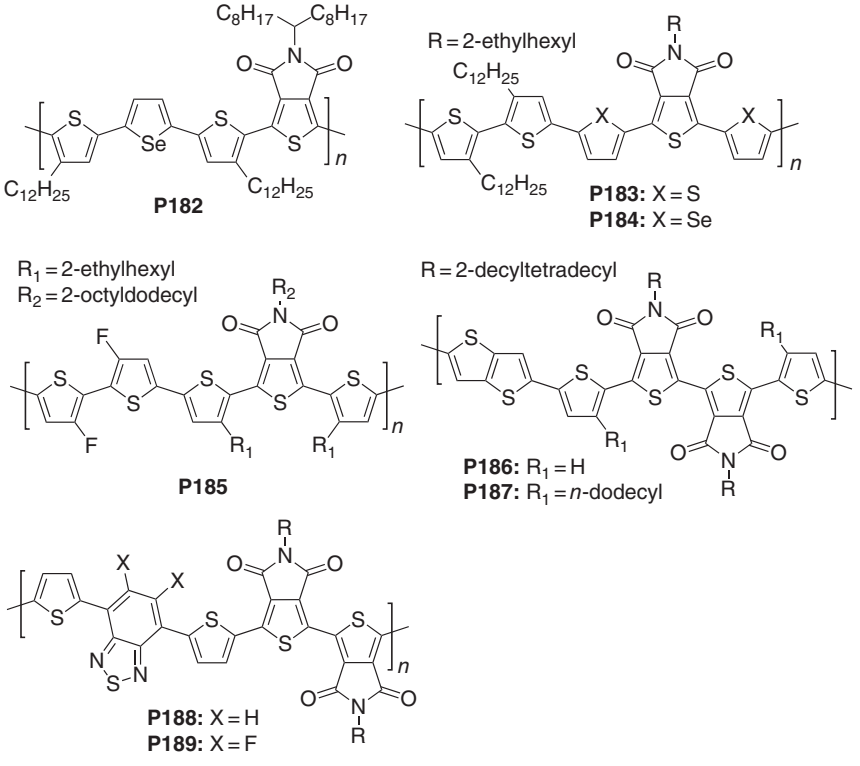

Figure 1.28 Chemical structures of the TPD-derived copolymers P182–P189. Source: Xiaopeng Xu.

Table 1.20 Optoelectronic properties and device performances of P182–P189.

Polymer	E_g^{opt} (eV)	HOMO/ LUMO (eV)	Acceptor	V_{oc} (V)	J_{sc} (mA cm^{-2})	FF	PCE (%)	References
P182	1.72	−5.49/−3.82	$PC_{71}BM$	0.88	10.74	0.62	5.80	[148]
P183	1.64	−5.50/−2.95	$PC_{71}BM$	0.92	4.73	0.461	2.04	[149]
P184	1.65	−5.52/−3.68	$PC_{71}BM$	0.80	4.53	0.420	1.52	[149]
P185	1.75	−5.55/−3.55	$PC_{71}BM$	0.96	10.50	0.514	5.52	[150]
P186	1.80	−5.61/−3.81	$PC_{71}BM$	0.91	13.45	0.672	8.22	[151]
P187	1.80	−5.59/−3.79	$PC_{71}BM$	0.89	14.15	0.721	9.08	[151]
P188	1.71	−5.72/−4.01	$PC_{71}BM$	1.02	9.48	0.668	6.46	[152]
P189	1.75	−5.85/−4.10	$PC_{71}BM$	0.96	2.55	0.636	1.56	[152]

BDT donor block has also been commonly used to pair with TPD acceptor block and develop high-performance conjugated polymers. The side chain effects on the overall properties of BDT–TPD-based polymers have been extensively studied (P190–P197) [153–155]. Beaujuge and coworkers found that linear side chains in BDT–TPD-based polymers could greatly impact the polymer self-assembling properties and device performances [154]. The N-alkyl substitutions on the BDT motifs triggered a critical change of preferential polymer orientation in thin films, resulting in a dramatic drop in bulk heterojunction (BHJ) device PCE [154]. A fine modulation of the number of aliphatic carbons in the linear N-alkyl-substituted TPD motifs did not significantly affect the preferential backbone orientation, yet this approach exhibited to be a main key to improve the device performance [154]. Among them, P195 with 2-ethylhexyloxy on the BDT block and heptyl on the TPD block achieved the optimized PCE of 8.5%. Zhu and coworkers reported a series of BDT–TPD-based polymers by introducing TT blocks into the polymer chains to extend the conjugation length and regulating their steric hindrance with side alkyl chains on BDT moiety (P198–P201) [156]. The additional alkyl chains on BDT moiety could significantly increase V_{oc} because of the decreased HOMO energy level. P200 with optimal length of alkyl side chain exhibited optimized thin-film morphology, contributing to higher PCE of 9.1% in the resulting PSCs. Recently, Huang and coworkers employed the bi-TPD block to mediate the crystallinity and developed P202 [157]. P202:Y6 BHJ blend film exhibited more favorable face-on backbone orientation and stronger crystallinity. As a result, charge transportation was enhanced, whereas the charge recombination was suppressed in the BHJ device, which contributed a high PCE of 14.2% in the fullerene-free devices. The chemical structures of P190–P202 are presented in Figure 1.29. The corresponding optoelectronic properties and device performances are listed in Table 1.21.

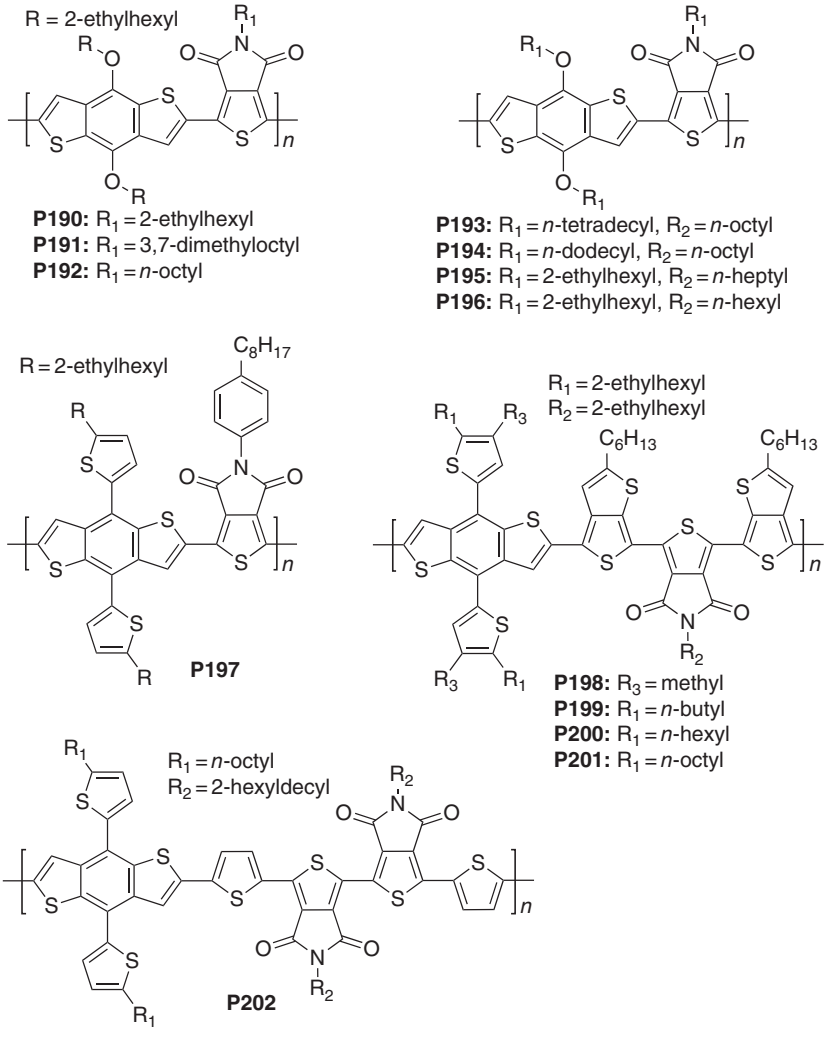

Figure 1.29 Chemical structures of the TPD-derived copolymers P190–P202. Source: Xiaopeng Xu.

1.3.4 MBG Polymers Based on Thieno[3,4-*b*]thiophene (TT)

BDT–TT-based polymers are quite representative high-performance polymers in the last decade (Figure 1.30). The TT monomer unit was designed because of its tendency to stabilizing the quinoidal structure that led to a medium energy bandgap around 1.6 ~ 1.8 eV [158]. This guaranteed an efficient light absorption in the solar spectrum with the highest photon flux around 700 nm. The quinoidal structure enhanced the planarity along the aromatic polymer backbone by providing a more rigid backbone as well. The extended π system in BDT unit enabled the polymer to form a better π–π stacking with a shorter distance between different polymer

Table 1.21 Optoelectronic properties and device performances of P190–P202.

Polymer	E_g^{opt} (eV)	HOMO/ LUMO (eV)	Acceptor	V_{oc} (V)	J_{sc} (mA cm^{-2})	FF	PCE (%)	References
P190	1.75	−5.48/−−	$PC_{71}BM$	0.87	8.1	0.56	4.0	[153]
P191	1.70	−5.57/−−	$PC_{71}BM$	0.81	9.7	0.67	5.7	[153]
P192	1.73	−5.40/−−	$PC_{71}BM$	0.85	11.5	0.68	6.8	[153]
P192	−−	−−/−−	$PC_{71}BM$	0.93	12.5	0.65	7.5	[154]
P193	−−	−−/−−	$PC_{71}BM$	0.93	8.3	0.53	4.1	[154]
P194	−−	−−/−−	$PC_{71}BM$	0.92	6.8	0.51	3.2	[154]
P195	−−	−−/−−	$PC_{71}BM$	0.97	12.6	0.70	8.5	[154]
P196	−−	−−/−−	$PC_{71}BM$	0.96	11.1	0.62	6.6	[154]
P197	1.78	−5.59/−3.62	$PC_{71}BM$	0.96	11.00	0.585	6.18	[155]
P198	1.61	−5.18/−3.26	$PC_{71}BM$	0.72	16.36	0.66	7.73	[156]
P199	1.63	−5.20/−3.27	$PC_{71}BM$	0.78	13.44	0.70	7.42	[156]
P200	1.64	−5.16/−3.26	$PC_{71}BM$	0.78	15.611	0.75	9.10	[156]
P201	1.61	−5.15/−3.27	$PC_{71}BM$	0.77	13.61	0.72	7.56	[156]
P202	1.78	−5.20/−3.45	Y6	0.83	25.6	0.667	14.2	[157]

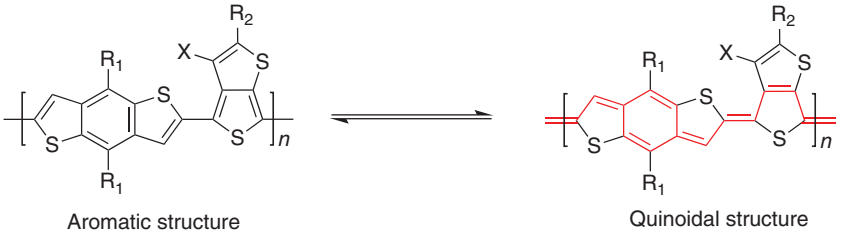

Figure 1.30 The aromatic form and quinoidal form of BDT-TT based polymers. Source: Xiaopeng Xu.

backbones and finally led to a high hole mobility [158]. The electron-donating ability of BDT block can be modulated by introducing alkoxy (P203–P209) [159–162], alkylthienyl (P210, P211) [163, 164], or alkoxyphenyl (P212) [165] side chains, or fluorine atom at the backbone (P208, P209) [162]. The electron-withdrawing property of TT block can be finely tuned by introducing ester (P203, P204) [159, 160], carbonyl (P205, P206) [159], or sulfuryl groups (P207) [161] at the 2-position, and/or introducing halogen atom (P204, P206, P207, P209–P215) [159–167] at the 3-position. In addition, introducing 2D side chains on the BDT block (P210–P215) [163–165] and/or on the 2-position of TT block (P213–P215) [166, 167] also extended the π-conjugation length of the resulting polymers for improving charge transport properties. He and coworkers introduced 2D side chains on both BDT and TT blocks and developed P213, which resulted in a strong and broad absorption [166]. Moreover, the 2D side chains could induce a modulation of the preferential

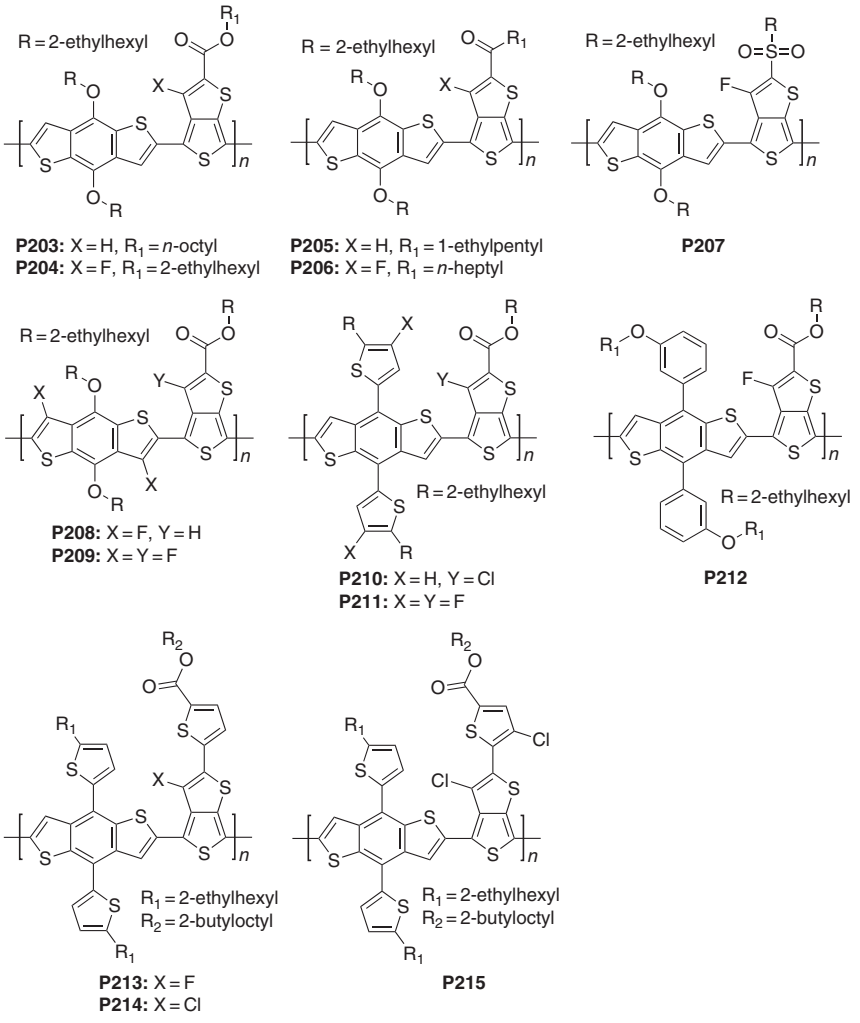

Figure 1.31 Chemical structures of the TT-derived copolymers P203–P215. Source: Xiaopeng Xu.

ordered microstructure that shortened the π–π distance to strengthen the π–π stacking between polymer backbones, which could be favorable toward higher J_{sc} and FF. As a result, P213:$PC_{71}BM$ devices realized a high PCE of 9.13%. The chemical structures of P203–P215 are presented in Figure 1.31. The corresponding optoelectronic properties and device performances are listed in Table 1.22.

Introducing π bridges between BDT and TT blocks to extend the conjugation area is beneficial for face-to-face packing and significant increase of photovoltaic efficiency [168]. Hou and coworkers developed a series of thiophene-bridged polymers (P216–P219) by introducing fluorine on the BDT side chains and/or 3-position of TT block [169]. They found that fluorination on the donor and the acceptor moieties has little influence on the optical properties, but a synergistic effect on lowering

Table 1.22 Optoelectronic properties and device performances of P203–P215.

Polymer	E_g^{opt} (eV)	HOMO/ LUMO (eV)	Acceptor	V_{oc} (V)	J_{sc} (mA cm^{-2})	FF	PCE (%)	References
P203	1.61	−5.01/−3.24	$PC_{71}BM$	0.62	13.2	0.63	5.15	[159]
P204	1.63	−5.15/−3.31	$PC_{71}BM$	0.74	14.5	0.690	7.40	[160]
P205	1.61	−5.12/−3.35	$PC_{71}BM$	0.70	14.7	0.641	6.58	[159]
P206	1.61	−5.22/−3.45	$PC_{71}BM$	0.76	15.2	0.669	7.73	[159]
P207	1.65	−5.12/−3.49	$PC_{71}BM$	0.76	14.1	0.58	6.22	[161]
P208	1.75	−5.41/−3.60	$PC_{71}BM$	0.68	11.1	0.422	3.2	[162]
P209	1.73	−5.48/−3.59	$PC_{71}BM$	0.75	9.1	0.394	2.7	[162]
P210	1.71	−5.43/−3.55	ITIC	0.91	14.53	0.58	7.57	[163]
P211	1.64	−5.47/−3.56	ITIC	0.94	16.0	0.605	9.1	[164]
P212	1.62	−5.45/−3.34	$PC_{71}BM$	0.86	16.4	0.622	9.0	[165]
P213	1.61	−5.32/−3.60	$PC_{71}BM$	0.73	17.78	0.704	9.13	[166]
P214	1.72	−5.45/−3.60	ITIC	0.91	15.79	0.613	8.81	[167]
P215	1.66	−5.43/−3.63	ITIC	0.87	14.52	0.574	7.38	[167]

their molecular energy levels. The V_{oc} of the resulting devices increased from 0.56 to 0.78 V, and the PCE improved from 4.5% to 8.6%. On the other hand, replacing the alkylthienyl side chains with *meta*-alkoxyphenyl groups, the optical absorption, molecular packing, and charge transport properties of the polymer (P220) were little changed, while the HOMO level could be reduced distinctly, so V_{oc} of the PSC device could be significantly enhanced from 0.60 to 0.78 V [170]. Replacing the electron-rich thiophene bridges with electron-deficient thiazole spacers is also favorable in obtaining deep HOMO levels of the corresponding polymers [171]. Yang and coworkers developed the thiazole-bridged P221 and P222 by changing the orientations of the thiazole relative to the TT moiety [171]. P222 with 2-position of thiazole attached to TT block exhibited a lower HOMO energy level, and better planar molecular configuration, together with preferable phase domains and good intermixing with $PC_{71}BM$. Consequently, a remarkable PCE of 9.72% was realized. Further lowering the HOMO level by introducing sulfur atoms on the BDT side chains and fluorine atom on the TT block, the resulting polymers (P223, P224) realized higher V_{oc}s in devices [172]. P224:$PC_{71}BM$-based PSCs achieved an impressive V_{oc} of 0.97 V and PCE of 10.30%. The chemical structures of P216–P224 are presented in Figure 1.32. The corresponding optoelectronic properties and device performances are listed in Table 1.23.

Expanding the π-conjugation system in the rigid BDT unit is conducive to lower positive charge density and exciton binding energy [173]. Yu and coworkers employed dithieno[2,3-*d*:2′,3′-*d*′]benzo[1,2-*b*:4,5-*b*′]dithiophene (DBD) as the donor building block along with side chain engineering and developed

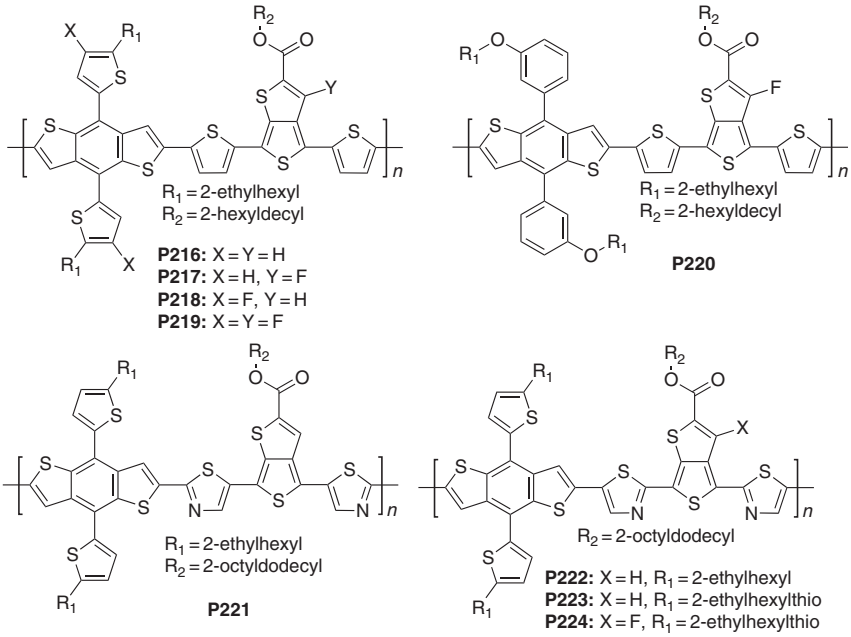

Figure 1.32 Chemical structures of the TT-derived copolymers P216–P224. Source: Xiaopeng Xu.

Table 1.23 Optoelectronic properties and device performances of P216–P224.

Polymer	E_g^{opt} (eV)	HOMO/ LUMO (eV)	Acceptor	V_{oc} (V)	J_{sc} (mA cm^{-2})	FF	PCE (%)	References
P216	1.61	−4.90/−3.10	$PC_{71}BM$	0.56	12.2	0.667	4.5	[169]
P217	1.65	−4.95/−3.12	$PC_{71}BM$	0.60	14.3	0.657	5.6	[169]
P218	1.64	−5.15/−3.27	$PC_{71}BM$	0.74	14.4	0.677	7.2	[169]
P219	1.64	−5.20/−3.30	$PC_{71}BM$	0.78	15.2	0.724	8.6	[169]
P240	1.70	−5.12/−3.49	$PC_{71}BM$	0.78	13.4	0.718	7.50	[170]
P241	1.73	−5.54/−−	$PC_{71}BM$	0.83	16.84	0.695	9.72	[171]
P242	1.70	−5.43/−−	$PC_{71}BM$	0.82	13.11	0.643	6.91	[171]
P243	1.71	−5.45/−3.52	$PC_{71}BM$	0.93	16.20	0.613	9.23	[172]
P244	1.74	−5.48/−3.51	$PC_{71}BM$	0.97	16.65	0.638	10.30	[172]

P225 and P226 [173]. Optimal structures of side alkyl chains in the polymers improved the compatibility of the polymer chains with $PC_{71}BM$, improving the morphology of the polymer:$PC_{71}BM$ blend film with concomitant enhancement of the crystallinity of the polymer chains in the blend film. Consequently, the device efficiency in P225 was enhanced up to 7.6%. Bathula et al. empolymed the linear shaped naphtho[2,3-*b*:6,7-*b*′]dithiophene (NDT) and "zigzag"

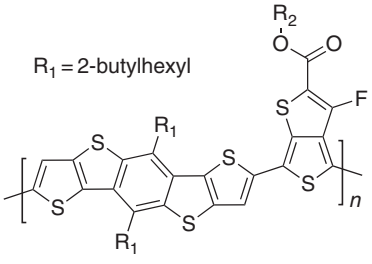

P225: R_2 = 2-butylocyl
P226: R_2 = 5,9-diethyltridecan-7-yl

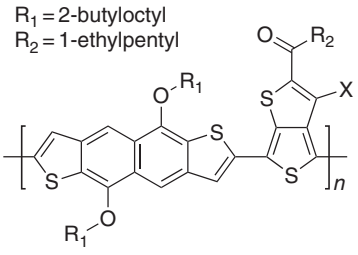

P227: X = H
P228: X = F

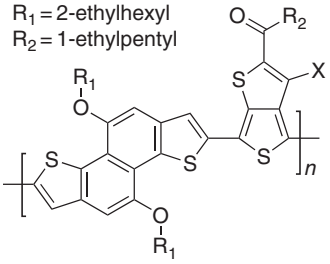

P229: X = H
P230: X = F

Figure 1.33 Chemical structures of the TT-derived copolymers P225–P230. Source: Xiaopeng Xu.

Table 1.24 Optoelectronic properties and device performances of P225–P230.

Polymer	E_g^{opt} (eV)	HOMO/ LUMO (eV)	Acceptor	V_{oc} (V)	J_{sc} (mA cm^{-2})	FF	PCE (%)	References
P225	1.68	−5.24/−−	$PC_{71}BM$	0.89	13.0	0.653	7.60	[173]
P226	1.67	−5.30/−−	$PC_{71}BM$	0.88	10.7	0.521	4.9	[173]
P227	1.65	−5.44/−3.79	$PC_{71}BM$	0.71	11.68	0.54	4.49	[174]
P228	1.64	−5.51/−3.87	$PC_{71}BM$	0.72	13.50	0.53	5.16	[174]
P229	1.60	−4.86/−3.26	$PC_{71}BM$	0.55	11.99	0.38	2.51	[175]
P230	1.69	−5.03/−3.34	$PC_{71}BM$	0.71	13.52	0.51	4.88	[175]

naphtho[1,2-*b*:5,6-*b*′]dithiophene (zNDT) as the donor blocks, respectively, and developed a series of MBG polymers (P227–P230) with extended π-conjugation [174, 175]. These polymers exhibited high field effect carrier mobilities up to ~10^{-3} cm^2 V^{-1} s^{-1}, showing the promising applications of this blocking in developing high-performance photovoltaics. The chemical structures of P225–P230 are presented in Figure 1.33. The corresponding optoelectronic properties and device performances are listed in Table 1.24.

1.4 WBG Polymers

As discussed in the introduction part, a very important molecular design strategy of WBG polymers is to introduce both the D unit with relatively weak electron-donating ability and the A unit with relatively weak electron-withdrawing ability due to a weak D unit will deep-shifts molecular HOMO level and a weak A unit will upshifts molecular LUMO level, respectively [176]. D units employed in high-performance WBG polymer donors are mostly thiophene or benzene fused building blocks with weak electron-donating ability, such as thiophene, BDT, IDT, and the related derivatives. Compared to D units, A units play a more important role in constructing WBG polymer donors due to their diversity [177, 178]. At present, the most common A units with weak electron-withdrawing ability for constructing high-performance WBG polymer donors include ester or cyano-substituted thiophene, thienopyrroledione, alkyloxy substituted benzothiadiazole, benzotriazole (BTA), benzodithiophene-4,8-dione (BDD), thiazole or pyrazine derivatives-based *N*-heterocycles (such as dithiazole, thiazolothiazole, benzodithiazole, thiadiazole, oxadiazole, pyrazine, quinoxaline, tetrazine, and et al.), and the related derivatives. In this contribution, the WBG polymer donors are divided into the following seven branching categories: (i) polythiophene (PT) derivatives; (ii) polymer donors with a backbone of benzodithiophene-*alt*-thiophene derivative; (iii) polymer donors based on benzothiadiazole derivatives; (iv) polymer donors based on BTA derivatives; (v) polymer donors based on thiazole, pyrazine, and their derivatives containing *N*-heterocycles; (vi) polymer donors based on BDD derivatives; and (vii) others. The following part will introduce the design strategies of these WBG polymer donors firstly, and then, some representative polymers and their photovoltaic properties will be analyzed.

1.4.1 WBG Polymers Based on Polythiophene (PT) Derivatives

Thiophene is one of the basic units of organic photovoltaic materials, and the corresponding PT and its derivatives have attracted great attention in the past decades due to their versatile and promising applications in many fields. Among them, as the most representative conjugated polymer donor, poly(3-hexylthiophene) (P231, $E_g > 1.9$ eV) with a simple chemical structure and low-cost synthetic pathway shows high hole mobility and crystallinity, which is beneficial to form a nanoscale interpenetrating fiber network in fullerene-based blend films and be considered as one of the most promising candidates for large-scale manufacturing of OSCs [179, 180]. However, P231 possesses a relatively high HOMO level of −4.90 eV due to its homopolymerized structure without electron-withdrawing unit, which makes it use to have a low V_{oc} in the $PC_{61}BM$- and $PC_{71}BM$-based OSCs [179]. Recently, the P231-based OSCs have achieved PCEs of 7 ~ 9% by developing fullerene derivatives (such as ICBA [180]) and non-fullerene small molecule (SM) acceptors with high LUMO levels (such as TrBTIC [181] and ZY-4Cl [182]) to increase V_{oc}. On the other hand, to deep-shift HOMO level of PT derivatives, some molecular modification strategies have also been carried out, such as introducing 2D-conjugated side

chains [183], ester or cyano groups [184], halogen atoms [185], and thiophene-fused electron-withdrawing units [150, 186, 187]. For example, a design concept of "side chain isolation" was proposed for developing a 2D-styryltriphenylamine-conjugated PT derivative P232 with red-shifted absorption spectrum and deep-shifted HOMO level. Matched with ICBA, the P232-based OSCs achieved a PCE of 3.6% with a high V_{oc} of 0.94 V [183]. Another strategy applied to decrease HOMO level of PT derivatives is to introduce electron-withdrawing groups into molecular backbone. In 2014, Zhang et al. synthesized a PT derivative P233 by attaching two electron-withdrawing carboxylate substituents on PT backbone [184], and the HOMO level of P233 (−5.26 eV) decreased by 0.36 eV in comparison with P231 (−4.90 eV). As a result, P233 achieved an improved PCE of 7.2% with a significantly increased V_{oc} of 0.91 V in the $PC_{71}BM$-based OSCs. Moreover, by using LBG SM acceptor ITIC instead of $PC_{71}BM$ in OSCs, P233 achieved a higher PCE of 10.16% with a J_{sc} of 16.5 mA cm^{-2}, which was the highest PCE in the OSCs based on PT derivatives [188]. Subsequently, a series of PT derivatives were designed and synthesized by introducing halogen atoms into the backbone of P233. The incorporation of chlorine or fluorine atoms into polymers both downshifted molecular HOMO levels, leading to higher V_{oc} in OSCs. Due to the suitable phase-separated morphology with favorable molecular packing and miscibility, chlorinated P236 achieved efficient exciton dissociation, improved charge collection, and weak charge recombination, resulting in the best PCE up to 12.38% [185]. In addition, constructing the D–A type PT derivatives by incorporating the thiophene-fused acceptor units has been proved to be an effective strategy to reduce molecular HOMO levels. In 2013, a PT derivative P238 with a lower HOMO level of −5.13 eV was synthesized by polymerizing thiophene-fused BDD acceptor unit with 2,2′-bithiophene (2T) donor unit, and an improved PCE of 6.88% with a higher V_{oc} of 0.83 V was achieved in its OSCs [186]. In addition to reduce molecular HOMO levels, the 3,3′-difluoro-2,2′-bithiophene (ff2T) unit has an improved planarity, more stable conformation, and additional noncovalent bonding interactions in comparison with the fluorine-free 2T unit, which leads to the improved crystallinity, extinction coefficient, and charge mobility, thus the related polymers can achieve higher V_{oc}, J_{sc}, and FF values simultaneously in OSCs [187]. In 2016, Fan et al. reported a ff2T-based PT derivative P239 and found that P239 shows a deeper HOMO level, improved extinction coefficient and crystallinity compared with that of non-fluorinated P238. Matching with $PC_{71}BM$, the OSCs yielded a PCE of 9.2% [187]. Subsequently, P239 was introduced as the hole-cascade material to optimize the blend morphology of PTB7-Th:N2200, and the ternary all-polymer OSCs achieved an improved PCE of 7.2% [189]. Wang et al. reported a TPD-based PT derivative P241 with low HOMO level of −5.55 eV by introducing the synergistic effects of fluorination and thiophene-fused acceptor unit (thienopyrroledione), and the corresponding $PC_{71}BM$-based OSCs achieved a PCE of 5.52% with a high V_{oc} of 0.96 V [150]. The chemical structures of representative PT derivatives are shown in Figure 1.34, and the corresponding photovoltaic parameters of OSCs are summarized in Table 1.25.

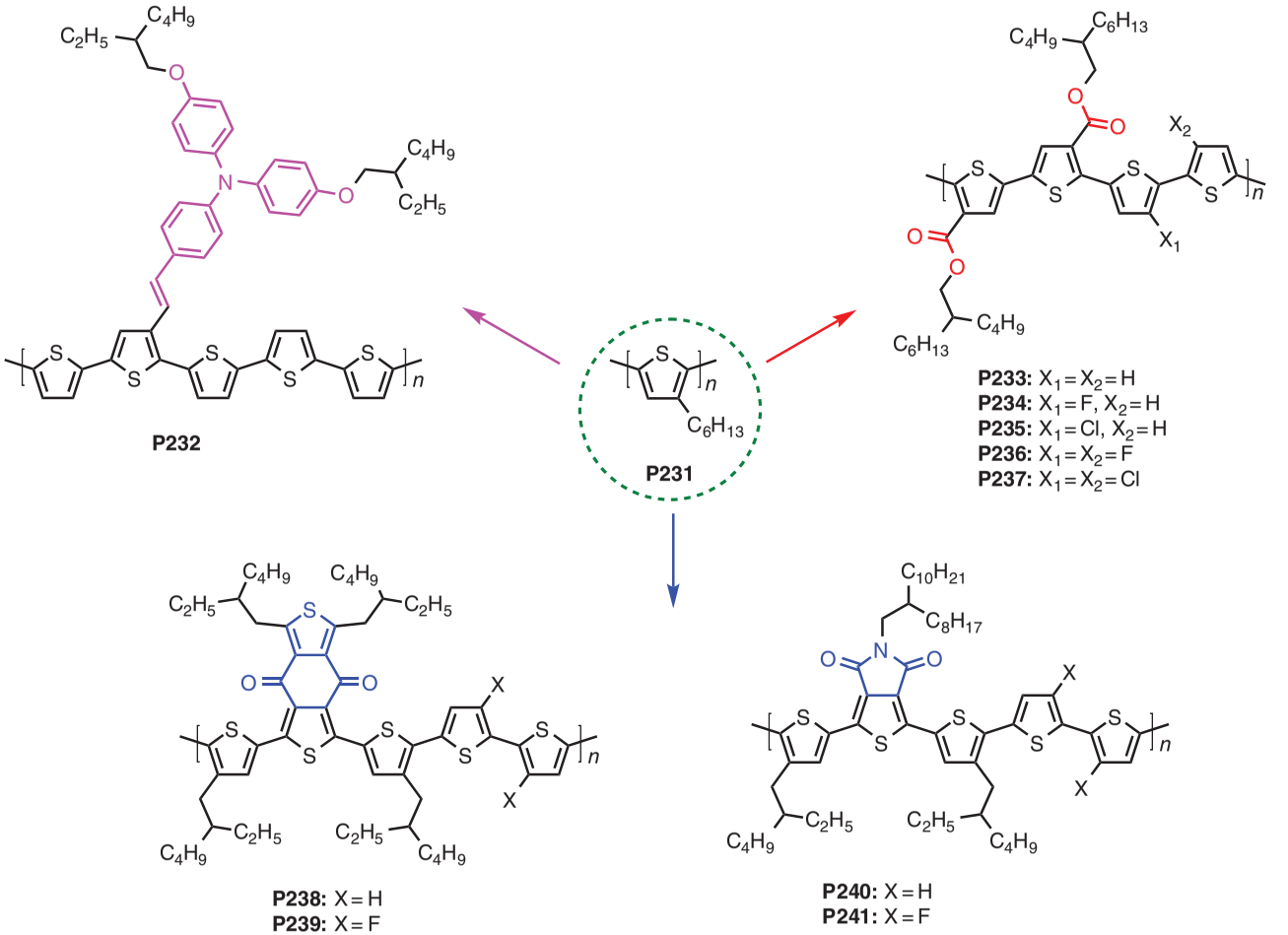

Figure 1.34 Chemical structures of the PT-derived copolymers P231–P241. Source: Qunping Fan.

1.4.2 WBG Polymers Based on Benzodithiophene-*alt*-Thiophene Derivatives

In 2008, BDT unit with a weak electron-donating, large and rigid coplanar fused-ring structure was firstly used in the synthesis of photovoltaic polymer materials [190]. Up to now, as one of the most popular and successful building blocks, BDT unit has been used in hundreds of high-performance photovoltaic materials [85]. Recently, the polymer donors with a backbone of benzodithiophene-*alt*-thiophene derivative have attracted great attentions due to their WBG of ~2.0 eV and low HOMO levels, which are complementary in absorption spectra and matching in energy levels with the booming LBG SM acceptors. Firdaus et al. developed a series of WBG polymers by polymerizing benzodithiophene and thiophene derivatives, such as non-fluorinated P242, difluorinated P243, and 2D-thienyl substituted P244 [191]. The synergistic effects of fluorination and 2D-conjugation decreased energy levels, improved absorption coefficient, and optimized molecular packing of polymers. As a result, the P244-based OSCs achieved the highest PCE of 9.8% with simultaneously improved V_{oc}, J_{sc}, and FF. In 2017, Park et al. reported a random WBG (2.02 eV) polymer donor P245 by introducing a methylcarboxyl substitution on thiophene unit [192]. Due to its good solubility, the P245-based OSCs fabricated by halogen-free solvents achieved a high PCE of 9.73%. Subsequently, Liu et al. synthesized a regioregular polymer P247 with a WBG of 1.99 eV [193]. Compared to its random analog P245, P247 has higher-order packing and improved absorption coefficient, which results in a higher PCE of 12.07% in its OSCs. Moreover, by introducing fluorine atom on the 2D-conjugated thienyl of polymer P245, Yao et al. developed polymer donor P246 with a similar WBG of 2.00 eV and a deeper HOMO level of −5.59 eV [194]. Matched with IT-4F, the P246-based OSCs achieved a high PCE of 14.7% due to the efficient charge transfer in device assisted by a large electrostatic potential difference between P246 and IT-4F. In the following work, Hou and coworkers reported a series of WBG polymer donors PDTB-EF-T (P248, P249, and P250) with deep HOMO level < -5.50 eV by introducing the synergistic electron-withdrawing effects of the fluorine atom and ester group [195]. Hence, a high V_{oc} of 0.90 V was achieved when matched with IT-4F, corresponding to a low E_{loss} of 0.62 eV. Moreover, the aggregation and molecular packing of PDTB-EF-T can be optimized well by side chain engineering of the ester, which results in the stronger interchain π–π interaction and ordering structure, and thus the improved charge transport and reduced recombination are achieved for the linear decyl-substituted PDTB-EF-T (P248)-based PSCs with a high PCE of 14.2%. Recently, Chen et al. reported a carboxylate-functionalized thienothiophene-based WBG polymer donor P251 [196]. Compared to its analog polymer 2TC-TT-BDTF T with two carboxylate groups on the outer thiophenes, P251 shows a higher planarity, stronger aggregation, red-shifted absorption, improved crystalline ordering, and larger charge carrier mobility. As a result, the P251-based OSCs demonstrated a greatly improved PCE of 11.15% in comparison with the 2TC-TT-BDTFT-based ones (9.65%). Very recently, Duan and coworkers introduced a cost-effective building block, 3,4-dicyanothiophene (DCT), for constructing a WBG polymer P253 with deep HOMO level for application as donor in OSCs [197]. Thanks to its stronger intermolecular interaction, more planar backbone, and larger dipole moment of the

Table 1.25 Optoelectronic properties and device performances of P231–P241.

Polymer	E_g^{opt} (eV)	HOMO/ LUMO (eV)	Acceptor	V_{oc} (V)	J_{sc} (mA cm^{-2})	FF	PCE (%)	References
P231	1.94	−4.90/−3.00	$PC_{61}BM$	0.61	9.4	0.53	3.0	[179]
P231	1.94	−4.90/−3.00	ICBA	0.87	11.35	0.75	7.4	[180]
P231	1.94	−4.90/−3.00	TrBTIC	0.88	13.04	0.719	8.25	[181]
P231	1.94	−4.90/−3.00	ZY-4Cl	0.88	16.49	0.65	9.46	[182]
P232	1.91	−5.10/−3.08	ICBA	0.94	6.55	0.584	3.6	[183]
P233	1.90	−5.26/−−	$PC_{71}BM$	0.91	11.0	0.72	7.2	[184]
P233	1.90	−5.26/−−	ITIC	0.94	16.50	0.6567	10.16	[188]
P234	1.93	−5.32/−2.98	ITIC-Th1	0.93	17.52	0.662	10.85	[185]
P235	1.92	−5.40/−3.03	ITIC-Th1	0.98	15.32	0.565	8.48	[185]
P236	1.91	−5.34/−3.01	ITIC-Th1	0.94	18.50	0.712	12.38	[185]
P237	1.95	−5.44/−3.00	ITIC-Th1	0.99	13.54	0.518	6.94	[185]
P238	1.77	−5.13/−3.23	$PC_{71}BM$	0.83	11.57	0.71	6.88	[186]
P239	1.74	−5.42/−3.53	$PC_{71}BM$	0.95	13.2	0.73	9.2	[187]
P240	1.84	−5.42/−3.31	$PC_{71}BM$	0.93	6.15	0.433	2.48	[150]
P241	1.75	−5.55/−3.55	$PC_{71}BM$	0.96	11.18	0.514	5.52	[150]

cyano group, P253 showed stronger aggregation in solution, higher π–π coherence length and higher relative dielectric constant in film compared to its cyano-free analog P252. Paired with SM acceptor IT-4F, the OSCs achieved PCEs of 2.3% and 11.2% for P252 and P253, respectively. Furthermore, by optimizing the alkyl chains of the DCT-containing polymers, an optimized polymer P254 was developed and achieved a higher PCE of 13.4%. The chemical structures of the polymers with a backbone of benzodithiophene-*alt*-thiophene derivatives are showed in Figure 1.35, and the corresponding photovoltaic parameters of OSCs are summarized in Table 1.26.

1.4.3 WBG Polymers Based on Benzothiadiazole (BT) Derivatives

BT with strong electron-withdrawing ability and stable quinoid structure is one of the most popular acceptor units in the synthesis of D–A-structured LBG and MBG photovoltaic materials [24, 198]. On the contrary, only few BT-based polymer donors with a WBG were successfully developed so far, by matching donor units with weak electron-donating ability [199], introducing alkyloxy substitution on BT units [199, 200], or designing thiophen-fused BT derivatives [4, 201] to decrease the ICT effects between D and A units. For example, Bo and coworkers reported a polymer donor P255 with a WBG of 1.97 eV by polymerizing fluorene with weak electron-donating ability and dodecyloxy-substituted BT derivative [199]. Matched with a WBG SM acceptor NI-T-NI, its OSCs obtained an impressively high V_{oc} of 1.30 V. On the other hand, attaching alkylphenyl with steric hindrance on the BDT unit and alkoxy chains on the BT unit could enlarge their E_g over 1.80 eV.

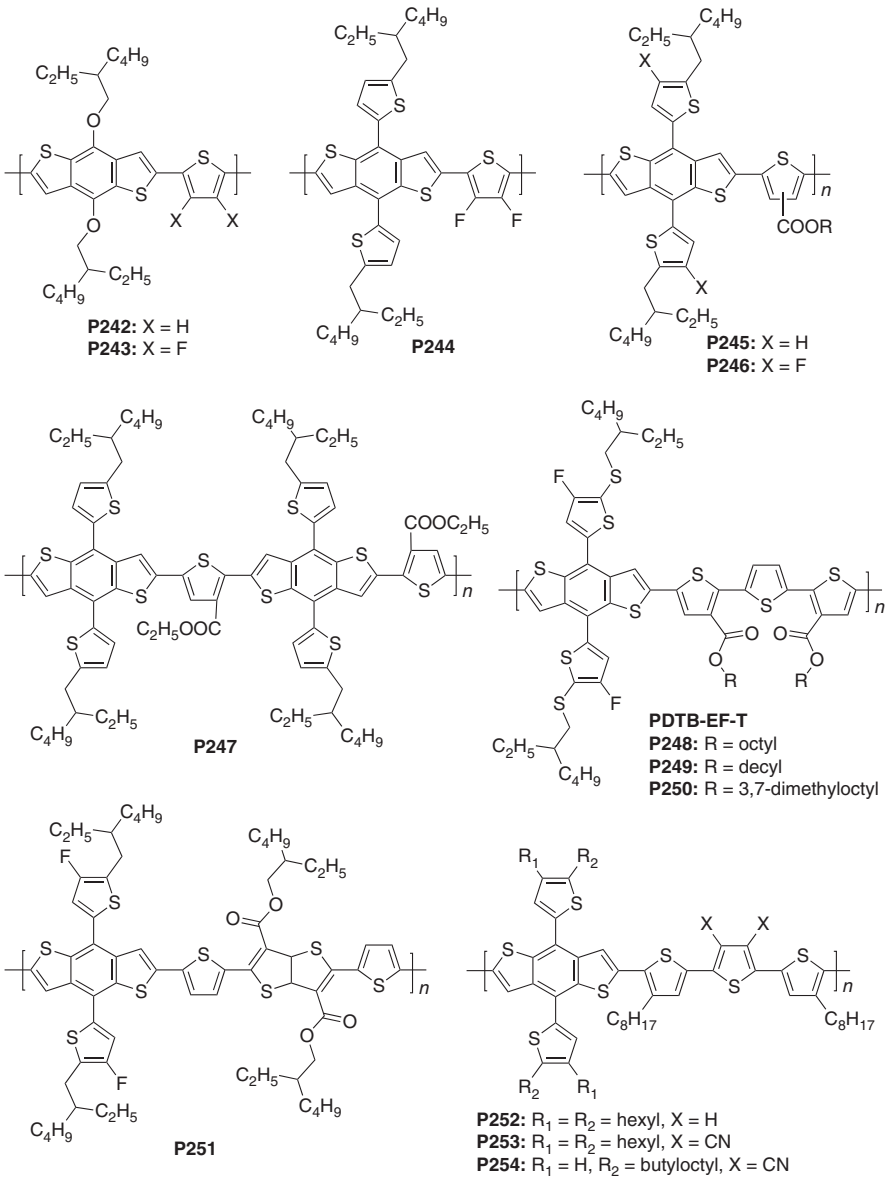

Figure 1.35 Chemical structures of the benzodithiophene-*alt*-thiophene-derived copolymers P242–P254. Source: Qunping Fan.

For example, Bo and coworkers synthesized a WBG (1.81 eV) polymer donor P256 with 4-alkyl-3,5-difluorophenyl substituted BDT as donor unit, alkyloxy-substituted BT as acceptor unit with two thiophenes as the spacers [200]. Matched with $PC_{71}BM$, its OSCs without any post-processing achieved a PCE of 8.24%. Using benzooxadiazole (BO) instead of BT, the corresponding polymer P257 showed a lower hole mobility, which resulted in a lower PCE of 5.67%. In 2017, Liu et al.

Table 1.26 Optoelectronic properties and device performances of P242–P254.

Polymer	E_g^{opt} (eV)	HOMO/ LUMO (eV)	Acceptor	V_{oc} (V)	J_{sc} (mA cm^{-2})	FF	PCE (%)	References
P242	2.1	−5.2/−−	ITIC	0.79	7.6	0.41	2.5	[191]
P243	2.1	−5.3/−−	ITIC	0.94	11.6	0.53	5.8	[191]
P244	2.0	−5.2/−−	ITIC	0.94	16.9	0.62	9.8	[191]
P245	2.02	−5.42/−3.40	ITIC	0.95	17.01	0.6008	9.73	[192]
P246	2.0	−5.59/−3.67	IT-4F	0.91	21.5	0.75	14.7	[194]
P247	2.07	−5.51/−3.46	FTIC	1.005	17.03	0.702	12.07	[193]
P248	1.93	−5.51/−3.59	IT-4F	0.896	20.05	0.64	11.5	[195]
P249	1.93	−5.50/−3.59	IT-4F	0.900	20.73	0.76	14.2	[195]
P250	1.94	−5.54/−3.60	IT-4F	0.904	20.31	0.61	11.2	[195]
P251	1.88	−5.41/−3.53	m-ITIC	0.97	16.57	0.6937	11.15	[196]
P252	2.00	−5.23/−2.89	IT-4F	0.78	7.1	0.41	2.3	[197]
P253	1.88	−5.62/−3.50	IT-4F	0.92	18.9	0.64	11.2	[197]
P254	1.88	−5.72/−3.52	IT-4F	0.91	21.2	0.69	13.4	[197]

reported a WBG polymer P258 based on a vertical-benzodithiophene (vBDT) building block [202]. Compared to traditional BDT-based polymers, the vBDT unit was connected *via* the phenyl group instead of the thiophene unit in P258, which led to larger torsion between the vBDT unit and the adjacent thiophenes, thus enlarged the bandgap of polymer and significantly changed the film morphology. Blended it with ITIC-Th, P258 achieved an improved PCE over 8%. At the same year, Chen and coworkers developed a highly crystalline polymer donor PBODT by polymerizing a BO-fused dithienobenzoxadiazole (DTBO) unit and tetra-thiophene (4T) unit [201]. Due to the weak electron-withdrawing ability of DTBO building block, P259 showed a WBG of 1.88 eV, which was significantly different from that of LBG polymer with a backbone of BO-*alt*-4T. The studies of variable temperature UV–vis, grazing-incident wide-angle X-ray scattering (GIWAXS), and organic field effect transistors indicated that P259 had strong self-aggregation effect, high crystallinity, and high hole mobility. Matched with SM acceptor ITIC and IDIC, the as-cast OSCs achieved the PCEs of 7.06% and 9.09% with high V_{oc} values of 1.00 and 0.93 V, respectively. Notably, when the OSCs processed with a single non-chlorinated solvent, a high PCE of 8.19% was still achieved. Very recently, Ding and coworkers synthesized a high-performance D–A copolymer donor P260 based on a BT-fused dithienobenzothiadiazole (DTBT) unit [4]. P260 shows a WBG of 1.98 eV, a deep HOMO level of −5.51 eV, and a high hole mobility of 1.59×10^{-3} cm^2 V^{-1} s^{-1}, which could be will matched with SM acceptor Y6. As a result, the P260:Y6-based OSCs gave a PCE of 18.22%. Then, Yan and coworkers replaced the fluorinated side chains with the chlorinated side chains and developed P261 [203]. They found the replacement of fluorine atoms with chlorine atoms did not change the conformation of the polymer backbone and the molecular packing so that the P261-based devices could

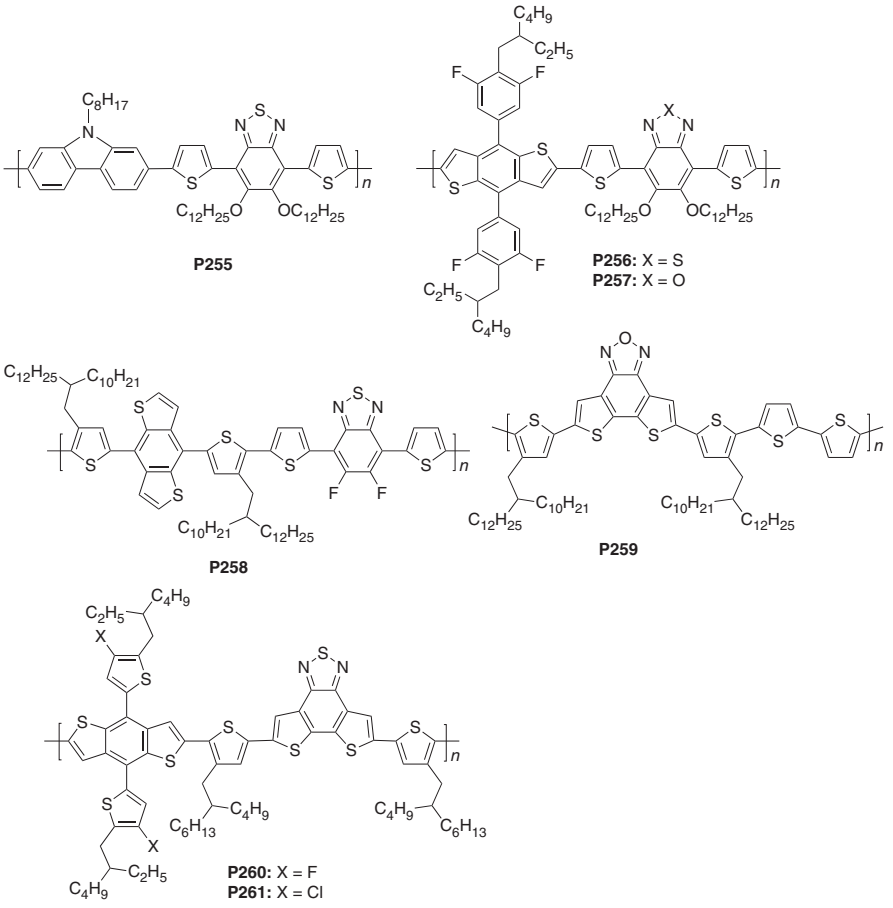

Figure 1.36 Chemical structures of the BT-derived polymers P255–P261. Source: Qunping Fan.

maintain a decent FF. P261:Y6:$PC_{71}BM$ devices achieved a higher PCE of 17.97% than P260:Y6:$PC_{71}BM$ devices (17.21%). The chemical structures of the polymer donors based on benzothiadiazole derivatives are showed in Figure 1.36, and the corresponding photovoltaic parameters of OSCs are summarized in Table 1.27.

1.4.4 WBG Polymers Based on Benzotriazole (BTA) Derivatives

BTA with a unique triazole structure has a relatively weak electron-withdrawing ability due to the lone-pair electrons on the 2-position of N contribute to the fused-triazole and its photovoltaic materials generally have strong self-aggregation and π–π stacking effects [204]. Therefore, the BTA-based polymer donors usually show a WBG, high crystallinity, high extinction coefficient, and good hole mobility. Consequently, the BTA-based polymer donors have developed rapidly and have been widely used for the efficient OSCs based on LBG SM acceptors in the past few years [205–208]. In the early studies, the high HOMO levels of BTA-based polymer donors limit their application in photovoltaic materials. To decrease the HOMO

Table 1.27 Optoelectronic properties and device performances of P255–P261.

Polymer	E_g^{opt} (eV)	HOMO/ LUMO (eV)	Acceptor	V_{oc} (V)	J_{sc} (mA cm^{-2})	FF	PCE (%)	References
P255	1.97	−5.23/−3.26	NI-T-NI	1.30	2.91	0.53	2.01	[199]
P256	1.81	−5.50/−−	$PC_{71}BM$	0.89	12.67	0.73	8.24	[200]
P257	1.82	−5.62/−−	$PC_{71}BM$	0.96	9.24	0.64	5.67	[200]
P258	1.94	−5.50/−3.56	ITIC-Th	0.93	15.2	0.56	8.1	[202]
P259	1.88	−5.44/−3.48	ITIC	1.00	10.7	0.664	7.06	[201]
P259	1.88	−5.44/−3.48	IDIC	0.93	14.1	0.693	9.09	[201]
P260	1.98	−5.51/−2.77	Y6	0.859	27.7	0.766	18.22	[4]
P261	2.00	−5.49/−3.49	Y6:$PC_{71}BM$	0.87	26.83	0.770	17.97	[203]

level of BTA-based polymers donors, You and coworkers synthesized a difluorinated benzotriazole (2fBTA) unit and developed a WBG polymer P263 [209]. Compared with its fluorine-free analog (P262), P263 obtained a dramatically improved PCE from ~4% to ~7%, owing to the higher V_{oc} and FF values. Recently, Li and coworkers designed and synthesized a series of thienyl BDT (BDT-T)-*alt*-2fBTA-structured high-performance polymer donors with WBG and deep HOMO level by modifying the 2D-conjugated thienyl of BDT unit [206–208, 210–212]. For example, polymer P265 was synthesized by introducing alkylthio substitutions into 2D-conjugated thienyls, targeting a deep-shifted HOMO level and improved crystallinity. Blending with ITIC, the P265-based OSCs obtained a PCE of 9.53% [206]. Subsequently, Fan et al. synthesized a polymer, P269 [207], *via* side chain engineering of P265. Compared with P265, P269 showed the increased steric hindrance on the BDT-T donor unit and the decreased steric hindrance on the 2fBTA acceptor unit, which resulted in stronger intermolecular π–π interactions, and more efficient charge separation and transport in its OSCs. Thus, the P269:ITIC-based OSCs achieved an improved PCE of 10.5%. Another 2fBTA-based polymer donor P266 was synthesized by attaching trialkylsilyl side chains into the 2D-conjugated thienyls [208]. Thanks to the σ* (Si)–π* (C) interaction deep-shifted the molecular HOMO level and increased absorption coefficient of P266, both higher V_{oc} and J_{sc} values were achieved in its OSCs. Fluorination of the 2D-conjugated thienyl on BDT unit has been convincingly established to be beneficial for deep-shifting molecular HOMO level and improving optical absorption, crystallinity, and charge transport of photovoltaic materials [169, 210, 211, 213]. Fan et al. reported a WBG polymer P268 based on difluorinated BDT-TF donor unit with mono-fluorinated thienyls and 2fBTA acceptor unit and found that the corresponding OSCs achieved improved photovoltaic parameters compared with those of the P270-based OSCs [210]. Subsequently, Xue et al. synthesized a tetra-fluorinated BDT-T2F donor unit with difluorinated thienyls and then developed another WBG polymer P267 with BTA unit [211]. In addition to deep-shift the molecular HOMO level and increasing absorption coefficient and hole mobility, fluorination on 2D-conjugated

thienyls of the polymers could suppress triplet formation to reduce charge carrier recombination in OSCs. With these favorable advantages, the P267:*m*-ITIC-based OSCs achieved a high PCE of 11.63%. It is well known that the introduction of chlorine atom and silicon atom substitutions into molecular backbone are two important strategies to deep-shift molecular HOMO level, improve absorption coefficient, and increase charge mobility of photovoltaic materials [208, 214]. By combining the chlorine and alkylsilyl substitutions into the 2D-conjugated thienyls of BDT-T unit, a BTA-based WBG polymer P272 was synthesized by Fan and coworkers and achieved a high PCE of 12.8% in its OSCs [212]. Yang and coworkers synthesized two BTA-based WBG polymer donors 273 and P274 with alkyloxy- or alkylthio-substituted 2D-biphenyl BDT units [215]. Using alkylthio chains instead of alkoxy chains, P274 showed a deeper HOMO level by over 0.20 eV compared to its counterpart P273, resulting in a significantly improved V_{oc}. Blending with ITIC, P274 achieved a higher PCE of 12.09% in its OSCs compared to the counterpart polymer P273 (9.20%). In the same year, Yang and coworkers synthesized a 2D–2D asymmetric BDT monomer [216]. The studies showed that this asymmetric structure had unique advantages in comparison with the conventional 2D symmetric BDT unit. The 2D-conjugated thienylthiol side chain on the BDT unit could reduce molecular HOMO level, broaden absorption spectra, and improve solubility. The bare rigid aryl of naphthalene as another 2D-conjugated side chain could be regarded as lever arms to stir up well the elongated ITIC and weaken the entanglements among polymer chains during the spin-coating process, which enabled a favorable morphology without post treatment. As a result, the corresponding BTA-based WBG polymer donor P275 with a 2D–2D asymmetric structure yielded a high PCE of 11.56% in its as-cast OSCs [216]. Currently, most high-performance WBG polymer donors are based on BDT units. Recently, Sun and coworkers developed a benzodifuran (BDF)-based polymer P276 [217], in which chlorinated thienyl BDF and BTA building blocks were used as the electron-donating and electron-withdrawing units, respectively. Blending with TTPT-T-4F, P276 obtained a remarkably higher PCE of 14.0% in OSCs compared to its analog BDT-based polymer P271 (12.72%). Yan and coworkers reported a polymer P277 with a WBG of 2.05 eV and strong aggregation properties, which was based on a BDT donor unit and a BTA acceptor unit [218]. Different with conventional BDT-based polymers with a BDT unit linked *via* the α positions of the thiophene units, the BDT units in P277 were connected *via* the phenyl group of the BDT unit. In the P277:O-IDTBR blend film, both the donor and acceptor could maintain their crystallinity and form small domains. With these favorite properties, P277 achieved a PCE of 11.6% with a high V_{oc} of 1.08 V in its OSCs. By introducing a siloxane-terminated side chain into BTA building block and its BTA-fused derivative, Huang and coworkers developed two WBG polymer donors P278 and P279 [219]. The resulting two polymers were successfully used to fabricate efficient ternary all-polymer OSCs with a LBG polymer acceptor N2200 and achieved a PCE of 9.17% with an active layer thickness of 350 nm. Subsequently, the P279:N2200-based all-polymer OSCs obtained a significantly improved PCE of 11.76% by the meticulous optimization of blend morphology in Liu's group [220].

To match the deep LUMO levels of the LBG SM acceptors, Huang and coworkers further reduced the HOMO levels of the polymer donor PTzBI series consist of a BDT electron-donating unit and a pyrrolo[3,4-*f*]benzotriazole-5,7(6*H*)-dione (TzBI) electron-withdrawing building block by introducing two 2D-conjugated difluorophenyl units on the 3,6-positions of BDT unit. The resulting WBG polymer donor P280 with 3-branched alkyl side chains of the TzBI unit showed the optimized molecular orientation and crystallinity [221]. Matching with SM acceptor IT-4F, the P280-based OSCs achieved a certified high PCE of 12.25% with both improved J_{sc} and V_{oc} on a device area of 1 cm^2. Notably, Huang and coworkers selected another SM acceptor Y6 with a similar LUMO level but a lower bandgap to match P280 for more complementary absorption and well-matched energy levels, the corresponding OSCs obtained an impressive PCE over 16% [222]. Recently, two BTA units-fused naphtho[1,2-*c*:5,6-*c*]bis(2-octyl[1-3]triazole) (TZNT) was also used as electron-withdrawing building block to construct high-performance WBG polymer donors [223, 224]. Peng and coworkers synthesized two WBG polymers, non-fluorinated P281 and fluorinated P282 with a backbone of TZNT-*alt*-bithiophene (DT) [223]. Compared to P281, P282 had a higher crystallinity, stronger absorption coefficient, and deeper HOMO level, leading to the higher PCEs of 10.60% and 11.48% in binary and ternary blend OSCs, respectively. Soon afterward, Peng and coworkers developed the others two TZNT-based WBG polymer donors P283 and P284 by using 2-alkylthio-substituted thienyl BDT (BDT-TS) unit or 2-alkylthio-3-fluorine-substituted thienyl BDT (BDT-TSF) unit instead of DT unit [224]. The rigid planar backbone of BDT-T and TZNT units imparted high crystallinity and good molecular stacking properties to these polymers. Using IT-4F as SM acceptor, the P284-based OSCs obtained a high PCE of 13.25% with a high V_{oc} of 0.93 V and a low E_{loss} of 0.59 eV. Furthermore, the P284:IT-4F-based homo-tandem devices with improved light-harvesting ability achieved a further increased PCE of 14.52%, which was the best value for homo-tandem OSCs. The chemical structures of the polymer donors based on BTA derivatives are showed in Figure 1.37, and the corresponding photovoltaic parameters of OSCs are summarized in Table 1.28.

1.4.5 WBG Polymers Based on Thiazole, Pyrazine, and Their Derivatives Containing *N*-Heterocycles

N-heterocycles-based acceptor building blocks with a weak electron-withdrawing ability, strong intramolecular noncovalent bonds and intermolecular interaction, such as bisthiazole (BTz) [225–227], thiazolo[5,4-*d*]thiazole (TTz) [228–231], benzo[1,2-*d*:4,5-*d*']bis(thiazole) (BBTz) [232], 1,3,4-thiadiazole (TDz) [233], 1,3,4-oxadiazole (ODz) [234], pyrazine (PAz) [235], quinoxaline (Qx) [236, 237], dithieno[3,2-f:2′,3′-h]quinoxaline (DTQx) [238], 1,2,4,5-tetrazine (TAz) [239], and related derivatives, have been widely used for constructing high-performance WBG polymer donors with a good planarity, deep HOMO level, high absorption coefficient, and strong crystallinity. In 2011, Zhang et al. reported a polymer donor P285 with a WBG of 2.07 eV by combining BTz as electron-withdrawing unit and alkyl-substituted IDT as weak electron-donating unit [225]. Blending with $PC_{71}BM$, its OSCs achieved a low PCE of 2.77% due to the limited absorption spectrum.

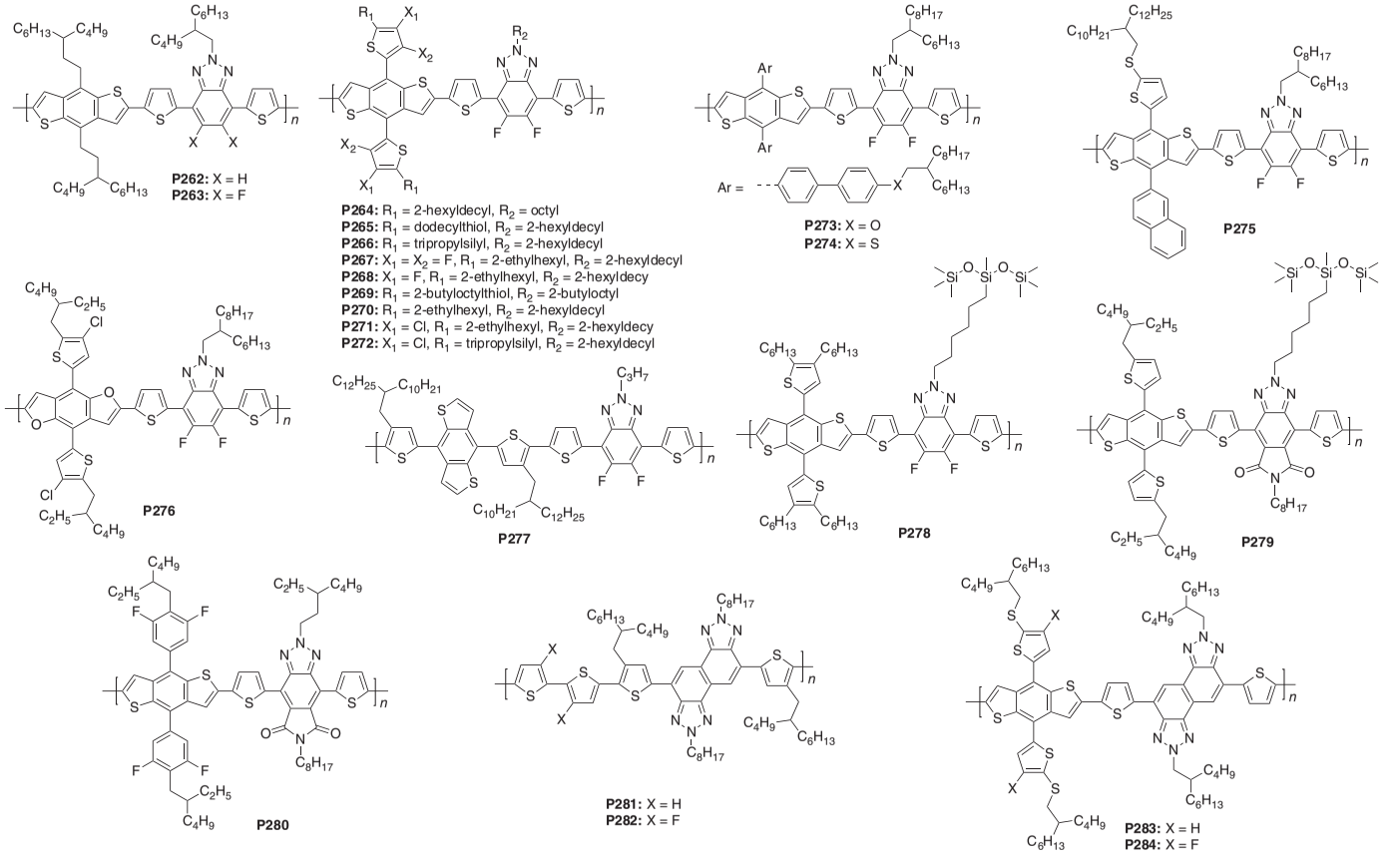

Figure 1.37 Chemical structures of the benzotriazole-derived polymers P262–P284. Source: Qunping Fan.

Table 1.28 Optoelectronic properties and device performances of P262–P284.

Polymer	E_g^{opt} (eV)	HOMO/ LUMO (eV)	Acceptor	V_{oc} (V)	J_{sc} (mA cm^{-2})	FF	PCE (%)	References
P262	1.98	−5.29/−2.87	$PC_{71}BM$	0.70	11.14	0.552	4.36	[209]
P263	2.00	−5.36/−3.05	$PC_{71}BM$	0.79	11.83	0.729	7.10	[209]
P264	1.94	−5.36/−3.42	ITIC	0.89	18.8	0.62	10.4	[210]
P265	1.93	−5.32/−3.08	ITIC	0.89	17.43	0.6148	9.53	[206]
P266	1.96	−5.40/−3.24	ITIC	0.94	17.32	0.6977	11.41	[208]
P267	2.00	−5.50/−3.02	m-ITIC	0.984	18.03	0.6554	11.63	[211]
P268	1.94	−5.36/−3.42	ITIC	0.89	18.8	0.62	10.4	[210]
P269	1.93	−5.37/−3.47	ITIC	0.89	19.0	0.62	10.5	[207]
P270	1.94	−5.18/−3.22	IT-4F	0.60	17.0	0.632	6.4	[212]
P271	1.94	−5.39/−3.41	IT-4F	0.80	17.7	0.683	9.7	[212]
P272	1.94	−5.56/−3.50	IT-4F	0.93	19.2	0.715	12.8	[212]
P273	1.93	−5.25/−3.49	ITIC	0.832	17.96	0.6156	9.20	[215]
P274	1.93	−5.46/−3.50	ITIC	0.914	18.52	0.7143	12.09	[215]
P275	1.91	−5.44/−3.49	ITIC	0.936	18.21	0.678	11.56	[216]
P276	1.86	−5.50/−3.39	TTPT-T-4F	0.86	22.17	0.736	14.0	[217]
P271	1.89	−5.48/−3.37	TTPT-T-4F	0.85	21.25	0.701	12.72	[217]
P277	2.05	−5.47/−3.42	O-IDTBR	1.08	16.26	0.636	11.6	[218]
P278	1.93	−5.23/−2.93	N2200	0.81	15.35	0.5638	7.00	[219]
P279	1.93	−5.31/−3.10	N2200	0.84	16.82	0.5187	7.34	[219]
P279	1.93	−5.31/−3.10	N2200	0.88	17.62	0.7578	11.76	[220]
P280	1.85	−5.38/−3.06	IT-4F	0.891	19.65	0.7409	12.96	[221]
P280	1.85	−5.38/−3.06	Y6	0.81	26.68	0.7411	16.02	[222]
P281	1.94	−5.16/−3.10	IT-M	0.75	10.15	0.581	4.42	[223]
P282	1.84	−5.24/−3.23	IT-M	0.80	17.33	0.725	10.05	[223]
P283	1.99	−5.39/−3.30	IT-4F	0.88	18.65	0.689	11.31	[224]
P284	1.97	−5.45/−3.41	IT-4F	0.93	19.23	0.741	13.25	[224]

Subsequently, using multi-alkyl thienyl-BDT unit instead of IDT unit, Zhang and coworkers reported another BTz-based WBG (1.89 eV) polymer donor P286 [226]. Compared to P285, P286 shows a red-shifted absorption onset from 600 to 650 nm, significantly improved planarity and crystalline structure, as well as increased hole mobility, leading to a higher PCE of 6.09% in the $PC_{71}BM$-based OSCs. Soon afterward, by replacing multi-alkyl thienyl-BDT unit with multi-alkoxyl phenyl-BDT unit in polymer backbone, Zhang and coworkers developed an efficient BTz-based polymer donor P287 [227]. Compared to P286, P287 exhibits a wider bandgap of 2.0 eV with strong absorption in the range of 300 ~ 620 nm and a lower-lying HOMO level of −5.36 eV. The OSCs based on P287:$PC_{71}BM$ showed a PCE of 8.1% with a high V_{oc} of 0.96 V, a J_{sc} of 10.9 mA cm^{-2} and a high FF of 76.7%, which was

among the highest values for the OSCs combined fullerene derivatives and polymer donors with a bandgap near to 2.0 eV. Moreover, blending with a LBG SM acceptor ITIC, its OSCs achieved a higher PCE of 10.3% with both improved V_{oc} of 1.01 V and J_{sc} of 14.1 mA cm^{-2}.

Compared to BTz unit, TTz unit has a larger fused-ring rigid structure, resulting in the stronger intermolecular aggregation and interaction of the corresponding polymers [228–230]. In 2016, Zhang and coworkers synthesized a polymer donor named PTZ1 (P288) by polymerizing BDT-T electron-donating unit and TTz electron-withdrawing unit for photovoltaic applications [228]. P288 with high crystallinity and favorable backbone orientation shows a desirable WBG of 1.97 eV, a deep HOMO level −5.31 eV, and a relatively high hole mobility >10^{-3} cm^2 V^{-1} s^{-1}. Consequently, single-junction OSCs based on P288:$PC_{71}BM$ obtained a PCE of 7.7% with a high V_{oc} of 0.94 V. Moreover, its tandem PSCs based on P288 as a donor material in the front cell achieved an improved PCE of 10.3% with a high V_{oc} of 1.65 V. Blending P288 with IDIC, the fabricated OSCs achieved the highest PCE of 11.5%, while the OSCs still obtained a PCE of 9.6% with an active layer thickness of 210 nm and a relatively high PCE of 10.5% with a device area of up to 0.81 cm^2 [229]. By incorporating a sulfur atom into 2D-conjugated alkylthienyl groups, Su et al. reported another similar WBG (1.96 eV) polymer P289 [230]. The P289-based OSCs with SM acceptors ITIC or IDIC achieved PCEs more than 8%. Moreover, by inserting ITIC into the binary P289:IDIC system, the active layer shows smooth and gradient energy levels, improved crystallinity, and optimized morphologies, which results in efficient exciton separation, charge transport and collection. Consequently, the optimized ternary OSCs based on P289:ITIC:IDIC (1 : 0.1 : 0.9) obtained a higher PCE of 11.1% in comparison with those of binary OSC systems. Recently, Huang and coworkers reported a series of WBG polymer donor analogs (P290 and P291) composed of thienothiophene (TT) or TTz units [231] and studied their device performance with N2200 in all-polymer OSCs. Results show that all-polymer OSCs with the TTz-based P291 achieved a PCE as high as 8.4%, which largely outperform the analog P290-based ones with a PCE of only 0.7%. In 2019, Yang and coworkers developed a WBG (2.1 eV) polymer donor P292 with a backbone of BDT-T-*alt*-BBTz [232]. Compared to TTz unit, BBTz unit has a further enlarged fused-ring rigid structure by inserting a benzene ring into TTz unit, resulting in the weaker electron-withdrawing ability, deep HOMO level, and stronger intermolecular aggregation and interaction of the corresponding polymers. Blending P292 with a LBG SM acceptor ITIC-F, the OSCs obtained a high PCE of 13.3% with a high V_{oc} of 0.91 V, a high J_{sc} of 20.9 mA cm^{-2}, and an FF of 0.70. TDz unit with high polarizability and relatively weak electron-withdrawing ability, has been widely studied in optoelectronic field. By polymerizing BDT and TDz building blocks, Peng and coworkers synthesized a polymer donor P293 with a WBG over 2.07 eV and a low-lying HOMO level of −5.35 eV [233], which matches well with the typical LBG SM acceptor ITIC. By using a single green solvent of o-xylene, the as-cast OSCs achieved a large V_{oc} up to 1.10 V and an extremely low E_{loss} of 0.48 eV, as well as the desirable J_{sc} of 17.78 mA cm^{-2} and FF of 65.4%, leading to a high PCE of 12.80%. When adopting a homo-tandem device architecture, the PCE is further improved to 13.35% with an improved V_{oc} of 2.13 V. After that,

by using ODz instead of TDz, Peng and coworkers reported another polymer donor P294 [234]. Compared to the TDz-based P293, P294 with a similar backbone has a wider bandgap of 2.12 eV and a deeper HOMO level of −5.68 eV. By adding 4% of copper(I) iodide as an additive to form coordination complexes with P294 for optimizing blend morphology, significantly improved device performances are achieved due to the improved absorption and crystallinity of photovoltaic materials. As a result, the PCE is elevated from 10.12% to 12.34%.

N-heterocyclic benzene derivatives, such as PAz [235], Qx [236, 237], DTQx [238], and TAz [239], also have been applied in the synthesis of WBG photovoltaic materials. Chen et al. firstly introduced F atom into PAz-based electron-withdrawing unit and successfully applied it in constructing a polymer donor P296 for OSCs [235]. Compared to its non-fluorinated counterpart P295, P296 had a better planarity, improved absorbance with red-shifted spectrum and higher absorption coefficient, reduced HOMO level, and optimized molecular packing and morphological properties. Blending with MeIC, the P296-based OSCs delivered a PCE of 12.3%, which was much higher than that of the P295-based control OSCs (10.2%). In addition to high efficiency and good stability, the application of OSCs requires the realization of low-cost devices. Sun et al. demonstrated a low-cost WBG polymer donor P297 with a simple backbone of thiophene-*alt*-(6,7-difluoro-2-(2-hexyldecyloxy)quinoxaline), which was synthesized by only two-step simple reactions with high overall yield of 87.4% from cheap raw materials [236]. More important, the P297-based OSCs achieved a high PCE of 12.70%, and the corresponding as-cast devices with thickness insensitivity also obtained a high PCE of 10.41%, which indicated that P297 was a promising polymer donor for commercial application of OSCs. By attaching an additional methyl substituent in the Qx unit of low-cost polymer donor P297, Sun et al. reported another similar polymer donor P298 [237]. Compared to P297, P298 showed an upshifted HOMO level of −5.52 eV, stronger molecular crystallization, and better hole transport capability. Impressively, the OSCs based on P298:TPT10 with near zero HOMO offset achieved a high PCE of 16.32% due to the efficient exciton dissociation and hole transfer. Recently, Hou and coworkers fused two thiophene units along with Qx to design DTQx, which is quite similar with DTBT [238]. The resulting polymer P299 achieved a high PCE of 18.0% in the ternary devices using BTA3 and BTP-eC9 as the acceptor materials. In 2019, Peng and coworkers synthesized a TAz-containing WBG polymer P300 [239]. The studies showed that P300 had a strong aggregation property, which resulted in serious phase separation and large domains when blending with Y6. To address the above defect, Peng and coworkers developed a new strategy of platinum(II) complexation to regulate molecular crystallinity and packing of TAz-based polymers, optimize blend morphology, and improve PCE of the resulting OSCs. Compared to binary polymer P300, the TAz-based ternary polymer P301 had bulky benzene ring on the platinum(II) complex to increase steric hindrance along the polymer main chain, which was beneficial to inhibit molecular aggregation strength and regulate blend morphology, and thus improved PCE to 16.35% in OSCs [239]. The chemical structures of the polymer donors based on thiazole, pyrazine, and their derivatives containing *N*-heterocycles are showed in Figure 1.38, and the corresponding photovoltaic parameters of OSCs are summarized in Table 1.29.

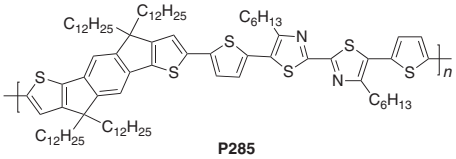

P285

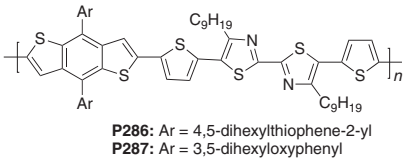

P286: Ar = 4,5-dihexylthiophene-2-yl
P287: Ar = 3,5-dihexyloxyphenyl

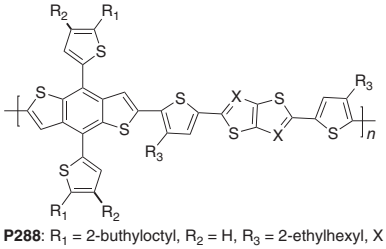

P288: R_1 = 2-buthyloctyl, R_2 = H, R_3 = 2-ethylhexyl, X = N
P289: R_1 = 2-buthyloctylthio, R_2 = H, R_3 = 2-ethylhexyl, X = N
P290: R_1 = R_2 = *n*-hexyl, R_3 = *n*-octyl, X = CH
P291: R_1 = R_2 = *n*-hexyl, R_3 = *n*-octyl, X = N

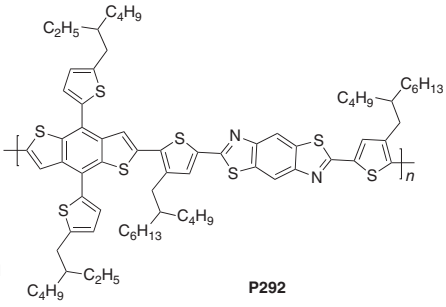

P292

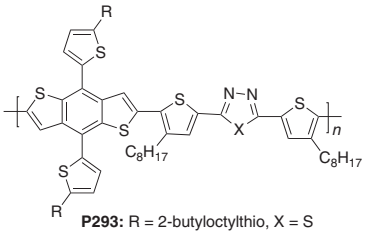

P293: R = 2-butyloctylthio, X = S
P294: R = 2-butyloctyl, X = O

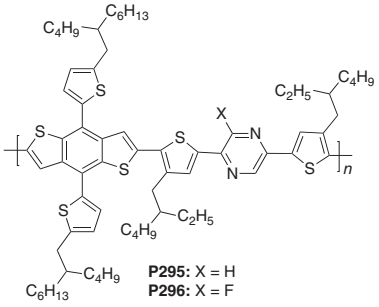

P295: X = H
P296: X = F

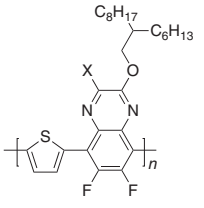

P297: X = H
P298: X = Me

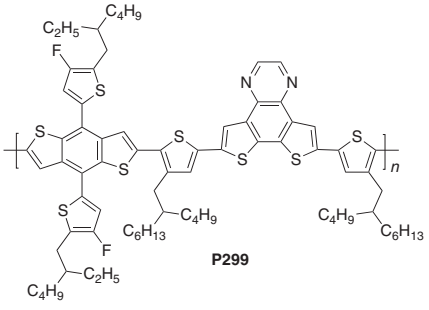

P299

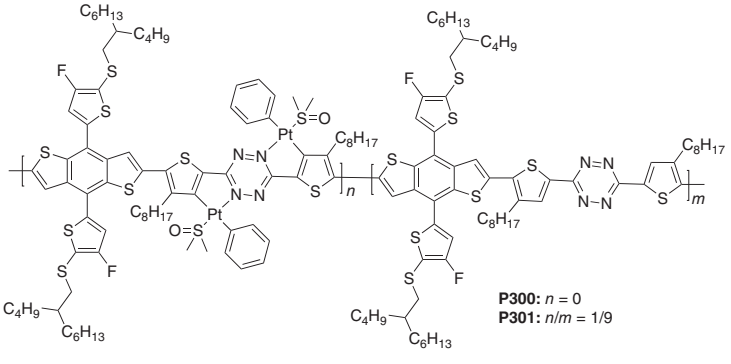

P300: *n* = 0
P301: *n*/*m* = 1/9

Figure 1.38 Chemical structures of the polymer donors based on thiazole, pyrazine, and their derivatives containing N-heterocycles P285–P301. Source: Qunping Fan.

Table 1.29 Optoelectronic properties and device performances of P285–P301.

Polymer	E_g^{opt} (eV)	HOMO/ LUMO (eV)	Acceptor	V_{oc} (V)	J_{sc} (mA cm^{-2})	FF	PCE (%)	References
P285	2.07	−5.26/−2.80	$PC_{71}BM$	0.90	7.43	0.414	2.77	[225]
P286	1.89	−5.21/−3.25	$PC_{71}BM$	0.92	10.53	0.629	6.09	[226]
P287	2.0	−5.36/−3.36	$PC_{71}BM$	0.96	10.9	0.767	8.1	[227]
P287	2.0	−5.36/−3.36	ITIC	1.01	14.1	0.723	10.3	[227]
P288	1.97	−5.31/−3.33	$PC_{71}BM$	0.95	11.3	0.72	7.7	[228]
P288	1.97	−5.31/−3.33	IDIC	0.92	16.4	0.762	11.5	[229]
P289	1.96	−5.44/−3.48	ITIC	1.01	15.4	0.523	8.13	[230]
P289	1.96	−5.44/−3.48	IDIC	0.928	14.7	0.591	8.06	[230]
P289	1.96	−5.44/−3.48	ITIC:IDIC	0.953	17.4	0.669	11.1	[230]
P290	2.01	−5.04/−3.03	N2200	0.75	2.0	0.46	0.7	[231]
P291	1.91	−5.20/−3.29	N2200	0.87	14.4	0.67	8.4	[231]
P292	2.10	−3.30/−5.40	ITIC-F	0.91	20.9	0.70	13.3	[232]
P293	2.07	−5.39/−2.80	ITIC	1.10	17.78	0.654	12.8	[233]
P294	2.12	−5.68/−2.89	ITIC-Th	1.06	17.1	0.681	12.34	[234]
P295	2.00	−5.44/−3.56	MeIC	0.95	15.54	0.688	10.2	[235]
P296	1.95	−5.48/−3.70	MeIC	0.96	17.29	0.738	12.3	[235]
P297	1.92	−5.54/−2.98	IDIC	0.969	17.81	0.736	12.7	[236]
P298	1.95	−5.52/−2.76	TPT10	0.88	17.25	0.748	16.32	[237]
P299	2.05	−5.39/−2.86	BTP-eC9	0.82	26.0	0.752	16.0	[238]
P299	2.05	−5.39/−2.86	BTA3:BTP-eC9	0.84	26.9	0.796	18.0	[238]
P300	1.93	−5.50/−3.50	Y6	0.80	25.1	0.649	13.03	[239]
P301	1.94	−5.53/−3.51	Y6	0.81	26.45	0.763	16.35	[239]

1.4.6 WBG Polymers Based on Benzodithiophene-4,8-dione (BDD) Derivatives

Benzodithiophene-4,8-dione (BDD) and its derivatives with a rigid large planarity and two fused electron-withdrawing C=O bonds have been widely used to construct high-performance polymer donors for photovoltaic applications [240–244]. Among these BDD-based polymers, the polymer donors (namely PBDB-T series) with a molecular backbone of BDT-*alt*-BDD display some unique properties, such as high absorption coefficient, WBG, temperature-dependent absorption spectra, deep-lying HOMO level, and high carrier mobility [240–251]. In 2012, Hou and coworkers developed a BDD-based WBG (1.80 eV) polymer donor with a 2D-conjugated thienyl BDT derivative, namely PBDB-T (P302) [241]. P302 displayed a strong aggregation effect in solution state, and the studies indicated that device efficiency of the P302:$PC_{61}BM$-based OSCs could be easily affected by the processing temperature used in solution preparation. By matching P302 with a LBG SM

acceptor ITIC, Hou and coworkers reported a high PCE of 11.21% [252]. After that, the following-up reports using P302 congeners sprang up in fullerene-based and SM-acceptor-based OSCs. In 2015, Zhang et al. synthesized a PBDB-T derivative, namely PM6 (PBDB-TF, P303) [242], by attaching a fluorine atom on 2D-conjugated thienyl substituents of polymer. Compared to P302, fluorinated P303 showed obviously downshifted HOMO level, stronger crystallinity, and smaller π–π stacking distance. Matching with $PC_{71}BM$, its OSCs obtained a PCE of 9.2%. P303 also could match different types of LBG SM/polymer acceptors very well with respect to absorption, energy levels, and morphological compatibility. In this regard, blending P303 with typical SM acceptor ITIC, the OSCs achieved a PCE of 9.7% with a V_{oc} up to 1.04 V [253]; with a strongly crystalline SM acceptor IDIC, the as-cast OSCs achieved the PCEs exceeded 11% with different active layer thicknesses [254]; with a tetra-fluorinated SM acceptor IT-4F, the OSCs delivered a PCE of 13.5% [255]; and with polymerized small molecular acceptors (PSMAs) such as PZ1 [256], PF1-TS4 [257], PF2-DTSi [258], PF3-DTCO [259], PFBDT-IDTIC [260], PN1 [261], and PYT [262], the all-PSCs provided the PCEs of 9 ~ 13%. Notably, matching P303 with the star SM acceptors of Y6 series, the OSCs have achieved promising PCEs of up to 15 ~ 18% [263–265]. Compared to fluorine atom, chlorine atom is more easily introduced into photovoltaic materials by low-cost strategy [214]. Fan et al. developed another P302 derivative, namely PM7 (PBDB-TCl, P304) [243], by attaching a chlorine atom on 2D-conjugated thienyl substituents of polymer. Compared to the halogen-free P302, P304 showed lower HOMO level, higher absorption coefficient, enhanced crystallinity, and higher carrier mobility. Moreover, the P304:IT-4F-based OSCs achieved a high PCE of 13.1%, which was much higher than the P302:IT-4F-based ones (5.8%). By combining the advantages of sulfur atom and fluorine atom substituents on thienyl BDT, Hou and coworkers synthesized a WBG polymer donor P305 with high absorption coefficient and deep HOMO level, and the corresponding P305:IT-4F-based OSCs also achieved a PCE more than 13% [244]. Introducing halogen atoms, such as fluorine and chlorine, on the 4-position of thiophene π-bridges of P302, the synthesized polymers P307 [245] and P309 [246] exhibited deeper HOMO level and smaller bandgap of ~1.78 eV, leading to improved photovoltaic performance in OSCs. Aiming to enhance the carrier transport ability, Qin et al. enlarged the 2D-conjugated side groups of P302 from thiophene to benzo[*b*]thiophen and synthesized a new polymer P310 [247]. Due to P310 had good solubility and enhanced aggregation effect in tetrahydrofuran (THF), the THF-processed P310:IT-M-based OSCs achieved a PCE of 12.10%. Liu et al. synthesized a series of PBDT-T derivatives, P311–P313 and found that the subtle atom changes in 2D-benzene on BDT unit can profound effect the electronic structure and self-assembly of polymers [248]. Among these polymers, P311 achieved a much higher PCE of 10% with a record FF of 80.5% in the $PC_{71}BM$-based OSCs due to the formation of optimal interpenetrating network morphology. By further attaching two chlorine atoms on the thiophene π-bridges of P311, an optimized WBG polymer donor P314 with a deeper HOMO level and improved crystallinity was synthesized by Ye et al. and achieved a higher PCE of 12.7% [249]. Moreover, Li et al. found that introducing fluorination on 2D-benzene on BDT unit also could significantly

reduce the HOMO level of polymers, and the resulting WBG polymer donor P315 with 2D-conjugated alkoxyl-fluorophenyl side chains obtained an increased PCE of 11.7% in comparison with non-fluorinated P312 (6.2%) [250]. Xu et al. designed a WBG polymer donor P316 based on 2D-conjugated *m*-alkoxyphenyl BDT and BDD units [251]. Matching with $PC_{71}BM$, the P316-based OSCs achieved a PCE of 8.4% with a high V_{oc} of 0.95 V. Consequently, the photovoltaic performance of P316 in devices was further improved by pairing it with ITIC, and the related OSCs achieved a PCE of 10.8% [266].

In addition to optimizing 2D-conjugated groups on BDT unit and introducing halogen atoms into thiophene π-bridges of P302, the modification of fused-ring building blocks of BDT and BDD units also have attracted great attentions. Chao et al. synthesized a new electron-withdrawing fused-ring building block of 2,3-bis(2-ethylhexyl)benzo[1,2-*b*:4,5-*c*′]dithiophene-4,8-dione (TTDO) *via* the design of cyclohexane-1,4-dione embedded into a thieno[3,4-*b*]thiophene [267]. Then, by polymerizing TTDO with fluorinated thienyl BDT, they developed a WBG (1.80 eV) polymer donor, P317. Blended with SM acceptor Y6, the P317-based OSCs obtained a PCE of 16.1% with a high FF of 77.1%. Compared to BDT unit, dithieno[2,3-*d*;2′,3′-*d*′]benzo[1,2-*b*;4,5-*b*′]dithiophene (DTBDT) with extended π-conjugation and larger molecular planarity could effectively improve the charge carrier transport of the related photovoltaic materials. Inspired these, Huo et al. reported a WBG (1.85 eV) polymer P318 by polymerizing an electron-rich DTBDT unit and an electron-deficient BDD unit [268]. P318 had a highly rigid backbone since both DTBDT and BDD units were rigid and planar, and its OSCs with a $PC_{71}BM$ acceptor achieved a high PCE of 9.7%, which was the highest value reported in the OSCs based on WBG polymer donors. By using NDT with extended π-conjugation and larger molecular planarity as electron-donating unit, Peng and coworkers developed WBG polymer donors P319 and P320 for efficient OSCs [269, 270]. Compared to its analogous polymers (P302 and P306), P319 and P320 showed higher crystallinity and stronger aggregation, which induced large phase separation with poorer morphology. To optimize the morphology, P319 and P306 were blended with SM acceptor Y6-T for forming the ternary blend devices. As expected, the optimized ternary OSCs achieved a PCE as high as 16.57%. Ternary copolymerization strategies have proven advantageous in boosting the photovoltaic performance of OSCs [271]. Cui et al. reported a WBG terpolymer P321 by incorporating an electron-withdrawing unit of ester-substituted thiophene into polymer P303 to downshift molecular HOMO level and broaden absorption [272]. In the P321:IT-4F-based OSCs, a high PCE of 15.1% was obtained. Soon afterward, Sun et al. synthesized a fluorine and ester-functionalized thiophene (FE-T) with electron-withdrawing ability and then developed another WBG terpolymer donor P322 by incorporating FE-T as the third component into polymer P303 to fine-tune the energy levels and crystallinity [273]. Blending P322 with an SM acceptor Y6, the OSCs achieved a high PCE of 16.4% with a small E_{loss} of 0.53 eV. Moreover, by incorporating 1 mol% concentration of iridium (Ir) complexes into the polymer-conjugated backbone of P303, Wang et al. developed a WBG terpolymer donor P323 [274]. The studies indicated that the introduction of small amount

Ir-complexes could rationally modify the molecular aggregations and carefully control the corresponding blend morphology and physical mechanisms. As a result, the P323:Y6-based OSCs delivered a high PCE of 17.32%, which was much better than that of the P303:Y6-based ones (15.39%). The chemical structures of the polymer donors based on BDD derivatives are showed in Figure 1.39, and the corresponding photovoltaic parameters of OSCs are summarized in Table 1.30.

1.4.7 Other WBG Polymers

In addition to the above-summarized WBG polymers with some typical acceptor units, there still has many other building blocks employed to construct high-performance WBG polymer donors (Figure 1.40, Table 1.31). Cao et al. synthesized a fused pentacyclic aromatic lactam building block (thieno[2′,3′:5,6]pyrido[3,4-*g*]thieno[3,2-*c*]isoquinoline-5,11(4*H*,10*H*)-dione [TPTI]) with weak electron-withdrawing ability and then developed a D-A conjugated polymer donor P324 with a backbone of TPTI-*alt*-thiophene [275]. P324 possessed a WBG (1.86 eV) and a deep HOMO level, and the corresponding P324:$PC_{71}BM$-based OSCs afforded an outstanding PCE up to 7.80% with a high V_{oc} of 0.87 V, which was one of the best PCEs in OSCs based on WBG polymer donor. Liao et al. reported a series of readily accessible and scalable polymer donors (P325–P328) with a backbone of BDT-*alt*-2,5-dithienyl TPD for application in OSCs blended with IT-4F [276]. All polymers readily dissolved in non-chlorinated solvents, and the corresponding active layers could be processed in ambient from xylene as solvent to fabricate OSCs with PCEs of 12 ~ 14%. In the P328:IT-4F-based OSC modules processed in ambient from a benign solvent, a certified PCE of 10.1% for a device area of 20.4 cm^2 was achieved. Moreover, the same module also delivered a power of ~40 μW cm^{-2} (PCE ~22%) under indoor lighting. Liu et al. designed a fused building block of 5H-dithieno[3,2-*b*:2′,3′-*d*]pyran-5-one with weak electron-withdrawing ability and then synthesized a polymer donor P329 with a WBG of 1.96 eV and a deep HOMO level of −5.45 eV [277]. Blending P329 with Y6, the OSCs provided a PCE over 14%. To fully exploit the potential of P329 series polymers, Ding and coworkers developed another WBG polymer donor P330 with a thiolactone unit of 5H-dithieno[3,2-*b*:2′,3′-*d*]thiopyran-5-one [278]. From P229 to P330, the simple replacement of lactone with thiolactone enhanced molecular π–π stacking, gifting P330 a higher hole mobility. When matched with Y6, its OSCs gave a high PCE up to 16.72%. The mechanism that how noncovalent conformation locked to improve the photovoltaic performance of WBG polymer donors was also investigated. By developing a model system with three structure-related polymers P331–P333, a clear correlation was found between the locking strength in polymer backbone and the photovoltaic performance [279]. Among three polymers, P331 with the strongest S···O and F···H double-side locking showed improved planarity, packing, crystallinity, and hole mobility compared to these of P332 with a S···O single-side locking and P333 with a weakened S···O locking caused by Cl–H steric repulsion, which gave the highest PCE of 16.23% in the P331:Y6-based OSCs, while the OSCs based on P332:Y6 and P333:Y6 achieved PCEs of 11.73% and 0.92%, respectively. He

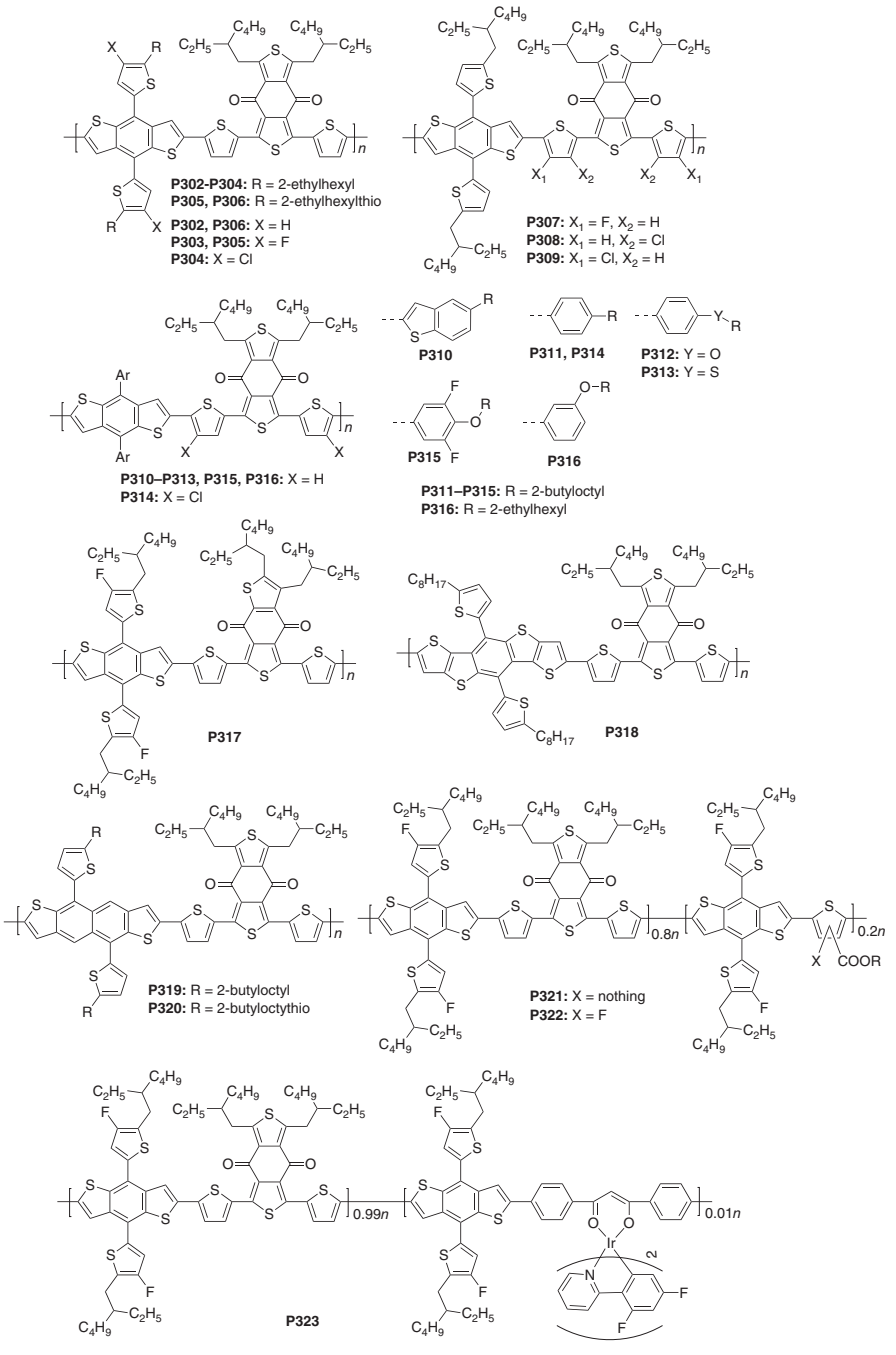

Figure 1.39 Chemical structures of the BDD derived polymers P302–P323. Source: Qunping Fan.

Table 1.30 Optoelectronic properties and device performances of P302–P323.

Polymer	E_g^{opt} (eV)	HOMO/ LUMO (eV)	Acceptor	V_{oc} (V)	J_{sc} (mA cm^{-2})	FF	PCE (%)	References
P302	1.80	−5.23/−3.18	$PC_{61}BM$	0.86	10.68	0.7227	6.67	[241]
P302	1.80	−5.23/−3.18	ITIC	0.899	16.81	0.742	11.21	[252]
P303	1.80	−5.50/−3.61	$PC_{71}BM$	0.98	12.7	0.74	9.2	[242]
P303	1.80	−5.50/−3.61	ITIC	1.04	16.0	0.58	9.7	[253]
P303	1.80	−5.50/−3.61	IDIC	0.97	17.8	0.69	11.9	[254]
P303	1.80	−5.50/−3.61	IT-4F	0.84	22.2	0.725	13.5	[255]
P303	1.80	−5.50/−3.61	PZ1	0.96	17.1	0.682	11.2	[256]
P303	1.80	−5.50/−3.61	PF2-DTSi	0.99	16.48	0.661	10.77	[258]
P303	1.80	−5.50/−3.61	PYT	0.93	21.78	0.6633	13.44	[262]
P303	1.80	−5.50/−3.61	Y6	0.83	25.3	0.748	15.7	[263]
P303	1.80	−5.49/−3.47	L8-BO	0.87	25.72	0.815	18.32	[265]
P304	1.80	−5.52/−3.57	IT-4F	0.88	20.9	0.711	13.1	[243]
P305	1.80	−5.40/−3.60	IT-4F	0.88	20.5	0.719	13.0	[244]
P307	1.78	−5.47/−3.46	C8-ITIC	0.94	19.6	0.72	13.2	[245]
P309	1.78	−5.48/−3.47	IT-4F	0.84	20.6	0.7109	12.33	[246]
P310	1.80	−5.36/−−	IT-M	0.96	17.97	0.70	12.1	[247]
P311	1.84	−5.43/−3.36	$PC_{71}BM$	0.93	13.1	0.805	10.0	[248]
P312	1.82	−5.30/−3.30	$PC_{71}BM$	0.88	11.1	0.727	7.2	[248]
P313	1.83	−5.45/−3.37	$PC_{71}BM$	0.93	11.6	0.715	7.8	[248]
P314	1.85	−5.59/−3.53	IT-4F	0.85	19.74	0.76	12.7	[249]
P312	1.81	−5.38/−3.57	IT-4F	0.72	16.8	0.512	6.2	[250]
P315	1.86	−5.50/−3.64	IT-4F	0.89	20.4	0.645	11.7	[250]
P316	1.90	−5.42/−3.36	$PC_{71}BM$	0.95	12.4	0.71	8.4	[251]
P316	1.90	−5.42/−3.36	ITIC	1.01	18.1	0.59	10.8	[266]
P317	1.80	−5.48/−3.68	Y6	0.84	24.8	0.771	16.1	[267]
P318	1.93	−5.36/−3.43	$PC_{71}BM$	0.92	14.11	0.75	9.74	[268]
P306	1.83	−5.47/−3.57	Y6-T	0.909	24.04	0.758	16.57	[270][a)]
P320	1.81	−5.43/−3.54						
P321	1.83	−5.48/−3.63	IT-4F	0.899	21.5	0.78	15.1	[272]
P322	1.83	−5.52/−3.72	Y6	0.877	25.402	0.737	16.42	[273]
P323	1.83	−5.55/−3.60	Y6	0.845	26.15	0.784	17.32	[274]

a) Device parameters from the ternary devices based on P306:319:Y6-T.

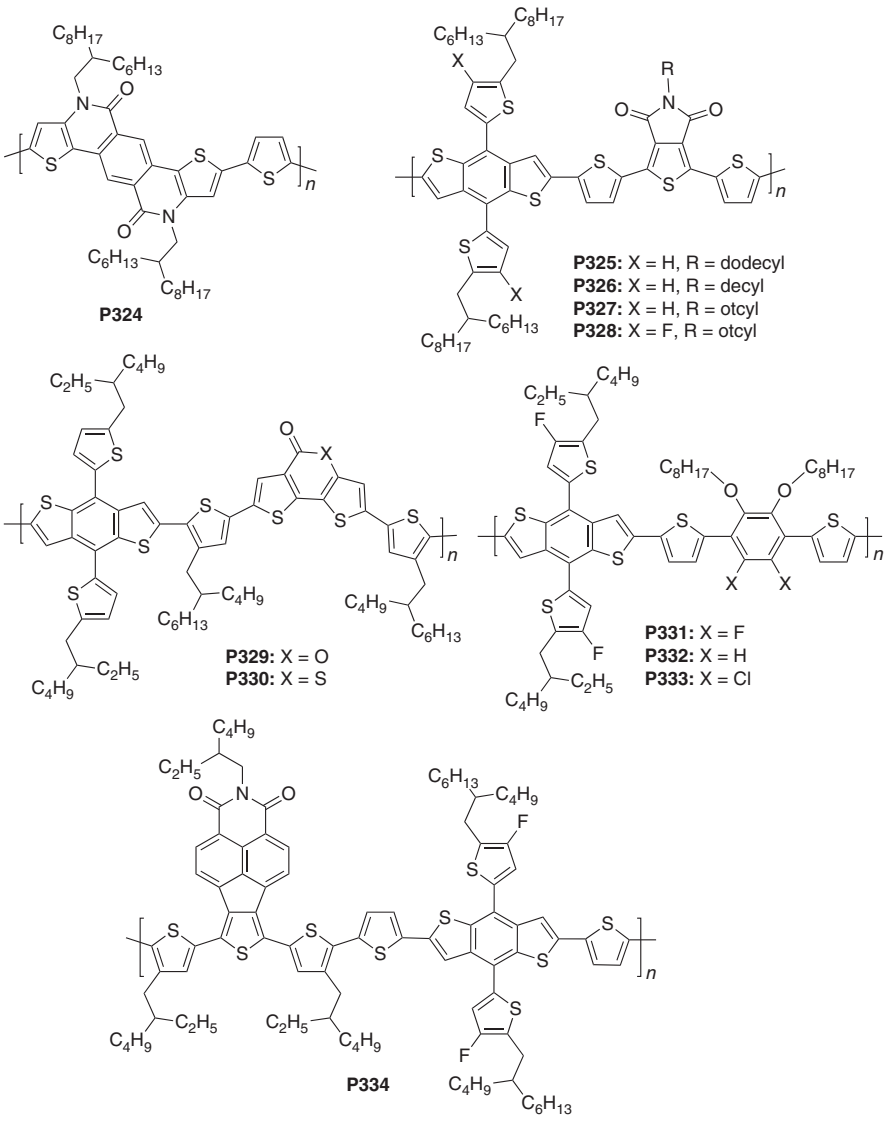

Figure 1.40 Chemical structures of the WBG polymer donors of P324–P334. Source: Qunping Fan.

and coworkers reported a new electron-deficient monomer naphthalenothiophene imide (NTI) and NTI-based copolymer P334 [280]. The strong electron-withdrawing ability of NTI could effectively lower the HOMO level of the polymer (−5.52 eV). The polymer chain modification resulted in the closed π–π stacking and ordered polymer packing of P334 and was proven to be an effective strategy to increase the device performance. OSC devices for P334:Y6 exhibited an efficiency of 16.72%, which was further enhanced to 17.35% by the third component $PC_{71}BM$.

Table 1.31 Optoelectronic properties and device performances of the WBG polymer donors of P324–P334.

Polymer	E_g^{opt} (eV)	HOMO/ LUMO (eV)	Acceptor	V_{oc} (V)	J_{sc} (mA cm^{-2})	FF	PCE (%)	References
P324	1.86	−5.42/−2.77	$PC_{71}BM$	0.87	13.69	0.656	7.8	[275]
P325	1.87	−5.48/−3.61	IT-4F	0.81	19.4	0.747	11.7	[276]
P326	1.88	−5.45/−3.57	IT-4F	0.81	19.6	0.742	11.8	[276]
P327	1.90	−5.49/−3.59	IT-4F	0.80	20.1	0.753	12.1	[276]
P328	1.90	−5.62/−3.73	IT-4F	0.92	21.6	0.723	14.4	[276]
P329	1.96	−5.45/−2.79	Y6	0.80	23.93	0.747	14.36	[277]
P330	1.96	−5.48/−2.83	Y6	0.85	25.41	0.749	16.22	[278]
P331	2.16	−5.44/−3.48	Y6	0.881	26.01	0.708	16.23	[279]
P332	2.18	−5.44/−3.48	Y6	0.846	22.44	0.618	11.73	[279]
P333	2.37	−5.04/−3.03	Y6	0.843	3.39	0.322	0.92	[279]
P334	1.79	−5.52/−3.43	Y6	0.872	26.31	0.73	16.72	[280]
P334	1.79	−5.52/−3.43	Y6:$PC_{71}BM$	0.875	26.45	0.75	17.35	[280]

1.5 Summary and Outlook

In this part, we have summarized several representative types of LBG, MBG, and WBG polymer donors and discussed the relationship between the chemical structures and the optical, electronic, and device performance. With the rapid development of non-fullerene acceptors, the number of publications of LBG and MBG polymers is far behind than WBG polymers in recent years, but it is undeniable that LBG and MBG polymers have made great contributions to the field of OSCs. Although WBG polymers have dominated the high performance in the current fullerene-free PSCs, LBG and MBG polymer donors will continue play an important role in OSCs, especially in semi-transparent, ternary, and tandem devices.

References

1 Yu, G., Gao, J., Hummelen, J.C. et al. (1995). *Science* 270: 1789.
2 Boudreault, P.-L.T., Najari, A., and Leclerc, M. (2011). *Chem. Mater.* 23: 456.
3 Thompson, B.C. and Frechet, J.M. (2008). *Angew. Chem. Int. Ed.* 47: 58.
4 Liu, Q.S., Jiang, Y.F., Jin, K. et al. (2020). *Sci. Bull.* 65: 272.
5 Lin, Y.B., Adilbekova, B., Firdaus, Y. et al. (2019). *Adv. Mater.* 31: 1902965.
6 Subbiah, J., Beaujuge, P.M., Choudhury, K.R. et al. (2009). *ACS Appl. Mater. Interfaces* 1: 1154.
7 Bin, H., Zhong, L., Zhang, Z.G. et al. (2016). *Sci. China Chem.* 59: 1317.
8 Cai, Y.H., Huo, L.J., and Sun, Y.M. (2017). *Adv. Mater.* 29: 1605437.

9 Jung, J.W., Liu, F., Russell, T.P., and Jo, W.H. (2015). *Adv. Mater.* 27: 7462.
10 Jung, J.W., Liu, F., Russell, T.P., and Jo, W.H. (2015). *Adv. Energy Mater.* 5: 1500065.
11 Zhou, H., Yang, L., Price, S.C. et al. (2010). *Angew. Chem. Int. Ed.* 49: 7992.
12 Zhou, H., Yang, L., Stoneking, S., and You, W. (2010). *ACS Appl. Mater. Interfaces* 2: 1377.
13 Dou, L., Liu, Y., Hong, Z. et al. (2015). *Chem. Rev.* 115: 12633.
14 Hildner, R., Köhler, A., Müller-Buschbaum, P. et al. (2017). *Adv. Energy Mater.* 7: 1700314.
15 Cheng, Y.-J., Yang, S.-H., and Hsu, C.-S. (2019). *Chem. Rev.* 109: 5868.
16 Brus, V.V., Lee, J., Luginbuhl, B.R. et al. (2019). *Adv. Mater.* 31: 1900904.
17 Mühlbacher, D., Scharber, M., Morana, M. et al. (2006). *Adv. Mater.* 18: 2884.
18 Bijleveld, J.C., Shahid, M., Gilot, J. et al. (2009). *Adv. Funct. Mater.* 19: 3262.
19 Chen, H.Y., Hou, J.H., Hayden, A.E. et al. (2010). *Adv. Mater.* 22: 371.
20 Scharber, M.C., Koppe, M., Gao, J. et al. (2010). *Adv. Mater.* 22: 367.
21 Gasparini, N., Jiao, X.C., Heumueller, T. et al. (2016). *Nat. Energy* 1: 16118.
22 Albrecht, S., Janietz, S., Schindler, W. et al. (2012). *J. Am. Chem. Soc.* 134: 14932.
23 Jo, J.W., Jung, J.W., Jung, E.H. et al. (2015). *Energy Environ. Sci.* 8: 2427.
24 You, J., Dou, L., Yoshimura, K. et al. (2013). *Nat. Commun.* 4: 1446.
25 Shi, S., Liao, Q., Tang, Y. et al. (2016). *Adv. Mater.* 28: 9969.
26 Zhou, H., Yang, L., Price, S.C. et al. (2010). *Angew. Chem. Int. Ed.* 49: 7992.
27 Yau, C.P., Fei, Z., Ashraf, R.S. et al. (2014). *Adv. Funct. Mater.* 24: 678.
28 Hendriks, K.H., Heintges, G.H.L., Gevaerts, V.S. et al. (2013). *Angew. Chem. Int. Ed.* 52: 8341.
29 Wang, M., Hu, X., Liu, P. et al. (2011). *J. Am. Chem. Soc.* 133: 9638.
30 Vohra, V., Kawashima, K., Kakara, T. et al. (2015). *Nat. Photonics* 9: 403.
31 Jin, Y., Chen, Z., Dong, S. et al. (2016). *Adv. Mater.* 28: 9811.
32 Jin, Y., Chen, Z., Xiao, M. et al. (2017). *Adv. Energy Mater.* 7: 1700944.
33 Kawashima, K., Fukuhara, T., Suda, Y. et al. (2016). *J. Am. Chem. Soc.* 138: 10265.
34 Kawashima, K., Tamai, Y., Ohkita, H. et al. (2015). *Nat. Commun.* 6: 10085.
35 Nielsen, C.B., Ashraf, R.S., Treat, N.D. et al. (2015). *Adv. Mater.* 27: 948.
36 Wang, C., Xu, X., Zhang, W. et al. (2016). *Adv. Energy Mater.* 6: 1600148.
37 Bianchi, L., Zhang, X., Chen, Z. et al. (2019). *Chem. Mater.* 31: 6519.
38 Zhou, P., Zhang, Z.G., Li, Y. et al. (2014). *Chem. Mater.* 26: 3495.
39 Wee, X.K., Yeo, W.K., Zhang, B. et al. (2009). *Bioorg. Med. Chem.* 17: 7562.
40 Yuen, J.D. and Wudl, F. (2013). *Energy Environ. Sci.* 6: 392.
41 Mei, J., Graham, K.R., Stalder, R., and Reynolds, J.R. (2010). *Org. Lett.* 12: 660.
42 Wang, E., Mammo, W., and Andersson, M.R. (2014). *Adv. Mater.* 26: 1801.
43 Zhang, G., Fu, Y., Xie, Z., and Zhang, Q. (2011). *Macromolecules* 44: 1414.
44 Wang, E., Ma, Z., Zhang, Z. et al. (2010). *Chem. Commun.* 47: 4908.
45 Stalder, R., Mei, J., Subbiah, J. et al. (2011). *Macromolecules* 44: 6303.
46 Ma, Z., Wang, E., Vandewal, K. et al. (2011). *Appl. Phys. Lett.* 99: 143302.
47 Ma, Z., Sun, W., Himmelberger, S. et al. (2014). *Energy Environ. Sci.* 7: 361.

48 Xu, X., Cai, P., Lu, Y. et al. (2013). *J. Polym. Sci., Part A: Polym. Chem.* 51: 424.
49 Cao, K., Wu, Z., Li, S. et al. (2013). *J. Polym. Sci., Part A: Polym. Chem.* 51: 94.
50 Fang, L., Zhou, Y., Yao, Y.-X. et al. (2013). *Chem. Mater.* 25: 4874.
51 Jung, E.H. and Jo, W.H. (2014). *Energy Environ. Sci.* 7: 650.
52 Xu, X., Li, L., Liu, B., and Zou, Y. (2011). *Appl. Phys. Lett.* 98: 063303.
53 Zhang, M., Gu, Y., Guo, X. et al. (2013). *Adv. Mater.* 25: 4944.
54 Zheng, Y.Q., Wang, Z., Dou, J.H. et al. (2015). *Macromolecules* 48: 5570.
55 Hu, H., Jiang, K., Kim, J.-H. et al. (2016). *J. Mater. Chem. A* 4: 5039.
56 Deng, Y., Liu, J., Wang, J. et al. (2014). *Adv. Mater.* 26: 471.
57 Chen, M.S., Niskala, J.R., Unruh, D.A. et al. (2013). *Chem. Mater.* 25: 4088.
58 Yue, W., Ashraf, R.S., Nielsen, C.B. et al. (2015). *Adv. Mater.* 27: 4702.
59 Randell, N.M., Radford, C.L., Yang, J. et al. (2018). *Chem. Mater.* 30: 4864.
60 Nielsen, C.B., Turbiez, M., and McCulloch, I. (2013). *Adv. Mater.* 25: 1859.
61 Mei, J., Graham, K.R., Stalder, R. et al. (2011). *Chem. Mater.* 23: 2285.
62 Kanimozhi, C., Yaacobi-Gross, N., Chou, K.W. et al. (2012). *J. Am. Chem. Soc.* 134: 16532.
63 Chen, M.S., Lee, O.P., Niskala, J.R. et al. (2013). *J. Am. Chem. Soc.* 135: 19229.
64 van Franeker, J.J., Heintges, G.H.L., Schaefer, C. et al. (2015). *J. Am. Chem. Soc.* 137: 11783.
65 Li, W., Hendriks, K.H., Furlan, A. et al. (2013). *J. Am. Chem. Soc.* 135: 18942.
66 Choi, H., Ko, S.-J., Kim, T. et al. (2015). *Adv. Mater.* 27: 3318.
67 Hendriks, K.H., Li, W., Wienk, M.M., and Janssen, R.A. (2014). *J. Am. Chem. Soc.* 136: 12130.
68 Li, W., Furlan, A., Roelofs, W.S. et al. (2014). *Chem. Commun.* 50: 679.
69 Sonar, P., Singh, S.P., Li, Y. et al. (2014). *Energy Environ. Sci.* 4: 2288.
70 Zoombelt, A.P., Mathijssen, S.G.J., Turbiez, M.G.R. et al. (2010). *J. Mater. Chem.* 20: 2240.
71 Jo, J., Gendron, D., Najari, A. et al. (2010). *Appl. Phys. Lett.* 97: 203303.
72 Peng, Q., Huang, Q., Hou, X.B. et al. (2012). *Chem. Commun.* 48: 11452.
73 Dou, L., You, J., Yang, J. et al. (2012). *Nat. Photonics* 6: 180.
74 Dou, L., Gao, J., Richard, E. et al. (2012). *J. Am. Chem. Soc.* 134: 10071.
75 Li, W., Hendriks, K.H., Furlan, A. et al. (2014). *Adv. Mater.* 26: 1565.
76 Li, W., Hendriks, K.H., Furlan, A. et al. (2015). *J. Am. Chem. Soc.* 137: 2231.
77 Dou, L., Chang, W.H., Gao, J. et al. (2013). *Adv. Mater.* 25: 825.
78 Ashraf, R.S., Meager, I., Nikolka, M. et al. (2015). *J. Am. Chem. Soc.* 137: 1314.
79 Jung, J.W., Liu, F., Russell, T.P., and Jo, W.H. (2013). *Chem. Commun.* 49: 8495.
80 Bijleveld, J.C., Zoombelt, A.P., Mathijssen, S.G.J. et al. (2009). *J. Am. Chem. Soc.* 131: 16616.
81 Yiu, A.T., Beaujuge, P.M., Lee, O.P. et al. (2012). *J. Am. Chem. Soc.* 134: 2180.
82 Hendriks, K.H., Li, W., Heintges, G.H.L. et al. (2014). *J. Am. Chem. Soc.* 136: 11128.
83 Feng, K., Yang, G., Xu, X. et al. (2018). *Adv. Energy Mater.* 8: 1602773.
84 Zhang, G., Xu, X., Bi, Z. et al. (2018). *Adv. Funct. Mater.* 28: 1706404.
85 Yao, H., Ye, L., Zhang, H. et al. (2016). *Chem. Rev.* 116: 7397.
86 Hou, J., Park, M.H., Zhang, S. et al. (2008). *Macromolecules* 41: 6012.

87 Subbiah, J., Purushothaman, B., Chen, M. et al. (2015). *Adv. Mater.* 27: 702.
88 Huo, L., Hou, J., Zhang, S. et al. (2010). *Angew. Chem.* 122: 1542.
89 Peng, Q., Liu, X., Su, D. et al. (2011). *Adv. Mater.* 23: 4554.
90 Chen, W., Xiao, M., Han, L. et al. (2016). *ACS Appl. Mater. Interfaces* 8: 19665.
91 Stuart, A.C., Tumbleston, J.R., Zhou, H. et al. (2013). *J. Am. Chem. Soc.* 135: 1806.
92 Dong, Y., Yang, H., Wu, Y. et al. (2019). *J. Mater. Chem. A* 7: 2261.
93 Shin, J., Kim, M., Lee, J. et al. (2015). *RSC Adv.* 5: 106044.
94 Zhang, M., Gu, Y., Guo, X. et al. (2013). *Adv. Mater.* 25: 4944.
95 Gong, X., Li, G., Li, C. et al. (2015). *J. Mater. Chem. A* 3: 20195.
96 Shin, J., Kim, M., Kang, B. et al. (2017). *J. Mater. Chem. A* 5: 16702.
97 Chen, W., Du, Z., Han, L. et al. (2015). *J. Mater. Chem. A* 3: 3130.
98 Shin, J., Kim, M., Lee, J. et al. (2017). *Chem. Commun.* 53: 1176.
99 Lee, J., Kim, J.-H., Moon, B. et al. (2015). *Macromolecules* 48: 1723.
100 Wang, J., Xiao, M., Chen, W. et al. (2014). *Macromolecules* 47: 7823.
101 Li, Z., Zhang, T., Xin, Y. et al. (2016). *J. Mater. Chem. A* 4: 18598.
102 Liu, D., Zhu, Q., Gu, C. et al. (2016). *Adv. Mater.* 28: 8490.
103 Liu, D., Wang, J., Gu, C. et al. (2018). *Adv. Mater.* 30: 1705870.
104 Ren, J., Bao, X., Han, L. et al. (2015). *Polym. Chem.* 6: 4415.
105 Duan, C., Furlan, A., van Franeker, J.J. et al. (2015). *Adv. Mater.* 27: 4461.
106 Kranthiraja, K., Gunasekar, K., Cho, W. et al. (2015). *J. Mater. Chem. C* 3: 796.
107 Fan, L., Cui, R., Guo, X. et al. (2014). *J. Mater. Chem. C* 2: 5651.
108 Huo, L., Huang, Y., Fan, B. et al. (2012). *Chem. Commun.* 48: 3318.
109 Zhang, Y., Gao, L., He, C. et al. (2013). *Polym. Chem.* 4: 1474.
110 Ashraf, R.S., Schroeder, B.C., Bronstein, H.A. et al. (2013). *Adv. Mater.* 25: 2029.
111 Fei, Z., Ashraf, R.S., Huang, Z. et al. (2012). *Chem. Commun.* 48: 2955.
112 Xu, Y.X., Chueh, C.C., Yip, H.L. et al. (2012). *Adv. Mater.* 24: 6356.
113 Hu, H., Jiang, K., Yang, G. et al. (2015). *J. Am. Chem. Soc.* 137: 14149.
114 Nguyen, T.L., Choi, H., Ko, S.J. et al. (2014). *Energy Environ. Sci.* 7: 3040.
115 Kang, H., Uddin, M.A., Lee, C. et al. (2015). *J. Am. Chem. Soc.* 137: 2359.
116 An, M., Xie, F., Geng, X. et al. (2017). *Adv. Energy Mater.* 7: 1602509.
117 Li, D., Xiao, Z., Wang, S. et al. (2018). *Adv. Energy Mater.* 8: 1800397.
118 Chen, H., Hu, Z., Wang, H. et al. (2018). *Joule* 2: 1623.
119 Feng, L.W., Chen, J., Mukherjee, S. et al. (2020). *ACS Energy Lett.* 5: 1780.
120 Xu, X., Li, K., Li, Z. et al. (2015). *Polym. Chem.* 6: 2337.
121 Xu, X.P., Wu, Y.L., Fang, J.F. et al. (2014). *Chem. Eur. J.* 20: 13259.
122 Wu, H., Zhao, B., Wang, W. et al. (2015). *J. Mater. Chem. A* 3: 18115.
123 Wang, M., Ma, D., Shi, K. et al. (2015). *J. Mater. Chem. A* 3: 2802.
124 Fan, Q., Xiao, M., Liu, Y. et al. (2015). *Polym. Chem.* 6: 4290.
125 Fan, Q., Jiang, H., Liu, Y. et al. (2016). *J. Mater. Chem. C* 4: 2606.
126 Yuan, J., Qiu, L., Zhang, Z.G. et al. (2016). *Nano Energy* 30: 312.
127 Xu, S., Feng, L., Yuan, J. et al. (2017). *ACS Appl. Mater. Interfaces* 9: 18816.
128 Qiao, Z., Wang, M., Zhao, M. et al. (2015). *Polym. Chem.* 6: 8203.
129 Putri, S.K., Kim, Y.H., Whang, D.R. et al. (2017). *Org. Electron.* 47: 14.
130 Zheng, Z., Awartani, O.M., Gautam, B. et al. (2017). *Adv. Mater.* 29: 1604241.

131 Zhang, Y., Ren, F., Li, Q. et al. (2018). *J. Mater. Chem. C* 6: 4658.
132 Li, G., Lu, Z., Li, C., and Bo, Z. (2015). *Polym. Chem.* 6: 1613.
133 Fang, T., Lu, Z., Lu, H. et al. (2015). *Polymer* 71: 43.
134 Zhang, F., Bijleveld, J., Perzon, E. et al. (2008). *J. Mater. Chem.* 18: 5468.
135 Liu, L., Zhang, G., He, B. et al. (2017). *Mater. Chem. Front.* 1: 499.
136 Yu, T., Xu, X., Li, Y. et al. (2017). *ACS Appl. Mater. Interfaces* 9: 18142.
137 Zou, Y., Najari, A., Berrouard, P. et al. (2010). *J. Am. Chem. Soc.* 132: 5330.
138 Hu, X., Shi, M., Zuo, L. et al. (2011). *Polymer* 52: 2559.
139 Zhang, Y., Zou, J., Yip, H.-L. et al. (2011). *J. Mater. Chem.* 21: 3895.
140 Li, Z., Tsang, S.W., Du, X. et al. (2011). *Adv. Funct. Mater.* 21: 3331.
141 Chu, T.Y., Lu, J., Beaupre, S. et al. (2011). *J. Am. Chem. Soc.* 133: 4250.
142 Chu, T.-Y., Lu, J., Beaupré, S. et al. (2012). *Adv. Funct. Mater.* 22: 2345.
143 Xu, B., Yi, X., Huang, T.-Y. et al. (2018). *Adv. Funct. Mater.* 28: 1803418.
144 Amb, C.M., Chen, S., Graham, K.R. et al. (2011). *J. Am. Chem. Soc.* 133: 10062.
145 Fei, Z., Ashraf, R.S., Han, Y. et al. (2015). *J. Mater. Chem. A* 3: 1986.
146 Zhong, H., Li, Z., Deledalle, F. et al. (2013). *J. Am. Chem. Soc.* 135: 2040.
147 Schroeder, B.C., Ashraf, R.S., Thomas, S. et al. (2011). *Chem. Commun.* 48: 7699.
148 Wang, D.H., Pron, A., Leclerc, M., and Heeger, A.J. (2013). *Adv. Funct. Mater.* 23: 1297.
149 Huang, J., Zhao, Y., He, W. et al. (2012). *Polym. Chem.* 3: 2832.
150 Wang, K., Xu, Z., Guo, B. et al. (2016). *RSC Adv.* 6: 63338.
151 Qiao, X., Chen, W., Wu, Q. et al. (2017). *Chem. Commun.* 53: 3543.
152 Qiao, X., Wu, Q., Wu, H. et al. (2017). *Adv. Funct. Mater.* 27: 1604286.
153 Piliego, C., Holcombe, T.W., Douglas, J.D. et al. (2010). *J. Am. Chem. Soc.* 132: 7595.
154 Cabanetos, C., Labban, A.E., Bartelt, J.A. et al. (2013). *J. Am. Chem. Soc.* 135: 4656.
155 Yuan, J., Dong, H., Li, M. et al. (2014). *Adv. Mater.* 26: 3624.
156 Zhang, C., Zhou, Z., Wu, H. et al. (2017). *Adv. Electron. Mater.* 3: 1700213.
157 Zhao, J., Li, Q., Liu, S. et al. (2020). *ACS Energy Lett.* 5: 367.
158 Lu, L. and Yu, L. (2014). *Adv. Mater.* 26: 4413.
159 Chen, H.Y., Hou, J.H., Zhang, S.Q. et al. (2009). *Nat. Photonics* 3: 649.
160 Liang, Y., Xu, Z., Xia, J. et al. (2010). *Adv. Mater.* 22: E135.
161 Huang, Y., Huo, L., Zhang, S. et al. (2011). *Chem. Commun.* 47: 8904.
162 Son, H.J., Wang, W., Xu, T. et al. (2011). *J. Am. Chem. Soc.* 133: 1885.
163 Wang, H., Chao, P., Chen, H. et al. (2017). *ACS Energy Lett.* 2: 1971.
164 Chang, C., Li, W., Guo, X. et al. (2018). *Org. Electron.* 58: 82.
165 Li, W., Guo, B., Chang, C. et al. (2016). *J. Mater. Chem. A* 4: 10135.
166 Chao, P., Wang, H., Qu, S. et al. (2017). *Macromolecules* 50: 9617.
167 Chao, P., Wang, H., Mo, D. et al. (2018). *J. Mater. Chem. A* 6: 2942.
168 Huang, Y., Guo, X., Liu, F. et al. (2012). *Adv. Mater.* 24: 3383.
169 Zhang, M., Guo, X., Zhang, S., and Hou, J. (2014). *Adv. Mater.* 26: 1118.
170 Zhang, M., Guo, X., Ma, W. et al. (2014). *Adv. Mater.* 26: 2089.
171 Liu, F., Zhou, Z., Zhang, C. et al. (2017). *Adv. Mater.* 29: 1606574.

172 Zhu, D., Bao, X., Ouyang, D. et al. (2017). *Nano Energy* 40: 495.
173 Son, H.J., Lu, L., Chen, W. et al. (2013). *Adv. Mater.* 25: 838.
174 Koti, R.S., Sanjaykumar, S.R., Hong, S.J. et al. (2013). *Sol. Energy Mater. Sol. Cells* 108: 213.
175 Bathula, C., Song, C.E., Badgujar, S. et al. (2013). *Polym. Chem.* 4: 2132.
176 Ma, Y., Kang, Z., and Zheng, Q. (2017). *J. Mater. Chem. A* 5: 1860.
177 Xu, X.P., Zhang, G.J., Li, Y., and Peng, Q. (2019). *Chin. Chem. Lett.* 30: 809.
178 Fan, Q., Méndez-Romero, U.A., Guo, X. et al. (2019). *Chem. Eur. J.* 14: 3085.
179 Kim, Y., Choulis, S.A., Nelson, J. et al. (2005). *Appl. Phys. Lett.* 86: 063502.
180 Guo, X., Cui, C.H., Zhang, M.J. et al. (2012). *Energy Environ. Sci.* 5: 7943.
181 Xu, X.P., Zhang, G.J., Yu, L.Y. et al. (2019). *Adv. Mater.* 31: 1906045.
182 Yang, C., Zhang, S., Ren, J. et al. (2020). *Energy Environ. Sci.* 13: 2864.
183 Zhang, Z.G., Zhang, S., Min, J. et al. (2012). *Macromolecules* 45: 113.
184 Zhang, M., Guo, X., Ma, W. et al. (2014). *Adv. Mater.* 26: 5880.
185 Wang, Q., Li, M., Zhang, X. et al. (2019). *Macromolecules* 52: 4464.
186 Qian, D., Ma, W., Li, Z. et al. (2013). *J. Am. Chem. Soc.* 135: 8464.
187 Fan, Q., Su, W., Guo, X. et al. (2016). *Adv. Energy Mater.* 6: 1600430.
188 Qin, Y., Uddin, M.A., Chen, Y. et al. (2016). *Adv. Mater.* 28: 9416.
189 Su, W., Fan, Q., Guo, X. et al. (2016). *J. Mater. Chem. A* 4: 14752.
190 Tumbleston, J.R., Collins, B.A., Yang, L. et al. (2008). *Nat. Photonics* 8: 385.
191 Firdaus, Y., Maffei, L.P., Cruciani, F. et al. (2017). *Adv. Energy Mater.* 7: 1700834.
192 Park, G.E., Choi, S., Park, S.Y. et al. (2017). *Adv. Energy Mater.* 7: 1700566.
193 Liu, Y., Lu, H., Li, M. et al. (2018). *Macromolecules* 51: 8646.
194 Yao, H.F., Cui, Y., Qian, D.P. et al. (2019). *J. Am. Chem. Soc.* 141: 7743.
195 Li, S., Ye, L., Zhao, W. et al. (2018). *J. Am. Chem. Soc.* 140: 7159.
196 Chen, J., Wang, L., Yang, J. et al. (2019). *Macromolecules* 52: 341.
197 Zhang, B., Yu, Y., Zhou, J. et al. (2020). *Adv. Energy Mater.* 10: 1904247.
198 Fan, Q., Su, W., Guo, X. et al. (2017). *J. Mater. Chem. A* 5: 5106.
199 Zhang, X., Zhang, J., Lu, H. et al. (2015). *J. Mater. Chem. C* 3: 6979.
200 Li, G., Gong, X., Zhang, J. et al. (2016). *ACS Appl. Mater. Interfaces* 8: 3686.
201 Jiang, H., Wang, Z., Zhang, L. et al. (2017). *ACS Appl. Mater. Interfaces* 9: 36061.
202 Liu, Y., Chen, S., Zhang, G. et al. (2017). *J. Mater. Chem. A* 5: 15017.
203 Zeng, A.P., Ma, X.L., Pan, M.A. et al. (2021). *Adv. Funct. Mater.* 31: 2102413.
204 Min, J., Zhang, Z.G., Zhang, S., and Li, Y. (2012). *Chem. Mater.* 24: 3247.
205 Gao, L., Zhang, Z.G., Xue, L.W. et al. (2016). *Adv. Mater.* 28: 1884.
206 Bin, H.J., Zhang, Z.G., Gao, L. et al. (2016). *J. Am. Chem. Soc.* 138: 4657.
207 Fan, Q., Su, W., Guo, X. et al. (2017). *J. Mater. Chem. A* 5: 9204.
208 Bin, H.J., Gao, L., Zhang, Z.G. et al. (2016). *Nat. Commun.* 7: 13651.
209 Price, S.C., Stuart, A.C., Yang, L. et al. (2011). *J. Am. Chem. Soc.* 133: 4625.
210 Fan, Q., Su, W., Meng, X. et al. (2017). *Solar RRL* 1: 1700020.
211 Xue, L., Yang, Y., Xu, J. et al. (2017). *Adv. Mater.* 29: 1703344.
212 Su, W., Li, G., Fan, Q. et al. (2019). *J. Mater. Chem. A* 7: 2351.

213 Li, G.D., Xu, Q.Q., Chang, C.M. et al. (2019). *Macromol. Rapid Commun.* 40: 1800660.
214 Zhao, Q., Qu, J., and He, F. (2020). *Adv. Sci.* 7: 2000509.
215 Chen, W., Huang, G., Li, X. et al. (2018). *ACS Appl. Mater. Interfaces* 10: 42747.
216 Liu, D., Zhang, K., Zhong, Y. et al. (2018). *J. Mater. Chem. A* 6: 18125.
217 Li, X., Weng, K., Ryu, H.S. et al. (2020). *Adv. Funct. Mater.* 30: 1906809.
218 Chen, S., Liu, Y., Zhang, L. et al. (2017). *J. Am. Chem. Soc.* 139: 6298.
219 Fan, B.B., Zhu, P., Xin, J.M. et al. (2018). *Adv. Energy Mater.* 8: 1703085.
220 Zhu, L., Zhong, W.K., Qiu, C.Q. et al. (2019). *Adv. Mater.* 31: 1902899.
221 Fan, B.B., Du, X.Y., Liu, F. et al. (2018). *Nat. Energy* 3: 1051.
222 Fan, B.B., Zhang, D.F., Li, M.J. et al. (2019). *Sci. China Chem.* 62: 746.
223 Tang, D.S., Wan, J.H., Xu, X.P. et al. (2018). *Nano Energy* 53: 258.
224 Feng, K., Yuan, J., Bi, Z. et al. (2019). *iScience* 12: 1.
225 Zhang, M., Guo, X., Wang, X. et al. (2011). *Chem. Mater.* 23: 4264.
226 Wang, K., Guo, X., Guo, B. et al. (2016). *Macromol. Rapid Commun.* 37: 1066.
227 Guo, B., Li, W., Guo, X. et al. (2017). *Nano Energy* 34: 556.
228 Guo, B., Guo, X., Li, W. et al. (2016). *J. Mater. Chem. A* 4: 13251.
229 Guo, B., Li, W., Guo, X. et al. (2017). *Adv. Mater.* 29: 1702291.
230 Su, W., Fan, Q., Guo, X. et al. (2017). *Nano Energy* 38: 510.
231 Cao, Z.X., Chen, J.L., Liu, S.J. et al. (2019). *Chem. Mater.* 31: 8533.
232 Wen, S., Li, Y., Rath, T. et al. (2019). *Chem. Mater.* 31: 919.
233 Xu, X.P., Yu, T., Bi, Z.Z. et al. (2018). *Adv. Mater.* 30: 1703973.
234 Xu, X.P., Li, Z.J., Bi, Z.Z. et al. (2018). *Adv. Mater.* 30: 1800737.
235 Chen, K., Ma, R.J., Liu, T. et al. (2020). *J. Mater. Chem. A* 8: 7083.
236 Sun, C.K., Pan, F., Bin, H.J. et al. (2018). *Nat. Commun.* 9: 743.
237 Sun, C., Qin, S., Wang, R. et al. (2020). *J. Am. Chem. Soc.* 142: 1465.
238 Xu, Y., Cui, Y., Yao, H.F. et al. (2021). *Adv. Mater.* 33: 2101090.
239 Xu, X.P., Feng, K., Bi, Z.Z. et al. (2019). *Adv. Mater.* 31: 1901872.
240 Zheng, Z., Yao, H.F., Ye, L. et al. (2020). *Mater. Today* 35: 115.
241 Qian, D.P., Ye, L., Zhang, M.J. et al. (2012). *Macromolecules* 45: 9611.
242 Zhang, M.J., Guo, X., Ma, W. et al. (2015). *Adv. Mater.* 27: 4655.
243 Fan, Q.P., Zhu, Q.L., Xu, Z. et al. (2018). *Nano Energy* 48: 413.
244 Zhao, W.C., Li, S.S., Yao, H.F. et al. (2017). *J. Am. Chem. Soc.* 139: 7148.
245 Fei, Z., Eisner, F.D., Jiao, X. et al. (2018). *Adv. Mater.* 30: 1705209.
246 Wu, Y., An, C., Shi, L. et al. (2018). *Angew. Chem. Int. Ed.* 57: 12911.
247 Qin, Y.P., Ye, L., Zhang, S.Q. et al. (2018). *J. Mater. Chem. A* 6: 4324.
248 Liu, T., Huo, L.J., Chandrabose, S. et al. (2018). *Adv. Mater.* 30: 1707353.
249 Ye, L., Xie, Y., Weng, K. et al. (2019). *Nano Energy* 58: 220.
250 Li, W., Li, G., Guo, H. et al. (2019). *J. Mater. Chem. A* 7: 1307.
251 Xu, Z., Fan, Q., Meng, X. et al. (2017). *Chem. Mater.* 29: 4811.
252 Zhao, W.C., Qian, D.P., Zhang, S.Q. et al. (2016). *Adv. Mater.* 28: 4734.
253 Wang, Y., Fan, Q., Guo, X. et al. (2017). *J. Mater. Chem. A* 5: 22180.
254 Fan, Q., Wang, Y., Zhang, M. et al. (2018). *Adv. Mater.* 30: 1704546.
255 Fan, Q.P., Su, W.Y., Wang, Y. et al. (2018). *Sci. China Chem.* 61: 531.
256 Meng, Y., Wu, J., Guo, X. et al. (2019). *Sci. China Chem.* 62: 845.

257 Fan, Q., Su, W., Chen, S. et al. (2020). *Angew. Chem. Int. Ed.* 59: 19835.
258 Fan, Q.P., Su, W.Y., Chen, S.S. et al. (2020). *Joule* 4: 658.
259 Fan, Q., Ma, R., Liu, T. et al. (2020). *Solar RRL* 4: 2000142.
260 Yao, H., Bai, F., Hu, H. et al. (2019). *ACS Energy Lett.* 4: 417.
261 Wu, J., Meng, Y., Guo, X. et al. (2019). *J. Mater. Chem. A* 7: 16190.
262 Wang, W., Wu, Q., Sun, R. et al. (2020). *Joule* 4: 1070.
263 Yuan, J., Zhang, Y.Q., Zhou, L.Y. et al. (2019). *Joule* 3: 1140.
264 Ma, R.J., Liu, T., Luo, Z.H. et al. (2020). *ACS Energy Lett.* 5: 2711.
265 Li, C., Zhou, J.D., Song, J.L. et al. (2021). *Nat. Energy* 6: 605.
266 Fan, Q., Xu, Z., Guo, X. et al. (2017). *Nano Energy* 40: 20.
267 Chao, P., Chen, H., Zhu, Y. et al. (2020). *Adv. Mater.* 32: 1907059.
268 Huo, L.J., Liu, T., Sun, X.B. et al. (2015). *Adv. Mater.* 27: 2938.
269 Xu, X.P., Feng, K., Lee, Y.W. et al. (2020). *Adv. Funct. Mater.* 30: 1907570.
270 Xu, X.P., Feng, K., Yu, L.Y. et al. (2020). *ACS Energy Lett.* 5: 2434.
271 Dang, D., Yu, D., and Wang, E. (2019). *Adv. Mater.* 31: 1807019.
272 Cui, Y., Yao, H., Hong, L. et al. (2019). *Adv. Mater.* 31: 1808356.
273 Sun, H.L., Liu, T., Yu, J.W. et al. (2019). *Energy Environ. Sci.* 12: 3328.
274 Wang, T., Sun, R., Shi, M.M. et al. (2020). *Adv. Energy Mater.* 10: 2000590.
275 Cao, J.M., Liao, Q.G., Du, X.Y. et al. (2013). *Energy Environ. Sci.* 6: 3224.
276 Liao, C.Y., Chen, Y., Lee, C.C. et al. (2020). *Joule* 4: 189.
277 Liu, J., Liu, L., Zuo, C. et al. (2019). *Sci. Bull.* 64: 1655.
278 Xiong, J., Jin, K., Jiang, Y.F. et al. (2019). *Sci. Bull.* 64: 1573.
279 Wang, T., Qin, J., Xiao, Z. et al. (2020). *Nano Energy* 77: 105161.
280 Zhang, G.Y., Ning, H.J., Chen, H. et al. (2021). *Joule* 5: 1.